

Normal tissue effects and cytokine responses after fractionated X-ray or proton radiotherapy of the head and neck region in mice

Olga Zlygosteva

Supervisor:

Nina Frederike Jeppesen Edin

Eirik Malinen

Hilde Galtung

Randi Gussgard Syljuåsen

Department of Physics

Faculty of Mathematics and Natural Sciences

© Olga Zlygosteva, 2024

*Series of dissertations submitted to the
Faculty of Mathematics and Natural Sciences, University of Oslo
No. 2746*

ISSN 1501-7710

All rights reserved. No part of this publication may be
reproduced or transmitted, in any form or by any means, without permission.

Cover: UiO.

Print production: Graphic center, University of Oslo.

Acknowledgments

First of all, I want to thank my main supervisor Nina Frederike Jeppesen Edin and co-supervisor Eirik Malinen for this opportunity to do an exciting PhD project at University of Oslo. Thank you for your supervision, invaluable guidance, support, and mentorship over the years. Your diverse perspective and expertise have greatly contributed to the depth of my research. Special thanks to my co-supervisor Hilde Galtung and Tine Merete Sølund for feedback, support, encouragement, and fruitful discussions throughout my entire journey that have broadened my research horizons and provided valuable insights into interdisciplinary approaches.

I want to thank Inga Solgård Juvkam, my partner in crime, with whom we conducted all experiments in Oslo and Aarhus during long days full of problem solving and never-ending fun. I enjoyed our work together and extremely happy to find myself such a friend. Thank you for sharing all your knowledge and experience with me, for being supportive, patient, enthusiastic and fun. Your presence has made this journey not only intellectually rewarding but also deeply fulfilling on a personal level.

I am extremely grateful to be a part of convergence environment PROCCA funded by UiO:Life Science and thank Torunn Vistnes Espe for support and resources provided. Through PROCCA project I met many brilliant people, including PhD colleagues Thuy-Tien Maria Huynh and Anna Ivanova, from whom I also gained new insights.

I further want to thank my colleagues at BMF for their assistance, willingness to share their expertise, friendly and supportive environment: Ingunn Hanson, Anne Marit Rykkelid, Julia Marzioch, Joe Alexander Sandvik, Kathinka Elinor Pitman. Also, I would like to thank all people from Radium Hospital in Oslo for being open, supportive, and curious. I am also thankful to Mateusz Sitarz and Brita Singers Sørensen from DCPT in Aarhus for their collaboration and the opportunity to work on joint project. This thesis is a culmination of the efforts, support, and contributions of many individuals, and I am deeply grateful to each and every one of them.

A huge thank to my friends Daria Kotova and Anna Piterskaya, whom I met in the beginning of my PhD journey, for their support, countless cups of coffee, and shared moments of joy. I am also very grateful for all my friends from Russia who stood by me during all these years.

Of course, I could not have done any of this without my family. I am deeply grateful for my mom, my grandfather and my uncle who supported me with the

decision to move to Norway for PhD. My grandfather and my uncle have passed away unexpectedly in the last couple of years, but my heart is always with them. I extend special thanks to my mother for her constant belief in me and unwavering support during the challenging phases of my doctoral studies. Throughout my doctoral journey, I had the privilege to meet my partner and my dearest friend – Delmon Arous. Thank you for your invaluable support, help and happiness you've brought into my life. I deeply appreciate all that you've done. *To all of you, I express my love and dedicate this thesis.*

Olga Zlygosteva
January 2024, Oslo

Abstract

Proton therapy for head and neck cancers holds significant potential due to the physical properties of protons that allow for precise targeting of tumors while minimizing radiation exposure to surrounding healthy tissues. However, more knowledge regarding the biological mechanisms behind the normal tissue toxicities and differences in normal tissue responses between conventional X-ray and proton irradiation is needed. This project aimed to investigate early and late responses of normal tissues in the mouse head and neck area following fractionated X-ray or proton irradiation. Subgoals included studying the cytokine response in serum and saliva after X-ray and proton irradiation and correlating it to the late effects such as hyposalivation and fibrosis.

A preclinical model was established to study early and late radiation-induced effects in the head and neck (H&N) region in mice. The radiation field covered the oral cavity, swallowing structures and salivary glands. To find the dosage that induces clinically relevant endpoints such as oral mucositis, C57BL/6J mice were X-irradiated with total doses ranging from 26 to 75 Gy, given in 10 fractions over 5 or 10 days. The dose that induced symptoms comparable to those observed in patients was found to be 65 Gy. To compare normal tissue effects after X-rays and protons, two different treatment plans were used for protons, either with the Bragg Peak in the middle of the mouse (BP) or outside the mouse (transmission mode; TM). Unexpectedly, oral mucositis after proton irradiation was more pronounced and occurred earlier than after X-rays and the number of dose fractions had to be reduced for both proton protocols. The delivered physical doses were 41, 45, and 65 Gy given in 6, 7, and 10 fractions for BP, TM, and X-rays groups, respectively. Various dosimetry methods were used to assess delivered doses. The follow-up period was 105 days to study the early and late radiation-induced effects and included macroscopic and microscopic examinations of the skin, lips, oral mucosa, and salivary glands. Blood and saliva were collected at different time points before and after irradiation to assess saliva volume and cytokine levels.

The observations of oral mucositis in the tongue, the measurements of acinar cell number, fibrosis in the salivary glands and saliva volume showed much larger normal tissue effects after proton irradiation than after X-ray irradiation, despite the proton doses being 30% lower than the X-ray dose. Significant increase of the pro-inflammatory cytokines IL-1 α , TNF, TIMP1, G-CSF, KC, and MIP-1 α were observed in

Abstract

saliva after X-ray irradiation in mice. In addition, cytokines in saliva, but not in serum, were associated with late endpoints in the X-ray experiments. Despite more severe early and late effects observed after proton irradiation, the cytokine response from X-rays showed much higher values, while the proton irradiated group showed a relatively 'cold' cytokine response.

To our knowledge, this is the first head and neck mouse study that directly compares radiation-induced normal tissue effects and cytokine response following X-ray and proton radiotherapy using the same irradiation setup. The results indicate that the relative biological effectiveness of protons in normal tissue is considerably larger than the current clinical standard correction factor of 1.1, which should be considered in the future proton therapy clinical trials with H&N cancers. The surprising lower cytokine response after protons compared to X-rays highlights the importance of studying the mechanistic pathways with respect to immune responses, inflammatory responses, and the development of tissue damage after proton versus X-ray irradiation. In addition, the stronger association of cytokine levels in saliva with late effects but not in serum pointed to a higher potential of salivary cytokines to be used as biomarkers of local radiation-induced damage of salivary glands.

Sammendrag

Protonterapi har et betydelig potensial innen behandling av hode- og halskreft på grunn av de fysiske egenskapene til protoner som tillater presis bestråling av svulster med betydelig mindre bestråling av omkringliggende friskt vev. Det er imidlertid behov for mer kunnskap om de biologiske mekanismene bak normalvevstoksisitet og forskjellene i normalvevsresponser mellom konvensjonell røntgen- og protonbestråling. Dette prosjektet hadde som mål å undersøke tidlige og sene normalvevsresponser i hode- og halsområdet (H&N) på mus etter fraksjonert røntgen- eller protonbestråling. Delmål inkluderte å studere cytokinresponsen i serum og spytt etter røntgen- eller protonbestråling og korrelere den med seneffekter som hyposalivasjon og fibrose.

En preklinisk modell ble etablert for å studere tidlige og sene strålingsinduserte effekter i H&N-regionen hos mus. Strålefeltet dekket munnhulen, svelgestrukturer og spyttkjertler. For å finne det dose regime som induserer klinisk relevante endepunkter som oral mukositt, ble C57BL/6J-mus røntgenbestrålet med totale doser fra 26 til 75 Gy, gitt i 10 fraksjoner over 5 eller 10 dager. Dosen som induserte symptomer sammenlignbare med de som ble observert hos pasienter ble funnet å være 65 Gy. For å sammenligne normale vevseffekter etter røntgen og protoner ble det brukt to ulike behandlingsplaner for protoner, enten med Bragg Peak'en i midten av musen (BP) eller utenfor musen (transmisjonsmodus; TM). Overraskende fant vi at mukositt etter protonbestråling var sterkere og begynte tidligere enn etter røntgenstråling og antall dosefraksjoner måtte reduseres for begge protonprotokollene. De leverte fysiske dosene var 41, 45 og 65 Gy gitt i 6, 7 og 10 fraksjoner for henholdsvis BP-, TM- og røntgengruppene. Ulike dosimetrimetoder ble brukt for å måle leverte doser. Oppfølgingsperioden var 105 dager for å inkludere både tidlige og sene strålingsinduserte effekter og besto av makroskopiske og mikroskopiske undersøkelser av hud, lepper, munnslimhinne og spyttkjertler. Blod og spytt ble samlet på forskjellige tidspunkt før og etter bestråling for å vurdere spyttvolum og cytokinnivåer.

Observasjonene av mukositt i tungen og målingene av antall acinarceller, fibrose og spyttvolum viste mye større normalvevseffekter etter protonbestråling enn etter røntgenbestråling, til tross for at protondosene var 30 % lavere enn røntgendosen. Betydelig økning av de pro-inflammatoriske cytokinene IL-1 α , TNF, TIMP1, G-CSF,

Sammendrag

KC og MIP-1 α ble observert i spytt etter røntgenbestråling av mus. I tillegg var cytokiner i spytt, men ikke i serum, assosiert med seneffekter i røntgenforsøkene. Til tross for mer alvorlige tidlige og sene effekter observert etter protonbestråling, viste cytokinresponsen fra røntgenstråler mye høyere verdier, mens den protonbestrålte gruppen viste en relativt 'kald' cytokinrespons.

Så vidt vi vet, er dette den første musestudien som direkte sammenligner strålingsinduserte normale vevseffekter i hode- og hals med cytokinrespons etter røntgen- og protonstrålebehandling ved bruk av samme bestrålingsoppsett. Resultatene indikerer at den relative biologiske effektiviteten til protoner i normalt vev er betydelig større enn dagens kliniske standardkorreksjonsfaktor på 1.1, hvilket bør vurderes i fremtidige kliniske studier med protonbestråling av H&N-kreft. Den overraskende lavere cytokinresponsen etter protoner sammenlignet med røntgenstråler fremhever viktigheten av å studere de biologiske mekanismer vedrørende immunresponser, inflammatoriske responser og utvikling av vevsskade etter proton versus røntgenbestråling. I tillegg pekte den sterkere assosiasjonen av cytokinnivåer i spytt, men ikke i serum, til et høyere potensial for spyttcytokiner som biomarkører for lokal strålingsindusert skade på spyttkjertler.

Contents

Acknowledgments	i
Abstract	iii
Sammendrag	v
List of Papers	xi
Candidate's contribution	xiii
Abbreviations	xv

Introduction **1**

1 Introduction	3
2 Aims	7

Theoretic background **9**

3 Background	11
3.1 Radiation therapy of H&N cancers.	11
3.2 Radiation physics and basic radiobiology	12
3.3 Parameters of biological effectiveness of different radiations	14
3.4 Radiation-induced normal tissue side effects in H&N area	15
3.4.1 Oral mucositis	15
3.4.2 Salivary glands effects	16
3.5 Strategies to reduce or alleviate normal tissue toxicity after radiotherapy.	18
3.5.1 Advantages of altered fractionation schemes	18
3.5.2 The use of cytokines as biomarkers for normal tissue toxicities	19
3.6 Clinical normal tissue side effects from proton and X-ray therapy	20
3.7 Preclinical normal tissue side effects from proton and X-ray therapy	22

Materials and Methods	25
4 Materials and Methods	27
4.1 Animals	27
4.2 Overview of animal experiments	27
4.3 Design of irradiation set-up.	29
4.4 Irradiation Procedure	29
4.4.1 X-ray experiments	29
4.4.2 Proton experiments	30
4.5 Dosimetry.	31
4.6 Blood and saliva sampling	32
4.7 Evaluation of early effects	32
4.8 Evaluation of late effects.	33
4.9 Cytokine analysis	33
Summary of papers	35
5 Summary of papers	37
Comparing X-ray fractionation schedules	41
6 Comparing X-ray fractionation schedules	43
6.1 Saliva volume	43
6.2 Fibrotic area in SMG	43
6.3 Cytokine profiles	44
Discussion	47
7 Discussion	49
7.1 Methodological considerations	49
7.2 General discussion	53
Conclusions and perspectives	63
8 Conclusions and perspectives	65
8.1 Conclusions.	65
8.2 Perspectives	66
References	67

I A preclinical model to investigate normal tissue damage following fractionated radiotherapy to the head and neck	77
II Cytokine Levels in Saliva Are Associated with Salivary Gland Fibrosis and Hyposalivation in Mice after Fractionated Radiotherapy of the Head and Neck	93
III Acute normal tissue responses in a murine model following fractionated irradiation of the head and neck with protons or X-rays	111
IV Proton compared to X-irradiation leads to more acinar atrophy and greater hyposalivation accompanied by a differential cytokine response	127

Contents

List of Papers

- Paper I** Juvkam IS[#], Zlygosteva O[#], Arous D, Galtung HK, Malinen E, Sølrand TM*, Edin NJ* (2023), **A preclinical model to investigate normal tissue damage following fractionated radiotherapy to the head and neck**, *Journal of Radiation Research*, 64(1), 44–52, DOI 10.1093/jrr/rrac066
- Paper II** Zlygosteva O, Juvkam IS, Aass HCD, Galtung HK, Sølrand TM, Malinen E*, Edin NFJ* (2023), **Cytokine Levels in Saliva Are Associated with Salivary Gland Fibrosis and Hyposalivation in Mice after Fractionated Radiotherapy of the Head and Neck**, *International journal of molecular sciences*, 24(20), 15218, DOI 10.3390/ijms242015218
- Paper III** Zlygosteva O[#], Juvkam IS[#], Arous D, Sitarz M, Sørensen BS, Ankjærgaard C, Andersen CE, Galtung HK, Sølrand TM, Edin NJ*, Malinen E* (2023), **Acute normal tissue responses in a murine model following fractionated irradiation of the head and neck with protons or X-rays**, *Acta oncologica (Stockholm, Sweden)*, 62(11), 1574–1580, DOI 10.1080/0284186X.2023.2254481
- Paper IV** Juvkam IS, Zlygosteva O, Sitarz M, Sørensen BS, Aass HCD, Edin NJ, Galtung HK, Sølrand TM*, Malinen E*, **Proton compared to X-irradiation leads to more acinar atrophy and greater hyposalivation accompanied by a differential cytokine response**, *Submitted*.

[#] These authors contributed equally to this work

* Joint senior authorship

List of Papers

Candidate's contribution

Paper I	Study design Methodology Writing FOTS applications Design and testing the irradiation setup Conducting dosimetry Conducting animal experiments Assisting in the examinations of the oral cavity Saliva sampling Visualisation Writing - original draft and revision
Paper II	Study design Conducting animal experiments Blood and saliva sampling Cytokine analysis Correlation analysis Visualisation Writing - original draft and revision
Paper III	Study design Methodology Writing FOTS application Design and testing the irradiation setup Conducting dosimetry Conducting animal experiments Assisting in the examinations of the oral cavity Saliva sampling Visualisation Writing - original draft and revision
Paper IV	Study design Conducting animal experiments Blood and saliva sampling Cytokine analysis Visualisation Writing - original draft and revision

Candidate's contribution

Abbreviations

BED	Biological Effective Dose
BP	Bragg peak
CT	Computed Tomography
DAHANCA	The Danish Head and Neck Cancer group
DNA	Deoxyribonucleic acid
FOTS	Forsøksdyrforvatningen tilsyns- og søknadssystem / application for performance of an animal experiment
G-CSF	Granulocyte colony-stimulating factor
HE	Hematoxylin and eosin
HNC	Head and neck cancers
H&N	Head and neck
IF-γ	Interferon gamma
IL-1α/IL-1β	Interleukin-1 alpha/beta
IL-6	Interleukin-6
IL-12p70	Bioactive isoform of Interleukin-12
IMRT	Intensity-modulated radiation therapy
IMPT	Intensity modulated proton therapy
in vitro	Studies performed with microorganisms, cells, or biological molecules outside their normal biological context
in vivo	Studies performed with the whole, living organisms or cells, usually animals, including humans, and plants
IP-10	Interferon gamma-induced protein 10
KC	Keratinocyte chemoattractant

Abbreviations

LET	Linear Energy Transfer (keV/ μm)
LQ	Linear-Quadratic
MC	Monte Carlo
MIP-1α	Macrophage inflammatory protein-1 alpha
MMP-9	Matrix Metalloproteinase-9
NF-κB	Nuclear Factor kappa B
NTCP	Normal tissue complication probability
OARs	Organs at risk
PT	Proton therapy
QUANTEC	Quantitative Analyses of Normal Tissue Effects in the Clinic
RBE	Relative biological effectiveness
ROS	Reactive oxygen species
RT	Radiotherapy
RTOG	Radiation Therapy Oncology Group
SCC	Squamous cell carcinoma
SD	Single dose
SF	Surviving fraction
SFED	Single fraction equivalent dose
SG	Salivary glands
SMG	Submandibular gland
SLG	Sublingual gland
SOBP	Spread-out Bragg peak
TIMP-1	Tissue Inhibitor of Metalloproteinase-1
TM	Transmission mode
TNF	Tumor Necrosis Factor

Introduction

Chapter 1

Introduction

**“For those of us who didn’t die, who are no longer sick,
but who don’t get well either”**

*From the book of Håvard Aagesen,
head and neck cancer survivor in Norway
(translated from Norwegian)*

H&N cancer is the seventh most common cancer worldwide, with more than 660,000 new cases and 325,000 deaths annually [1]. Improvements in diagnosing and treating cancer have resulted in higher rates of survival of H&N cancer patients. However, patients and survivors experience both disease-related after-effects and treatment-induced effects such as hearing loss, acute oral effects (e.g. mucositis, skin toxicity, dermatitis and hyposalivation that can lead to loss of taste, difficulties in eating, speaking, swallowing, teeth problems, infections in the oral cavity and malnutrition), osteoradionecrosis, and problems with body image and intimacy [2, 3, 4]. Although early effects are transient, they still may lead to unplanned interruptions and failure in treatment, while late effects and related malnutrition cause a significant reduction in quality of life, weight loss, and psychological distress after the completion of treatment [4].

Approximately 50% of all cancer patients receive radiation therapy (RT) during their course of illness as a main treatment or in combination with other treatment modalities [5]. Precise dose delivery is crucial for tumors located in regions surrounded by many critical organs at risk (OARs) such as those found in the H&N area. For many decades, X-ray beam therapy has been most widely used in the clinic. Advanced delivery techniques, such as intensity-modulated radiotherapy (IMRT) has contributed to great progress in dose conformity to tumor and in limiting the dose to normal tissue [6]. However, because of the physical properties of X-rays, further improvements in sparing of normal tissue seem to be challenging. In recent decades, the advantages of the beam properties of protons were translated into clinical settings and proton therapy (PT) was introduced to cancer patients. These advantages relate to the different dose deposition of protons versus X-rays (see Fig. 1.1). While X-rays give a maximum dose near the surface with declining, low-density dose deposition along their track, protons have a well-defined range and

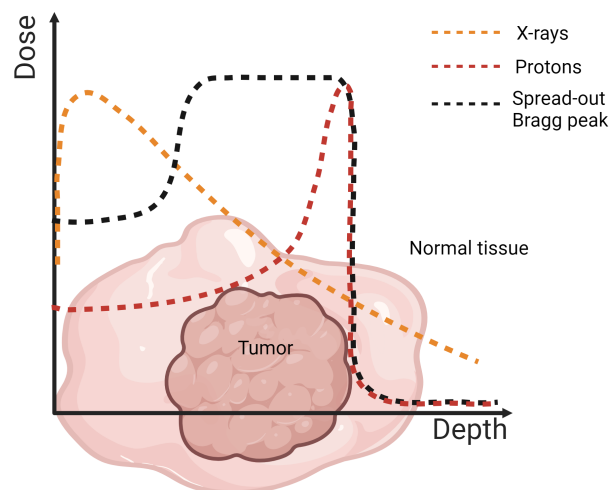


Figure 1.1: Depth dose distributions for X-rays, single and spread-out proton beam with Bragg peak as a function of depth in tumor surrounded by normal tissue. Created with BioRender.com.

deposit most of the energy at the end of their track in the so-called Bragg peak with no dose behind the end of the Bragg peak [7, 8]. By varying the proton energies, a spread-out Bragg Peak (SOBP) can be produced to cover the tumor volume with a substantially lower dose to surrounding normal tissue compared to X-rays (see Fig. 1.1), which potentially could lead to the reduction of normal tissue toxicities. Therefore, proton therapy is considered to be a beneficial treatment modality for H&N cancer patients. Despite all the advantages of the proton dose deposition, the position of the Bragg peak for proton beams depends on beam energy and tissue density and this represents a risk factor. If the delineations are inaccurate or if the tumor size or normal tissue quality/occurrence have changed during the treatment course, the position of the Bragg peak might be shifted, which can lead to an overdose to the normal tissue around the tumor [7]. Currently protons are assumed to be 10% more biologically effective than X-rays, but this might vary along the beam track with higher effectiveness towards the end of the track [9]. Thus, further research in this field and especially on normal tissue toxicities is needed to fully exploit the potential of proton particle therapy. Published clinical data from proton therapy have several limitations such as retrospective observations that might be not reliable or small number of patients, while preclinical data on proton versus X-ray radiation-induced effects usually are not directly comparable because of different setups. Therefore, it is important to design relevant preclinical studies to address the questions such as identifying biological mechanisms leading to clinical symptoms after proton versus X-ray irradiation and the possibilities to detect early signs of radiation-induced late effects using non-invasive methods to identify the risk of side effects.

With the establishment of two new proton therapy centers in Norway by 2025, it is planned that a high proportion of cancer patients undergoing proton therapy will be included in clinical trials. This has led to a comprehensive initiative to enhance

proton therapy research in the country. Preclinical data have an important role in the design and planning of clinical trials and are therefore in high demand.

Chapter 1. Introduction

Chapter 2

Aims

The overall aim of this project was to investigate normal tissue responses in the mouse H&N after X-ray or proton irradiation. In order to fulfill the main aim, the work was divided into subprojects with the following aims:

- to establish a preclinical model employing a clinically relevant radiation field to study various normal tissue effects in the H&N region after X-ray and proton irradiation (paper I and III);

- to monitor serum and salivary cytokines after X-ray and proton irradiation of the H&N and explore the potential of cytokine profiling as an early biomarker (paper II and IV);

- to examine and compare early and late normal tissue effects after X-ray and proton irradiation of the H&N (paper I, II, III and IV).

Chapter 2. Aims

Theoretic background

Chapter 3

Background

3.1 Radiation therapy of H&N cancers

More than 90% of H&N cancers are squamous cell carcinomas (SCC) that usually starts in the mucosal epithelium lining the oral cavity, pharynx and larynx [10]. The other less common H&N cancers originate in other cell types in the major or minor salivary glands (SG) [11].

The treatment of head and neck cancers (HNC) is complex and usually involves multiple modalities. According to the latest ESMO Clinical Practice Guidelines for Head and Neck Cancers, the early-stage SCC HNC can be treated by RT alone, while for locally advanced disease either surgery plus adjuvant chemoradiotherapy or chemoradiotherapy alone is recommended [12, 13]. The standard treatment for SG cancer without distant metastasis is surgery with post-operative RT. However, primary RT is recommended for patients with unresectable tumors or who are unsuitable for surgery due to comorbidities [14]. In the case of RT, IMRT or its variant volumetric-modulated arc therapy is recommended for treatment, which is the advanced form of three-dimensional conformal RT. However, radiotherapy of HNC is associated with significant acute and late toxicities including among others mucositis, dysphagia, xerostomia and hyposalivation. Therefore, there is a need for organ-sparing approaches such as proton therapy.

Despite of the potential and increased use of intensity-modulated proton therapy (IMPT) for HNC, it is not recommended for routine use because of limited clinical evidence [12]. However, randomized clinical trials are ongoing [15] and several countries use IMPT for HNC treatment especially where normal organ constraints cannot be met with IMRT [16]. Based on DAHANCA Radiotherapy Guidelines 2020 from Danish Head and Neck Cancer Group, the potential candidates for PT should be identified at the local oncology departments after the comparison of two treatment plans using protons and X-rays. The dosimetric differences regarding normal tissue complications are used to estimate the potential benefit of PT [17]. National guidelines for treatment of HNC in Norway are similar to the European recommendations and include conventional RT. As particle therapy is currently not available in Norway, only few HNC patients (with inoperable carcinomas in salivary glands, for example) are sent for treatment

abroad [18]. However, Norway will have two new proton therapy centres in operation from 2025, and proton therapy research is therefore highly relevant.

3.2 Radiation physics and basic radiobiology

As was mentioned in the introduction, the therapeutic use of protons is beneficial because of their favorable depth-dose profile. The physical property of protons makes it possible to focus the prescribed dose in the target volume while limiting the damage induced in surrounding healthy tissues [19].

Different biological effects after protons and X-rays may arise because of different radiation interactions with matter. X-rays are considered to be indirectly ionizing radiation as the damage to biomolecules occurs through the interaction with water that leads to generation of reactive oxygen species. There are three main ways on how X-rays can interact with matter depending on its energy and the atomic number of the elements of the matter [20, 21]. The photoelectric effect which predominantly occurs at lower X-ray energies up to 30 kV implies that an atomic electron absorbs all the energy of the incoming photon and is emitted from the atom. The photoelectric effect is the most important interaction for diagnostic imaging because of the high dependence on atomic number. The Compton effect, which can occur at any energy but is predominant at energies higher than 30 kV, implies that part of the energy is absorbed by the free or atomic electron with a simultaneous emission of a secondary photon. Compton effect is the most important interaction mechanism in tissue for energies used in RT. Pair production which occurs at energies higher than 1.022 MV implies that the incoming photon interacts with the electric field of an atomic nucleus in the irradiated material resulting in an electron-positron pair. In tissue, X-ray energies of more than 20 MeV are required for pair production to dominate over the Compton effect.

Compared to X-rays, protons are considered to be directly ionizing radiation and to directly interact with critical molecules such as DNA and proteins leading to ionization or excitation. There are two main ways protons can interact with matter depending on its energy and the atomic number of the elements of the matter [20, 21]. The first is electronic or Coulomb interactions, which imply that protons interact with electrons in the atomic shell with or without energy loss. There are two types of interactions: elastic scattering and inelastic collision. In elastic scattering, the proton is scattered and changes its direction, while in inelastic collision, the proton transfers energy to the hit electron which is excited or emitted from the atom depending on the transferred energy from the proton. The second mode of interaction is nuclear interactions, which imply that the protons interact with the atomic nuclei. In elastic nuclear scattering, the proton is scattered and changes its direction, while in inelastic nuclear scattering, the proton is deflected and emits bremsstrahlung. Lastly, a proton interaction with the nuclei itself can induce a nuclear reaction.

In biological tissue, X-rays undergo attenuation through absorption and scattering that leads to a decrease of the photon numbers with depth, while protons gradually lose energy through the few Coulomb collisions, slow down and

eventually stop with the release of energy (Bragg peak). The interaction difference between X-rays and protons is presented in Figure 3.2 with corresponding dose distributions.

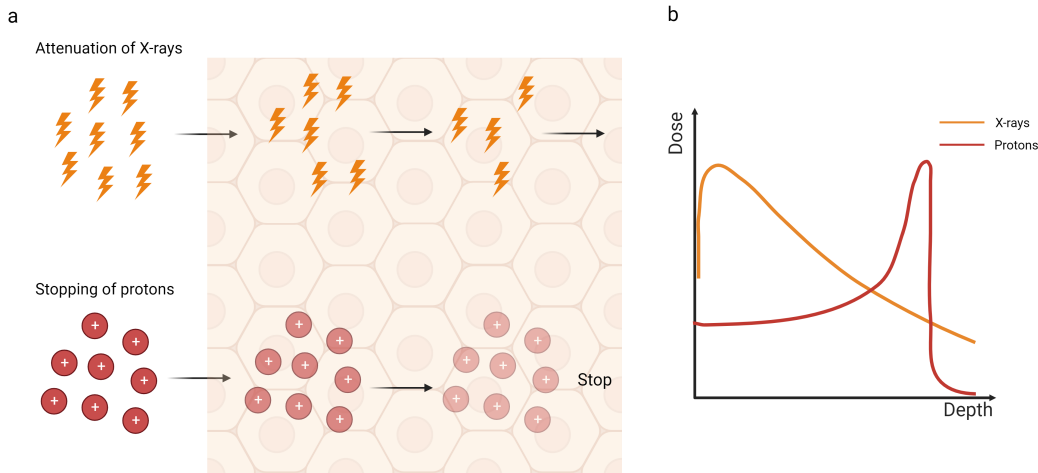


Figure 3.2: Attenuation of X-rays versus stopping of protons (a), dose distribution of X-ray and protons (b). Created with BioRender.com.

For particle irradiation, stopping power is used to describe the energy loss through collisions along the track in matter by the Bethe–Bloch formula, which gives the stopping power as a function of particle energy, charge, and velocity [21]. For quantification in radiobiology, the linear energy transfer (LET) is used, which refers to the energy absorbed by the matter per unit of distance travelled by the particle. LET only takes electronic interactions into account and is equal to electronic stopping power for large samples. In terms of X-rays, LET refers to the energy deposition of secondary electrons mainly from Compton scattering.

X-rays and protons are considered to be low LET radiation. However, the LET of protons vary and protons have a higher LET toward the distal edge of the Bragg peak because the interactions with matter increase with the decrease of the velocity of protons [22]. Despite the fact that LET is used in biology to characterize energy deposition resulting in cellular damage, it does not provide any information about the radial distribution around the track or the variability of energy density along the track. Therefore, two different radiations may have the same average LET, but differ widely in microscopic energy density distribution that can lead to different radiobiological effects [23].

Prediction of radiobiological response is a main challenge in radiotherapy. Survival curves serve as a valuable tool for evaluating the radiosensitivity in vitro following different types of radiation. The extensively validated linear-quadratic (LQ) model is used to describe the surviving fraction (SF) of cells as a function of radiation dose D , where α and β are two parameters [21]:

$$SF(D) = e^{(-\alpha D - \beta D^2)} \quad (3.1)$$

The α/β ratio indicates the intrinsic radiosensitivity. Cells and tissues with a high α/β ratio are more sensitive to radiation and early responding, while slower growing/more radioresistant late responding tissues have low α/β ratio. The survival curve's shape depends on the LET. As the LET increases, the slope of the curve becomes steeper and more linear with less shoulder which indicates a higher ratio of lethal to potentially lethal lesions or a less efficient repair of damage caused by high LET radiation. Conversely, a lower α/β ratio results in a more curved survival curve with a more pronounced shoulder arising from sublethal damage [21].

3.3 Parameters of biological effectiveness of different radiations

To account for differences in energy deposition patterns, the relative biological effectiveness (RBE) is used as a scaling parameter to measure the effectiveness of different radiations. RBE is defined as the ratio of the reference dose (for example, dose from Co-60 γ -rays or 250 kV X-rays) to the test dose that induce the same biological effect [19, 22]. It represents a complex function and depends on several variables such as the dose per fraction, LET, tissue types, biological end points, etc [24]. LET increases with the slowing down of protons with depth (Figure 3.3), and RBE increases with increasing LET with a slope depending on the biological endpoint [22]. Importantly, the region of maximum LET and therefore RBE is not at the top of the Bragg peak but at the distal dose fall-off with very low proton energies that are dosimetrically negligible [22]. Dose per fraction is another parameter that affects biological effectiveness. RBE increases with decreasing dose for cell survival. This is reported to be more pronounced for late-responding (low α/β) compared to early-responding (high α/β) tissues [22]. Therefore, the RBE also depends on the intrinsic radiosensitivity and repair proficiency of the cell and tissue type [25].

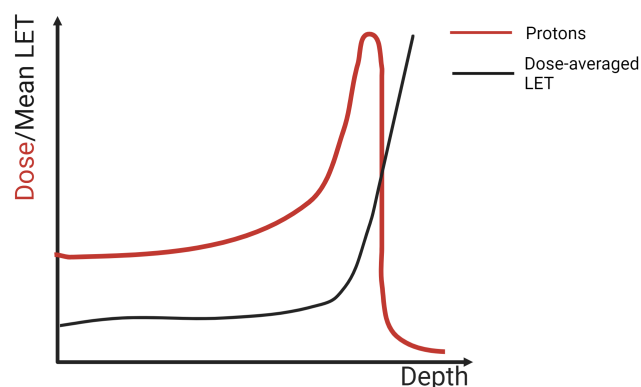


Figure 3.3: Schematic dose and dose-averaged LET as a function of depth for proton beam. Created with BioRender.com.

Despite the knowledge of different interactions and dose deposition mechanisms

of protons and X-rays, proton therapy dose planning is currently based on the practices developed for conventional X-ray treatment and tissue tolerance data are mostly derived from old studies using X-rays. The different energy deposition mechanisms of protons versus X-rays that lead to a differential response in normal tissues are not fully explored or implemented at the proton therapy centers today.

3.4 Radiation-induced normal tissue side effects in H&N area

Radiation-induced normal tissue effects can be divided into early and late effects [26]. As the focus in this project was to study radiation-induced oral mucositis and salivary gland dysfunction, the overview of these effects is presented in the following subsections.

3.4.1 Oral mucositis

Oral mucositis is a common and dose-limiting complication with incidence varying between 50-90% among HNC patients, depending on radiation field, dose, fractionation, and use of concurrent chemotherapy [27]. The oral mucosa is composed of two layers: stratified squamous epithelium and connective tissue below. Basement membrane formed by stem cells is located between the epithelium and connective tissue layer [28]. The renewing and proliferating mucosal cells have a very high cell turnover rate resulting in replacement of the lining every 7 to 14 days, which makes them vulnerable to the cytotoxic effects of RT [28, 29]. In literature, a five-stage model of the pathobiology of oral mucositis after RT is suggested (Fig. 3.4). The first “Initiation” stage results in DNA damage to cells within the RT field and the production of reactive oxygen species (ROS) that are crucial mediators of downstream signaling pathway activation and biological agents release from the epithelium and tissue macrophages [30, 31]. The next two stages of “Primary damage” and “Signal amplification” are usually combined and characterized by the innate immune response and the activation of p53, NF- κ B and other transcription factors. This stimulates the gene expression and release of pro-inflammatory cytokines, such as TNF, IL-1 β , and IL-6. The resultant cell damage and apoptosis in the basal epithelial stem cells lead to loss of renewable epithelium and disruption of oral mucosal integrity [31, 32, 33]. In addition, TNF activates NF- κ B by providing a positive feedback loop that contributes to signal amplification and leads to more cell death [31]. During the “Ulceration” stage, the oral mucosa presents with a pseudomembrane or ulceration which allows the microbial colonies and infection to penetrate the surface and increase the release of pro-inflammatory mediators [31]. The final stage of “Healing” occurs around 2–4 weeks after the termination of the treatment by signaling to basal epithelial cells to differentiate and migrate across the lesions [32, 33].

The association between cumulative radiation dose and the incidence of oral mucositis following radiotherapy depends on many factors including treatment

modalities and patient-related risk factors [34]. The first clinical signs of oral mucositis have been reported at cumulative doses of 10 to 30 Gy followed by ulceration in the mucosa of the tongue, gingiva, and palate [34, 35]. For nasopharyngeal or oropharyngeal tumors, patients that are receiving cumulative radiation doses > 50 Gy are more likely to develop severe oral mucositis [35]. One study presented the mean dose at which 50% of patients experience grade 3 oral mucositis (severe oral ulcers) to be 51 Gy (95% CI 40–61) based on generated dose–response curves [36].

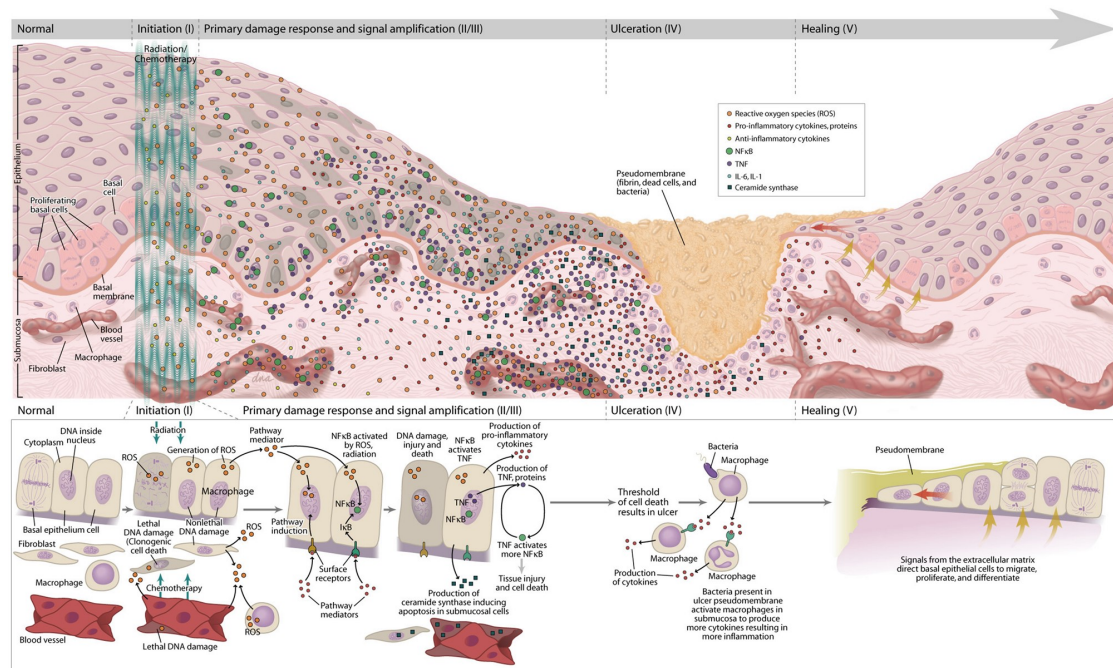


Figure 3.4: Five-stage model of the pathobiology of oral mucositis. Figure courtesy of Dr Stephen T. Sonis. Figure reprinted with permission from [32].

3.4.2 Salivary glands effects

It is estimated that more than 80% of HNC patients exhibit salivary gland hypofunction and xerostomia (dry mouth) after RT [37]. Salivary glands consist of three major cell types: saliva-producing mucous and serous acinar cells as well as myoepithelial and duct cells [38]. The SG cells are mostly postmitotic with a slow cell turnover time of 60–120 days and are expected to be relatively radioresistant. However, interestingly, changes in the amount and composition of saliva occurring early after RT suggest that their response to radiation has both early and late phases (Fig. 3.5) [38, 39].

The early response has been attributed to DNA damage, enhanced ROS production, impairment of microvessels and possibly inflammation [37, 38, 40]. The late effects result from an accumulation of chronic inflammation, neuronal and vascular changes, fibrosis, and senescence or dysfunction of adult progenitor cell populations [37, 38]. Moreover, it has been proposed that the senescent cells might

3.4. Radiation-induced normal tissue side effects in H&N area

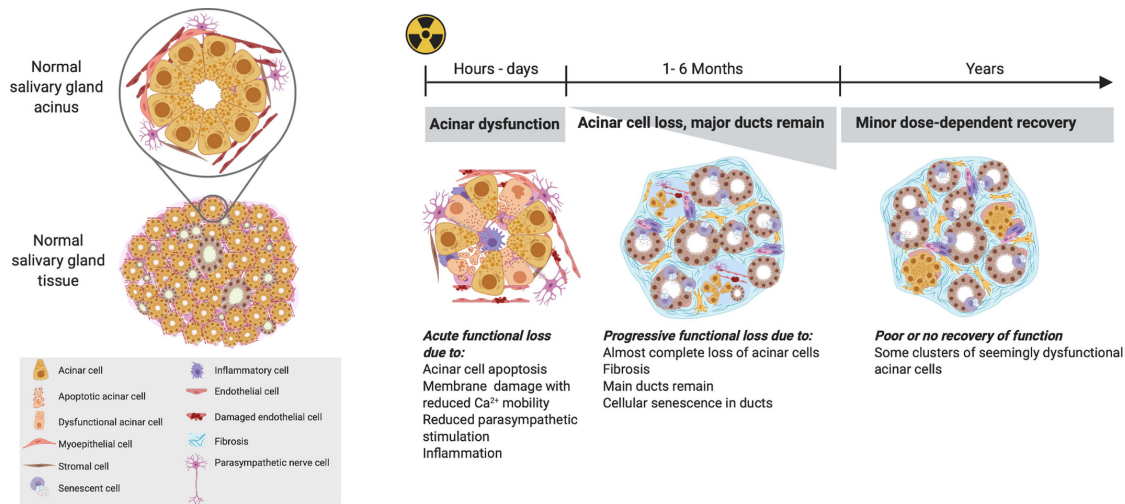


Figure 3.5: A schematic of the cellular and tissue responses of the salivary gland to RT over time. The left panel depicts a model of a salivary gland tissue with an acinus, the functional unit of the glands, enlarged. The right panel shows the early and late responses of salivary gland tissue to RT. Figure reprinted with permission from [38].

develop a unique secretory phenotype that produces several proinflammatory and profibrotic growth factors and is associated with reduced tissue regenerative capacities, inflammation, and fibrosis [38].

The incidence of SG damage following RT depends on both the radiation dose and the volume of the parotid or submandibular glands (SMG) included in the radiation field. The lowest observable gland function reduction was reported to occur at < 10-15 Gy mean dose, with a gradual further decrease at doses of 20-40 Gy and a strong reduction at doses > 40 Gy [41]. There are strong indications that total irradiation of parotid glands with doses exceeding 60 Gy results in permanent salivary damage with no functional recovery [42]. However, the risk of hyposalivation and xerostomia is mitigated when at least one parotid gland or even one SMG is spared [41]. The clear volume effect was demonstrated in a parotid gland irradiation study, where the increase in irradiated volume of parotid glands from 0%–40% to 90–100% resulted in a decrease in saliva flow ratio from 100% to less than 10% in patients with a mean parotid dose of 35–45 Gy [42].

The different RT-induced normal tissue side effects may contribute to the development and progression of each other. For example, a decrease in saliva flow and changes in its quality decrease the protective effect on the mucous membranes and teeth, affecting lubrication of food, eating, and speaking. Therefore, the salivary gland damage may contribute to the infectious ulceration of oral mucositis [27].

In conclusion, knowledge of the radiation-induced biological mechanisms leading to the clinical symptoms discussed above is vital for early detection of patients at risk and the development of new strategies for mitigation.

3.5 Strategies to reduce or alleviate normal tissue toxicity after radiotherapy

Reducing normal tissue toxicities in cancer patients will lead to improved quality of life. This can be done by changing the treatment in terms of radiation type, dose fractionation, radiation field configuration, combination treatments with systemic therapies, or mitigation strategies. The literature review below presents several promising strategies that are already implemented in clinics or that have been under active research.

3.5.1 Advantages of altered fractionation schemes

Several unconventional fractionated RT regimens for HNC have been assessed in the past decades including hypo- and hyperfractionation and accelerated fractionation [43, 44]. These regimens were believed to improve the therapeutic ratio through a differential response between tumors and normal tissues to fractionated radiotherapy [44]. According to classifications, hypofractionated RT employs a dose per fraction of more than 2.2 Gy, while hyperfractionated RT uses a dose per fraction of less than 1.8 Gy [45]. Accelerated RT employs a rate of dose-accumulation that exceeds 10 Gy/week and delivers the conventional number of dose fractions in a reduced treatment time to increase tumor control rate [45].

One of the largest meta-analyses with the aim to study the effect of altered fractionation on overall survival was conducted by the MARCH (Meta-Analysis of Radiotherapy in Carcinomas of Head and neck) Collaborative Group and included 15 randomized trials with in total 6515 patients [46]. The results showed a small but significant improvement in survival (8% at 5 years) and a more pronounced benefit in locoregional and local control with hyperfractionated radiotherapy compared to conventional radiotherapy (accelerated radiotherapy showed 2% survival improvement) [46]. The benefit was significantly higher in the youngest patients [46]. However, a study conducted by the Radiation Therapy Oncology Group (RTOG) showed that the patients given hyperfractionation had significantly more acute mucositis, compared to standard fractionation [44]. This is one of the major limiting factors of implementing altered fractionations in radiotherapy for HNC. Importantly, no significant increase of late effects was observed [44].

Even though altered fractionation in radiotherapy shows an improvement of survival in patients with HNC, the optimal fractionation schedule is still not known. Based on the LQ model, the biological effective dose (BED) and single fraction equivalent dose (SFED) can be calculated to compare different fractionation regimes [47]:

3.5. Strategies to reduce or alleviate normal tissue toxicity after radiotherapy

$$BED = nd \cdot \left(1 + \frac{d}{\alpha/\beta}\right), \quad (3.2)$$

$$SFED = \frac{\sqrt{1 + 4\frac{BED}{\alpha/\beta}} - 1}{\frac{2}{\alpha/\beta}}. \quad (3.3)$$

For both equations, n is the fraction number, d is the dose per fraction in Gy, and α/β ratio in Gy is a parameter derived from the LQ model. BED is an extrapolated dose given over infinitely many fractions needed to induce the same effect and is a useful parameter in clinical practice.

3.5.2 The use of cytokines as biomarkers for normal tissue toxicities

Several studies of the inter- and intra-patient variability in early and late side-effects have demonstrated that the risk of normal tissue toxicity is defined by biological determinants which are specific for each individual and for the individual radiation-induced pathogenesis [48]. The possibility to stratify cancer patients according to the risk of toxicity as well as to identify the development of the effects and their severity in an early phase would be an important tool to guide the choices of treatment modality, therapeutic interventions, or adaptive therapy selection in order to mitigate the risk or intensify the therapy [48, 49]. There is therefore a high interest in identifying relevant biomarkers, which are indicative measurable characteristics of the responses of a biological system [48]. Identification of biomarkers for the assessment and early diagnosis of oral mucositis, for example, might reduce the frequency of therapy termination, dosage re-modulation and allow a more tailored management of each patient [49]. In the last decade, the content of body fluids like blood and saliva has been studied to find potential diagnostic and prognostic biomarkers for HNC response and normal tissue toxicities [50].

Cytokines are potential candidates to be used as biomarkers in the clinic [51]. Cytokines are small glycoproteins produced by immune and stromal cells that regulate cell proliferation, survival, and migration and they play a crucial role in immune cell activation [50, 52]. Their release after chemo- and/or radiotherapy leads to amplification of damage responses [49]. Many studies have focused on changes in cytokine levels before and after X-ray radiotherapy treatment with the aim to correlate them with radiation-induced tissue toxicities. Several studies demonstrated a potential for using cytokine levels in saliva to identify HNC patients at risk for mucositis [51]. For example, an increase of pro-inflammatory cytokines including interleukin IL-1 β , IL-6 and TNF during or after RT was associated with greater severity of oral mucositis in patients with HNC which represents a potential tool for the early identification of patients at risk [53, 54]. Another study, focused on late effects in HNC survivors ≥ 5 years post-RT, did not find any significant associations between a selection of pro-inflammatory cytokines

and xerostomia, dysphagia, or chronic fatigue [55]. However, this study reported increased levels of some cytokines, for example IL-6 and IP-10, in HNC survivors group compared to healthy controls that may indicate persistent systemic changes in the survivors. Still, the studies of cytokine levels for prediction of the severity of late radiation-induced effects, which are also an important dose-limiting factor and the major contributor for reduced quality of life after RT, are limited.

While the number of cytokine studies is increasing, the predictive role of cytokines in the determination of early and late toxicity severity in HNC has still not been fully explored.

3.6 Clinical normal tissue side effects from proton and X-ray therapy

The evidence summarized in several reviews comparing PT and IMRT suggests that PT is a promising treatment option for patients with HNC [56].

For oropharyngeal SCC the tumor control rates are reported to be similar or better than those obtained with IMRT, while the first comparative results of patient-reported outcomes, which is a validated instrument for assessing symptom burden, show a reduction in subacute toxicity for patients, especially regarding taste and appetite, for IMPT [57, 58]. Lower rates of subacute and late swallowing-related morbidity were also reported for IMPT when measured by the rate of feeding tube dependency and/or severe weight loss based on a case matched analysis [59]. Finally, in one of the largest retrospective studies, the proportion of moderate-to-severe xerostomia was significantly lower in a group of patients who received IMPT at 18–36 months [56, 57]. The dosimetric advantage of protons over X-rays for the treatment of HNC were discussed in [60]. For both cases the use of IMPT can spare organs from up to 25 Gy of unnecessary irradiation compared with IMRT (Figure 3.6). All this may result in less hospitalizations and lower health care costs over time, and patients receiving IMPT may return to normal function and life during the first 3 months after treatment [57, 58]. Several retrospective case-matched studies of patients with nasopharyngeal SCC reported a lower requirement for feeding tube placement and opioid pain medication for IMPT patients compared to those treated with IMRT which was correlated to a reduction in the mean oral cavity dose [56, 61]. Reducing late complications and improving quality of life after RT of HNC is especially important because of the increasing number of young and physically fit patients with good prognosis [57, 62].

In 2010, the Quantitative Analyses of Normal Tissue Effects in the Clinic (QUANTEC) group presented a review of the published clinical evidence for normal tissue dose effect relationships including a report on salivary glands [63, 41]. The recommendations for H&N IMRT suggest that limiting the mean dose to at least 1 parotid gland to < 20 Gy, or to both glands to < 25 Gy leads to a significant reduction of severe xerostomia risk [63, 41].

Normal Tissue Complication Probability (NTCP) is a crucial concept in

3.6. Clinical normal tissue side effects from proton and X-ray therapy

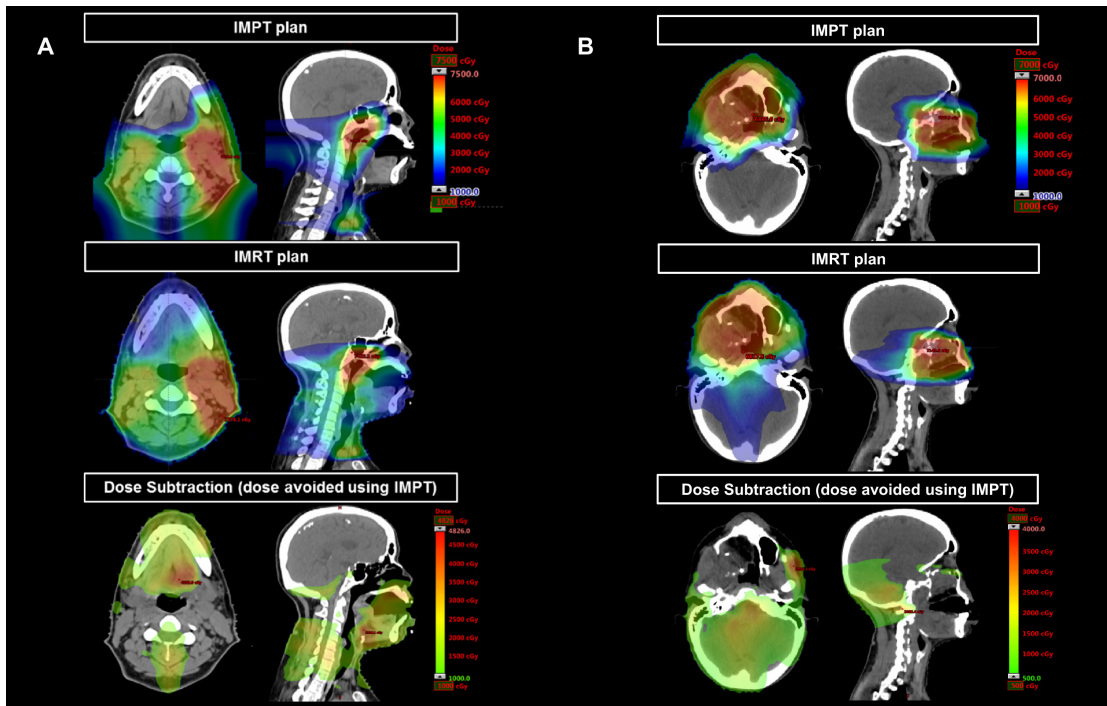


Figure 3.6: Comparative treatment plans using IMRT, IMPT, and subtraction plan (IMRT-IMPT). (A) A 56-year woman with T1N1 left sided nasopharyngeal carcinoma (4 nodes in left levels IIa, IIb, III, and Va). (B) A 47-year woman with T4N0 adenoid cystic carcinoma of the hard palate (surgery followed by adjuvant radiotherapy). Figure reprinted with permission from [60].

assessing the risk of normal tissue effects such as xerostomia. NTCP quantifies the likelihood of complications occurring in normal tissues as a consequence of various factors, including the radiation dose delivered to the SG, the volume of the glands irradiated, and individual patient characteristics. NTCP models were used to validate the QUANTEC xerostomia recommendations and allowed the clinicians to optimize treatment plans, balancing the therapeutic benefits of radiation with the preservation of SG function to enhance the overall quality of life for patients. Most of the NTCP studies found that the QUANTEC constraints perform well [63, 64]. However, NTCP models also highlighted that the dose to the SMG, SLG, and soft palate might be significant predictors of xerostomia, and sparing at least one SMG also appears to reduce xerostomia risk as it is responsible for 20–30% total saliva secretion [63, 41, 65]. In addition, recent findings indicate the presence of stem cell regions within the parotid glands, which play a critical role in maintaining gland functionality, and might suggest targeted partial-gland sparing [63]. A more comprehensive understanding of the biological mechanisms underlying normal tissue toxicities holds the potential to improve RT strategies.

To conclude, the data utilized for the development and validation of constraints primarily rely on IMRT studies with X-rays, and more clinical data from IMPT is needed. Furthermore, the studies listed above have several weaknesses because they are generally based on low amounts of evidence from small non-randomized studies due to a lack of large comparative randomized studies for PT of HNC [57].

Increasing number of IMPT patients and ongoing comparative randomized trials will provide more clinical data on the differences between IMPT and IMRT and patient-reported outcomes in the nearest future [61, 66].

3.7 Preclinical normal tissue side effects from proton and X-ray therapy

Despite the high theoretical potential of IMPT, the uncertainties and assumptions regarding PT discussed above might compromise its clinical potential [66]. Knowing that the proton dose distribution is highly sensitive to inter- and intra-fractional variations in anatomy, there is a concern that regions with higher LET and RBE towards the distal edge might occur in a normal tissue and cause severe toxicities [66]. In the current practice of PT, the fixed standard value for RBE of 1.1 is used in most facilities [66]. This value was deduced as an average of measured RBE values from in vivo experiments conducted in the early days of PT and neglected any dependency of RBE on dose, tissue type, endpoint or beam properties [24]. However, the awareness around RBE variation along the proton path has been raised and various in vitro and in vivo experiments have been conducted to accumulate data on variability of proton RBE [67].

The review that summarized RBE values for published in vitro data showed that the range of estimated RBE's was from 0.86 to 2.1 with an average of 1.22 ± 0.02 in the middle of the SOBP [68], while at the distal end of the depth dose distribution, RBE was around 1.6 [69]. The in vitro studies help to analyze relative RBE values and understand basic mechanisms, but in vivo studies enable better approximation of clinical treatments and are superior for studying more complex biological systems [68, 70].

The in vivo studies for clinical 80-250 MeV proton beams include a variety of tissue end points such as acute and late skin reactions, jejunal crypt cell survival, organ weight loss or the dose at which half the laboratory animals died (LD50) with the majority returning RBE values broadly consistent with 1.1 or a less pronounced increase than found in in vitro studies [68, 71].

A preclinical study that used zebrafish embryos survival data as an alternative in vivo model reported RBE of $1.13 \pm 0.08/1.41 \pm 0.08$ for 20/30 Gy single dose (SD) irradiation at the entrance plateau and $1.20 \pm 0.04/1.60 \pm 0.32$ for 20/30 Gy SD irradiation at the mid-SOBP position determined four days after irradiations with proton relative to 6 MV photon beams [69]. Another study investigated the early normal tissue damage of limb skin in mice after SD irradiation with protons and reported RBE values for mid-SOBP position of 1.00 (0.94–1.05) relative to 6 MV photons and 0.9 (0.85–0.97) relative to 240 kV photons [67]. However, this study demonstrated an enhanced biological effect in the position covering the very distal edge of the SOBP and the first part of the distal dose drop off. In the mice group positioned at the SOBP distal dose fall-off, 25% of the mice developed early skin damage compared with 0–8% in other groups [67]. Another study of early end point of intestinal crypt regeneration in mice showed that proton irradiations at

3.7. Preclinical normal tissue side effects from proton and X-ray therapy

the distal edge of the SOBP were more effective than at the mid-SOBP by a factor of 14%, while RBE values for mid-SOBP of 1.15 was reported regardless of the fractionation regime or dose (at least in the range of 1–10 fractions) [72]. A recent study with the goal to investigate the fundamental differences between proton- and X-ray-induced intestinal injuries in mice after SD irradiation at the mid-SOBP also reported increased biological effectiveness of protons with an RBE of 1.14 [73]. EdU staining, which labels the actively dividing cells in the jejunum crypts, showed that proton irradiation was more effective in eradicating regenerating jejunum crypts than X-ray irradiation [73].

For a late end point, a study of mice death at 180–240 days due to pneumonitis and progressive fibrosis after selective fractionated irradiation of the thorax reported a statistically insignificant increase by 6% in proton RBE from the mid to the end of the SOBP [71, 74][63, 66]. The average RBE values for mid-SOBP position for all fractionations and endpoints was 1.12 [74]. This study concluded that there is no need to further investigate the RBE value in consideration of the late tolerance of normal tissues because RBE for lung tolerance in mice did not significantly vary with fractionation and did not significantly differ from most early and late responding tissues studies [74]. Another study of radiation-induced myelopathy after rat spinal cord proton irradiation reported moderately increase of RBE values (reference MV photons) from 1.13 ± 0.04 for the entrance to 1.26 ± 0.05 at the distal end of SOBP for SD and from 1.06 ± 0.02 to 1.23 ± 0.03 for two equal fractions [69, 75].

Literature reviews and expert workshops display a need for more experimental data in order to address the RBE uncertainties. In addition, new preclinical tumor and normal tissue models in vivo as well as clinical studies might contribute to better understanding of biological effects and potential integration of RBE models into treatment planning algorithms. A substantial part of published studies is focused on acute reactions and are likely to underestimate the biological effects in late-responding tissues which are the major dose-limiting factors affecting the quality of life after RT [25, 70]. Therefore, more experimental studies should be conducted on a panel of relevant normal tissues models that include functional and tissue endpoints representing both acute and late radiation-induced reactions in animal systems to examine the dependence of RBE on dose/fraction, tissue types, and beam characteristics [70, 24]. Furthermore, the radiation schedule should simulate the clinical settings, including fractionation which should be adapted to beam availability [76]. It is recommended therefore to use shorter and hypofractionated schedules as a viable and clinically relevant option and include irradiation in the distal edge of SOBP [70, 76].

Chapter 3. Background

Materials and Methods

Chapter 4

Materials and Methods

All experiments in papers I-IV were conducted using laboratory animals (mice) as a preclinical model.

4.1 Animals

Nine-week-old C57BL/6J mice were purchased from Janvier company (France), kept in a 12-h light/12-h dark cycle under pathogen-free conditions and fed a standard commercial fodder with water given ad libitum. Standard housing with nesting material and refuge was provided. All experiments were approved by the Norwegian Food Safety Authority (ID 20889, 26246 and 27931) and Danish Animal Experiments Inspectorate (ID 2022-15-0201-01146) and performed in accordance with the animal welfare policy of Oslo University Hospital and Aarhus University. At the onset of experiments, animals were 12 weeks old.

4.2 Overview of animal experiments

In total, seven experiments were performed with the timelines presented in Figure 4.7.

Two pilot experiments (#1 and #2) were conducted with a small number of animals (n=3 and n=4, respectively) to establish all the procedures and endpoints and to determine the optimal X-ray voltages and doses. For experiment #1 both female and male mice were used, while for the other experiments only female mice were chosen because of aggressive behavior of males during the experiment. The following doses per fraction were used for the pilot experiments: 2.6 Gy, 3.9 Gy, 4.4 Gy, 5.1 Gy, 5.7 Gy with 2 fractions per day (8 AM and 4 PM) for 5 days. All reported doses are mean doses at the midpoint in the X-ray path through the mouse. The aim was to find the optimal dose for mice that induce the effects observed in patients such as oral mucositis.

The chosen doses did not induce signs of oral mucositis during the acute phase. Therefore, two larger experiments #3 and #4 (n=10) were conducted with higher doses: 7.5 Gy and 6.6 Gy with 2 fractions per day for 5 days, to observe the early

Chapter 4. Materials and Methods

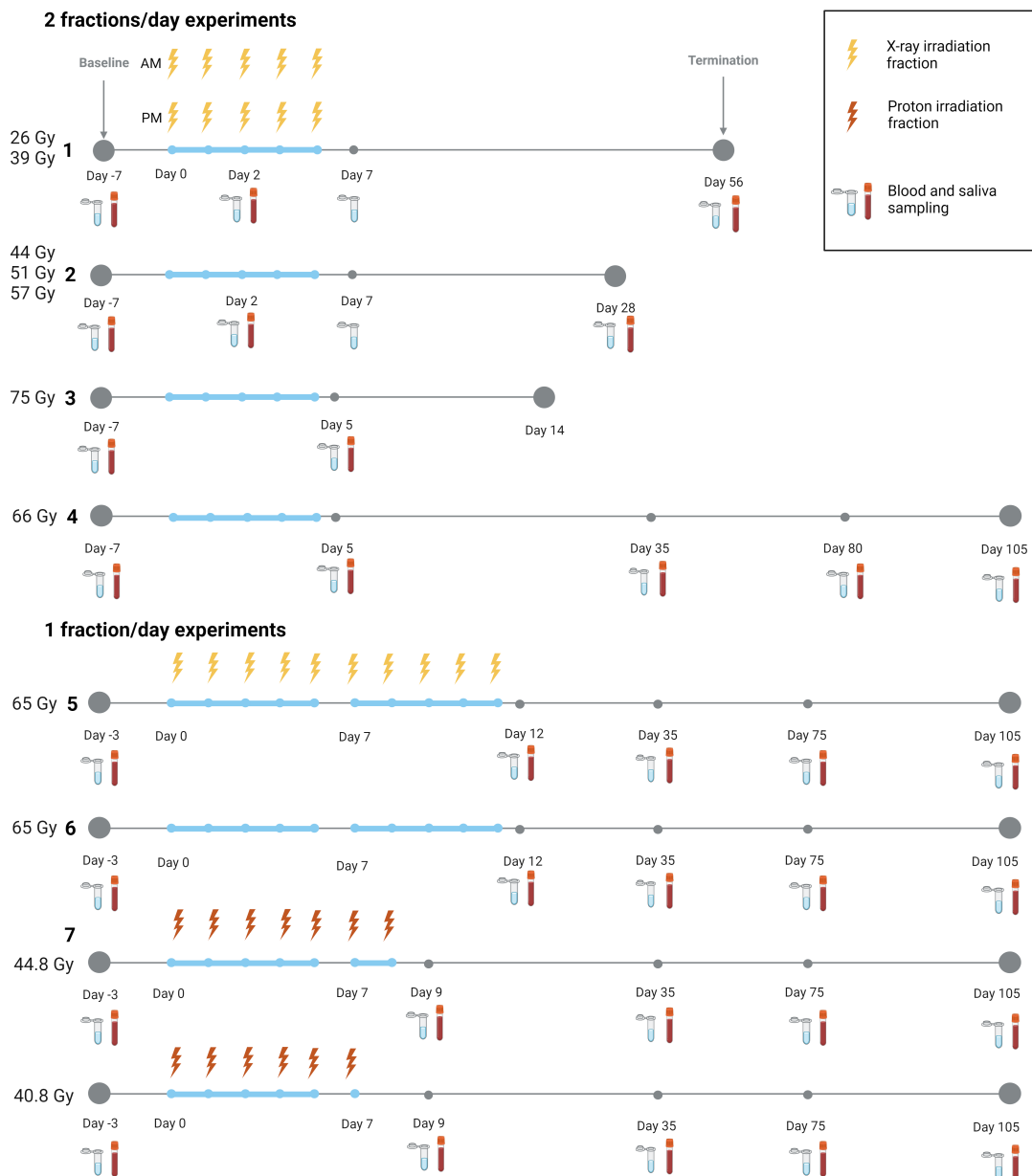


Figure 4.7: Overview and timelines of all animal experiments.

radiation-induced effects. The total dose of 75 Gy was not well tolerated by the mice and experiment #3 was terminated on day 14 due to unacceptable weight loss ($> 20\%$). Based on experiments # 1-3, the optimal dose was determined to be between 5.7 and 7.5 Gy per fraction (Gy/fr) and a dose of 6.6 Gy/fr in experiment #4 appeared to be optimal to reach the clinical endpoint (oral mucositis) and be well tolerated by the mice to survive the acute phase. Results from these experiments are presented in paper I and II.

As the main goal of the project was to compare the normal tissue effects after X-ray vs proton irradiation, we visited our collaborators at Danish Centre for Particle Therapy in Aarhus, Denmark, to discuss and plan proton experiments.

Based on our requirements of using the clinical gantry to get a vertical beam to mimic the X-ray experiments and the patient's treatment schedule, the decision of changing the fractionation scheme from 2 fractions per day to 1 fraction per day was made. Therefore, experiments #5 and #6 were conducted with the same dose 6.6 Gy/fr with 1 fraction per day (4 PM) for 10 days to test how the change in fractionation scheme influenced the induced effects. Surprisingly, the observed effects were larger and more consistent, and the mice could only tolerate these experiments when given saline injections to prevent dehydration. For experiment #7 (protons), approximately the same dose per fraction was chosen and two proton treatment plans were developed to encompass the LET effects – Bragg peak (BP) and Transmission mode (TM) (see the subsection below). However, the radiation treatment had to be terminated for the BP and TM groups after fraction #6 and #7, respectively, due to weight loss and early signs of oral mucositis. The early and late effects from these experiments are presented in papers III and IV.

The day of the first irradiation was denoted day 0. The maximum follow-up period in experiments # 4-7 was 105 days after onset of fractionated irradiation. Euthanasia in all experiments was performed through overdose of an anesthetic (Pentobarbitol, Exagon® Vet) by intraperitoneal injection to prevent tissue damage from cervical dislocation.

4.3 Design of irradiation set-up

The set-up for positioning of the animals during irradiation is presented in Figure 4.8a.

The animals were anesthetized using gas anesthesia with Sevoflurane 4 % in O_2 . The anesthetized mice were positioned laterally on the right (for X-rays and BP protons) or left (for TM protons) side in a custom-made foam holder. The different side for TM protons was chosen to achieve similar dose distributions as for X-rays. Lead (for X-rays) and brass (for protons) collimators were custom built to define a radiation field of 25×20 mm and placed on top of the foam holder to only irradiate the tissues of interest and avoid exposure to the eyes and brain. The radiation field covered the oral cavity, pharynx, and major salivary glands. A built-in X-ray imaging system was used to verify the anatomical location of the radiation field (see Fig. 4.8b). The irradiation was performed on two mice simultaneously.

4.4 Irradiation Procedure

4.4.1 X-ray experiments

X-ray irradiation was performed with Faxitron Multirad225 irradiation system (Faxitron Bioptics, Tucson, AZ, USA) at the Radium Hospital in Oslo, Norway. The following X-ray settings were used: (1) 180 kV X-ray potential, 10 mA current, 0.3 mm Cu filter, and 0.65 Gy/min dose rate, (2) 100 kV, 15 mA, 2.0 mm Al, and

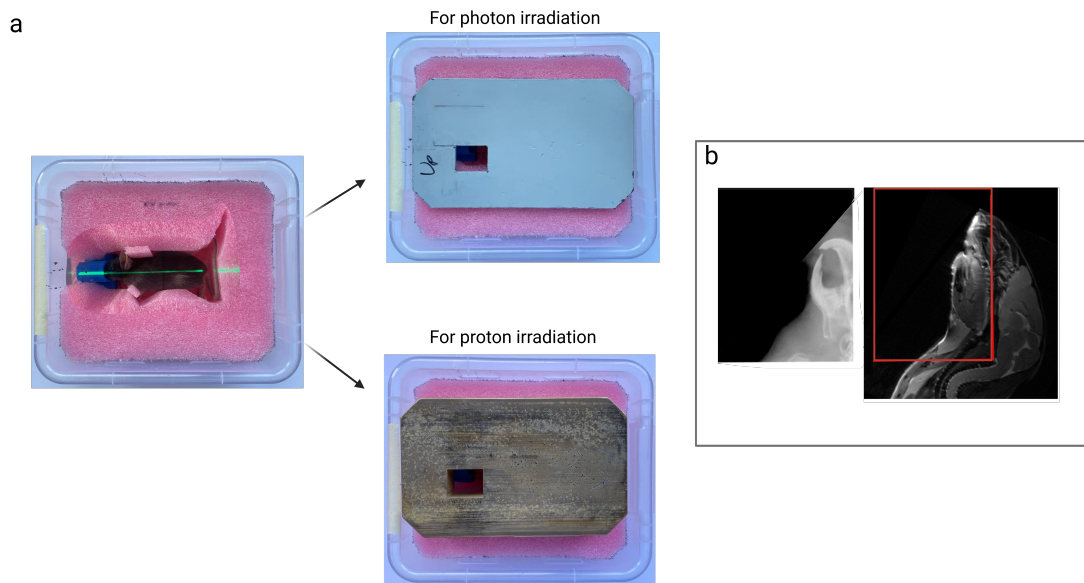


Figure 4.8: (a) The pictures of actual set-up for partial H&N irradiation. Plastic box with the foam base cut in the mouse shape with PMMA 3D-printed face mask for gas anesthesia and the mouse positioned for irradiation. Two different collimators of lead (for X-rays) or brass (for protons) were put on top of the foam to define the radiation field. (b) X-ray image of the radiation field and magnetic resonance image of the corresponding H&N region. The red rectangle shows the approximate radiation field.

0.75 Gy/min. (1) was used for the experiment #1, while (2) was used for the experiments # 2-6.

The schematic treatment plan and corresponding Monte Carlo (MC) simulation for X-ray experiments # 4-6 are presented in Figure 4.9 (left column). The X-ray group from the experiment #4 was irradiated with a total dose of 66 Gy given in 10 fractions over 5 days (paper I and II), while the X-ray groups from the experiment #5 and #6 were irradiated with a total dose of 65 Gy given in 10 fractions over 10 days (paper III).

4.4.2 Proton experiments

Proton irradiation was performed with Varian ProBeam clinical gantry with a pencil beam scanning dedicated nozzle (Varian, Medical Systems, Palo Alto, CA, USA) at the Danish center for particle therapy at Aarhus University Hospital in Aarhus, Denmark. Two different proton treatment groups were included. The schematic treatment plans and corresponding MC simulations for proton experiment #7 are presented in Figure 4.9 (middle and right column).

The TM group was irradiated with a total dose of 44.8 Gy given in 7 fractions over 7 days (5+2) with a single energy (70 MeV degraded by 1 cm solid water) pristine Bragg peak (paper III). In this ‘transmission mode’, the Bragg peak ended up outside the mouse. The BP group was irradiated with a total dose of 40.8 Gy

given in 6 fractions over 6 days (5+1) using a single energy (70 MeV degraded by 3 cm solid water) pristine Bragg peak (paper III). For this group, the distal edge of Bragg peak was around the middle of the mouse). The proton entrance energy / range was estimated by MC simulations to be 60 MeV / 31 mm and 24 MeV / 6.8 mm range for the TM and BP groups, respectively.

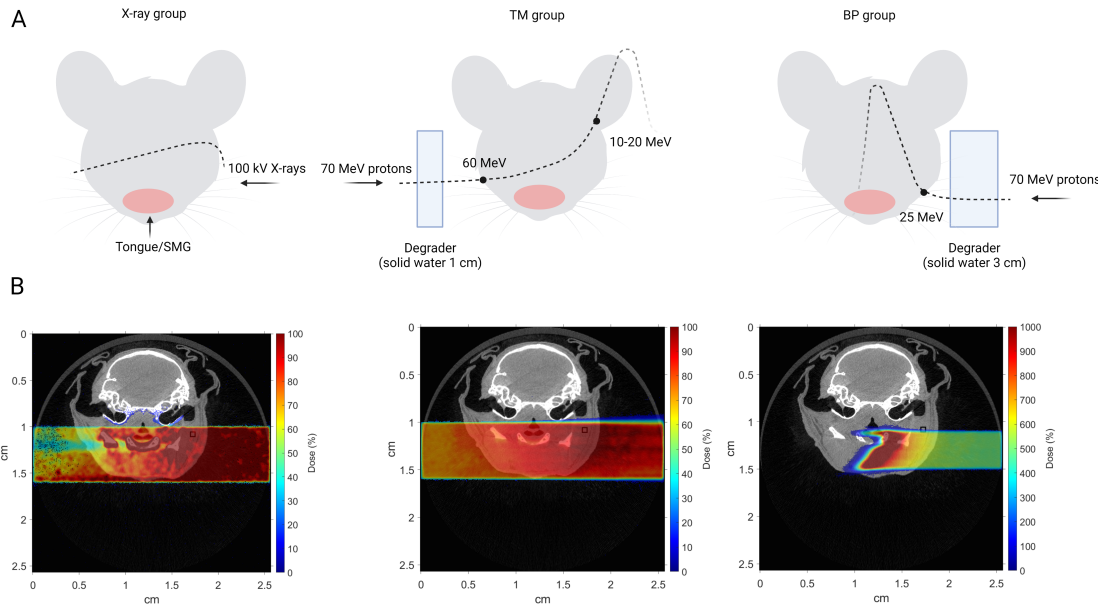


Figure 4.9: (a) Graphical treatment plan and (b) corresponding FLUKA MC simulations for the X-ray (left column) and proton (middle and right column) irradiation experiments.

4.5 Dosimetry

To verify the delivered doses several dosimetry approaches were used.

Absolute calibration of the X-ray system and unshielded beam was conducted using a FC65-G Farmer type ionization chamber (IBA Dosimetry, Germany) together with a MAX-4000 electrometer (Standard Imaging, USA) according to IAEA report TRS-277 [77]. Dosimetry for the collimated beam was performed using GafchromicTMEBT3 dosimeter films at a source-surface distance representing skin entrance of the mouse. EBT3 films (lot No. 02122001) were irradiated and processed according to the recommended protocols specified for radiochromic film dosimetry in the report of the AAPM Task Group 235 [78]. Alanine dosimetry was conducted to verify the dose distribution after X-ray and proton irradiation. Cylindrical pellets (batch BX608 and CD600; diameter 4.8 mm and height 2.7 mm) from Harwell Dosimetrers Ltd, UK consisting of 90.9% L-alpha-alanine, amino acid and 9.1% paraffin wax (binder) were used. Seven pellets were stacked on top of each other and placed in the Eppendorf tube. The tubes with pellets were

positioned inside the foam holder in the area of the mouse oral cavity/SG, covered by the collimators and irradiated with the same settings and dose per fractions as mice in all treatment groups X-ray, BP and TM. The pellets were read out by the RISO team from Danish Technical University, Denmark, using a specific read out procedure described in [79].

4.6 Blood and saliva sampling

Blood and saliva sampling were performed in all animals as baseline measurements 7 or 3 days before the first fraction (depending on the experiment). Additional blood and saliva samplings were performed on day 5, 9 or 12, and on day 35, 75 or 80 and 105 before termination (depending on the experiment). Blood sampling was collected from the tail vein into serum microvette tubes (Microvette, Sarstedt). Afterwards, the samples were centrifuged at 1000 g and 4 °C for 15 minutes, and the separated serum was stored at -80 °C. Saliva sampling collection was performed as previously described [80]. Mice were anesthetized with subcutaneous injection of Zoletil-mix (see below). Saliva production was stimulated using 0.375 mg/kg of pilocarpine (Pilocarpine hydrochloride, Sigma) that was intraperitoneally administered to the mice under anesthesia. The mice were positioned in the tube at 45 degrees with the cotton swab in the mouth and the saliva was collected for 15 minutes. The cotton swabs were then centrifuged at 7500 g and 4 °C for 2 minutes. The obtained volume was measured and stored at -80 °C for cytokine analysis. The saliva volume was used as a measurement of salivary gland function during the acute and late phases. In paper II, data from day 80 and 105 were pooled because of inter-animal variations due to the limited number of animals per group.

4.7 Evaluation of early effects

The development and progression of acute effects were observed during the first 2-3 weeks after the completion of fractionated irradiation. Assessment of overall activity, appearance and body weight (less than 20 % body weight loss was considered acceptable) was performed according to the score sheet for monitoring the welfare of the animals. Oral mucositis, skin and lip toxicity were graded using a modified scoring scheme based on the RTOG scoring criteria [81]. For this, macroscopic examinations of the oral cavity were performed every second day using magnifying glasses (3.5×) and a light source. Mice were anesthetized by subcutaneous injection of Zoletil-mix (Zoletil-mix: 10 ml Narcoxyl® or Rompun® (xylasin 20 mg/ml) + 0,5 ml Torbugesic® (butorphanol 10 mg/ml) + Zoletil® (zolazepam 125 mg and tiletamin 125 mg)). Analgesic treatment with Temgesic every 8 hours for 3-5 days in conjunction with saline treatment by subcutaneous injection to prevent dehydration was provided to all animals. In addition, easily digestible and nutrition rich gel fodder (DietGel Recovery, Clear H2O) was provided to avoid unnecessary mortality. The animals that reached humane

endpoints were euthanized.

4.8 Evaluation of late effects

Fibrosis and acinar atrophy of salivary glands as a radiation-induced late effects were assessed by histological examination of SMG section, and the percentage of fibrotic area was used in the prediction modelling as fibrosis score. The detailed methodology on decision tree regression analysis is presented in paper II. The SMGs were collected after euthanasia and fixated for 24 hours in 10 % formalin, dehydrated in ethanol and embedded in paraffin. Tissue sections of 4 μm were cut (Leica RM2155 microtome) and stained with hematoxylin and eosin (HE) and Masson Trichrome (Trichrome Stain kit, abcam) according to the protocol from the manufacturer. Images of the stained sections were acquired using a Nikon DS-Ri1 camera with a CFI Plan Fluor 10 \times objective (NA 0.30). The percentage of fibrotic area relative to the total area was extracted by thresholding in ImageJ based on 8-11 images of the SMG from each mouse.

4.9 Cytokine analysis

Both saliva and serum samples were thawed on ice, vortexed and spun down at 16 000 g for 5 minutes at 4 °C. The samples were diluted (saliva; 2:1 and serum; 1:1) with the RD1-W buffer (R&D Systems, Abington, UK). All samples from X-ray experiment with 2 fractions/day (fr/d) were analyzed with a custom made 12 plex kit (www.biotechne.com/g8AnddcM) including MIP-1 α , KC, IP-10, G-CSF, IFN- γ , IL-1 α , IL-1 β , IL-6, IL-12 p70, MMP-9, TIMP-1 and TNF (Bio-Techne Ltd, Abington, UK). All samples from X-ray (1 fr/d) and proton experiments were analyzed with a custom made 11 plex kit (www.biotechne.com/g8AnddcM) including MIP-1 α , KC, G-CSF, IFN- γ , IL-1 α , IL-1 β , IL-6, IL-12 p70, MMP-9, TIMP-1 and TNF (Bio-Techne Ltd, Abington, UK). A Luminex IS 200 instrument (Bio-Rad, Hercules, CA, USA) was used to record data. Total protein concentrations in saliva samples were estimated in mg/ml using NanoDrop 2000c (Thermo Scientific, Rockford, IL, USA). The salivary cytokine levels were adjusted to total protein concentration and presented as (pg of cytokine)/(mg of total protein). No significant differences were found in cytokine levels in control groups from X-ray and proton experiments and from X-ray experiments with different fractionation schemes. Therefore, cytokines in control groups were merged for the analysis.

Chapter 4. Materials and Methods

Summary of papers

Chapter 5

Summary of papers

Paper I. A preclinical model to investigate normal tissue damage following fractionated radiotherapy to the head and neck (published)

The primary objective of this investigation was to establish a preclinical model to study different early and late radiation-induced effects in the H&N region after fractionated irradiation. We used a clinically relevant radiation field covering the oral cavity, pharynx and major salivary glands and several different dose deliveries to achieve endpoints observed in RT-treated patients, such as oral mucositis and hyposalivation.

Ulcerations on the ventral surface of the tongue were observed for doses ranging from 66 to 75 Gy. However, the 75 Gy dose was not tolerable for mice and that group of mice was euthanized because of extensive weight loss. Therefore, we tested doses per fraction ranging from 2.2–7.5 Gy (with a total dose of 22–75 Gy in 10 fractions over 5 days) and determined that for the current fractionation scheme and irradiation setup, the optimal dose to obtain clinically relevant normal tissue responses was 6.6 Gy/fr.

Mice exposed to 6.6 Gy/fr experienced severe radiation dermatitis, featuring confluent moist desquamation affecting not only the lower lip but also the skin of the upper chest. We observed a clear relationship between radiation dosage and the occurrence of radiation dermatitis in the skin. Additionally, a significantly reduced saliva production was observed in the irradiated groups compared to the control.

Histological examinations of the tissues showed increased keratin thickness of the epidermis, keratin desquamation, and atrophy of sebaceous glands and hair follicles in the lip. Histological findings of mucosal ulcerations corresponded to the macroscopic observation of oral mucositis on the ventral surface of the tongue in mice exposed to 6.6 and 7.5 Gy/fr. In conclusion, we have developed a preclinical model to study radiation-induced effects in various tissues, including the skin, oral mucosa, and salivary glands in the H&N region. In this study we presented early radiation-induced effects after a range of the doses. In irradiated mice,

dose-dependent radiation dermatitis and oral mucositis were observed, along with reduced saliva production compared to the control group. The optimal total dose for inducing similar effects as seen in H&N cancer patients was determined to be around 66 Gy. This preclinical model provides a valuable tool for investigating normal tissue responses after irradiation including late effects.

Paper II. Cytokine levels in saliva are associated with salivary gland fibrosis and hyposalivation in mice after fractionated radiotherapy of the head and neck (published)

In this study our established model with radiation field from the paper I was used. The dose was 66 Gy given in 2 fractions per day over 5 days, the number of mice per group was 10. Blood and saliva samples were screened for cytokines. The aim of this study was to monitor the levels of cytokines in both saliva and serum after fractionated radiotherapy in mice and to investigate any potential associations between the cytokine levels and salivary gland fibrosis and hyposalivation.

A significant increase of fibrotic area in the submandibular gland tissue and a decrease in saliva production were found in the irradiated mice compared to controls and were considered as late endpoints. A significant increase in pro-inflammatory cytokine levels of IL-1 α , TNF, and TIMP-1 on days 35, 80, and 105 post-irradiation compared to controls was found. Additionally, the levels of G-CSF and KC were significantly higher on days 35 and 80 in the irradiated group. In serum, only MIP-1 α exhibited a significant decrease on days 35, 80, and 105 in the irradiated mice compared to controls, while no significant changes were observed in the other cytokines.

We tested the correlation of salivary cytokines with the late endpoints and found the strongest correlation on day 35. Additionally, we found a much stronger correlation between salivary cytokines and endpoints compared to serum cytokines and endpoints, which supports our hypothesis that saliva cytokines are more specific and more sensitive to the local damage of salivary glands than serum cytokines. Decision tree regression analysis with the feature matrix of cytokine levels as dependent variable and the concatenated endpoint vector as independent variable showed a significant contribution of IL-1 α in predicting late endpoints.

In conclusion, this is the first study of the alterations in cytokine levels in mouse saliva following irradiation of H&N region. We found a differential secretion of cytokines in the saliva of irradiated mice but not in serum compared to the control group. There was a strong correlation between salivary cytokine levels and the late endpoints, whereas cytokines in serum only showed weak correlations with the endpoints. These findings supported the theory that these cytokines, known for their involvement in inflammatory responses and fibrosis formation, play a crucial role in the development of late effects induced by radiation. In addition, we concluded that saliva compared to serum might be the better candidate for

biomarkers of radiation-induced damage of salivary glands.

Paper III. Acute normal tissue responses in a murine model following fractionated irradiation of the head and neck with protons or X-rays (published)

For this study, we conducted additional X-rays experiments with 65 Gy total dose but delivered in 1 fraction per over 10 days using our established model with radiation field from the paper I. The aim of this preclinical study was to investigate the acute responses of normal tissues following proton and X-ray irradiation in the H&N region to gain a deeper understanding of the differences in the biological effects between these two types of radiation.

To study the effects of LET, we included two proton groups. The BP group received irradiation with a pristine BP that covered half of the H&N region in mice, with the distal edge of the BP focusing on the area of interest, namely the salivary glands. This setup aimed to emulate the irradiation of normal tissues located behind a tumor, simulating a clinical scenario. In contrast, the TM group received irradiation with a more uniform dose distribution where the BP was positioned outside of the mouse. This approach was designed to create a proton plan with a dose distribution similar to that of X-rays, facilitating direct comparison of their biological effectiveness.

To assess the dose distribution, we performed alanine dosimetry for both proton and X-ray irradiation. The results revealed that the depth dose profiles within the irradiation field were nearly identical for TM proton group and X-rays with approximately the same dose per fraction. For the BP proton group, a steep dose gradient was observed as expected. The total doses received by X-ray, BP and TM groups were 65, 40.8 and 44.8 Gy, respectively.

Surprisingly, despite the very similar dose distributions and the lower proton doses, the proton TM group exhibited significantly higher biological effects compared to the X-ray group, and similar to the BP group. After proton irradiation, oral mucositis appeared earlier, had a higher severity score, and affected a greater percentage of the mice compared to X-ray irradiation. Tongue mucositis was observed in all mice subjected to proton irradiation, while it was only present in 80% of mice exposed to X-rays. However, the mean severity score for lip dermatitis was quite similar between the X-ray and proton groups. The reduction in saliva production was observed the day after termination of radiotherapy for both proton and X-ray irradiation compared to the control. The TM and X-ray groups demonstrated significantly decreased saliva volume compared to controls on day 35, while the BP group showed better recovery of saliva production.

In conclusion, our findings indicated an increased acute tissue response in the oral mucosa following proton irradiation compared to X-ray irradiation while the skin reactions were similar, even though the doses were about 30% lower for protons. In terms of RBE, the estimated values for oral mucositis and dermatitis

were very high, but large confidence intervals prevented us to draw any firm conclusions.

Paper IV. Proton compared to X-irradiation leads to more acinar atrophy and greater hyposalivation accompanied by a differential cytokine response (submitted)

This paper is a continuation of paper III where early tissue effects after proton vs X-ray irradiation were described. The aim of this study was to investigate late salivary gland effects and possibly correlate them to molecular responses by monitoring the cytokines levels in serum and saliva at different time points before and after fractionated irradiation.

To our knowledge this study is the first H&N mouse study that directly compares radiation-induced normal tissue effects following proton and X-ray irradiation using the same irradiation setup. The total doses received by X-ray, BP and TM groups were 65, 40.8 and 44.8 Gy, respectively. The dose distributions from the proton and X-ray treatment plans verified by alanine dosimetry (the results were presented in paper III), show that the TM and X-ray plans had very similar dose distribution in the tissues while the mice irradiated with the BP plan only received a dose in one side of the head with the Bragg peak positioned in the midplane of the animal. The results indicated significantly fewer acinar cells and a tendency towards larger gland size reduction and more fibrosis in the SMG irradiated by either proton plan compared to X-rays. In addition, more pronounced decrease of saliva volume after protons compared to X-irradiation was observed, with the highest reduction in saliva production in the TM group.

Cytokine analysis showed different responses after proton versus X-ray irradiation. The levels of pro-inflammatory cytokines IL-1 α and TNF in saliva were significantly increased after exposure to X-rays compared to protons and controls. The cytokine response after X-ray was displayed as waves immediately after the termination of radiation treatment and at day 70, while the cytokine response was lower and more similar for the different time points in the two proton groups compared to the X-ray group. In contrast, protons induced more severe oral mucositis compared to X-rays as was discussed in paper III. Thus, early and late cytokine responses did not reflect the more severe tissue effects induced by protons. This might indicate that the contribution of pro-inflammatory cytokines to the mechanisms responsible for the early and late responses after proton versus X-ray irradiation is different with other factors involved in the proton response.

In conclusion, proton irradiation caused more severe late tissue responses compared to X-rays, even with similar dose distribution and lower doses. Moreover, a difference in cytokine regulation following proton and X-ray irradiation was observed, where protons induced a relatively 'cold' cytokine response compared to X-ray irradiation.

Comparing X-ray fractionation schedules

Chapter 6

Comparing X-ray fractionation schedules

Due to practical limitations of the proton irradiations, the original plan to give 2 fr/d for 5 days had to be changed to 1 fr/d for 10 weekdays. Therefore, a new reference experiment with X-rays had to be conducted. In this section, the effects in SMG and cytokine response in the two X-ray experiments with similar total doses of 66 Gy (2 fr/d) and 65 Gy (1 fr/d) in 10 fractions are compared in addition to the main goal of the project. The saliva data and cytokine levels in serum and saliva from mice irradiated with 2 fr/d (66 Gy total dose) of X-rays at different time points after irradiation were reported and discussed in paper II. The similar data from the X-ray experiment with 1 fr/d (65 Gy total dose) were reported and discussed in paper IV.

6.1 Saliva volume

A significant reduction in saliva volume was observed on day 12 (the day after the last irradiation) in the mice X-irradiated with 1 fr/d compared to controls, while the mice irradiated with 2 fr/d did not show any difference from controls at this early time point. However, for both groups irradiated with 1 or 2 fr/d, the saliva volume was significantly reduced on day 35, 70/80 and 105 (Fig. 6.10). Interestingly, better recovery of saliva volume was seen by day 105 for the mice irradiated with 1 fr/d than with 2 fr/d.

6.2 Fibrotic area in SMG

All X-irradiated mice (1 or 2 fr/d) showed an increased percentage of fibrotic area in the SMG at day 105 compared to controls. However, the mice irradiated with 2 fr/d demonstrated significantly larger fibrotic area compared to the mice irradiated with 1 fr/d (Fig. 6.11).

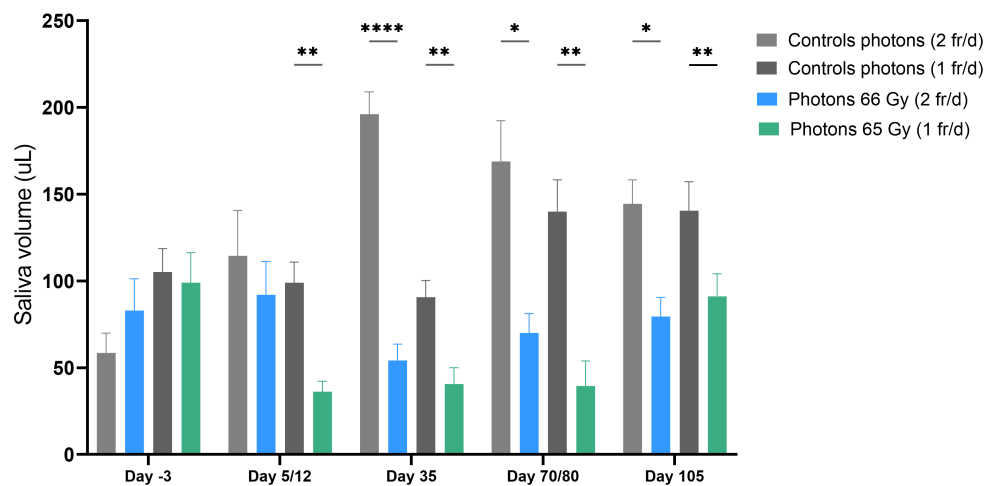


Figure 6.10: Saliva volume after X-ray irradiation with different fractionation schemes (controls n = 9, X-rays 1 fr/d n = 9, X-rays 2 fr/d n = 10). Data is represented as mean \pm SEM (*p<0.05, **p<0.01, ***p<0.001).

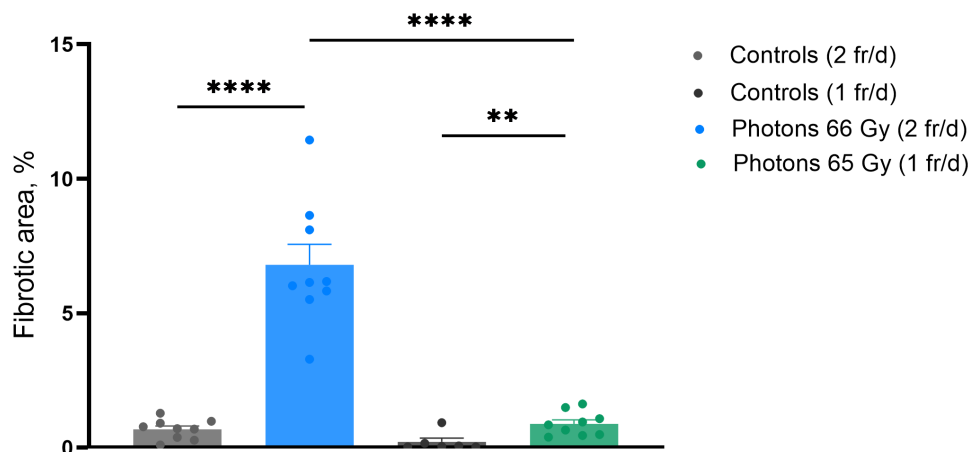


Figure 6.11: Fibrotic area in SMG at day 105 in controls and irradiated groups after different fractionated irradiation (controls n = 9, X-rays 1 fr/d n = 9, X-rays 2 fr/d n = 10). Data is presented as mean \pm SEM (**p<0.01, ****p<0.0001).

6.3 Cytokine profiles

The levels of the detected serum and salivary cytokines at different time points before and after X-ray irradiation with either 1 fr/d or 2 fr/d are presented in Fig. 6.12. In the serum samples, the MIP-1 α level was significantly lower for 1 fr/d compared to 2 fr/d and controls on day 5/12 and the TIMP-1 level was significantly lower for 1 fr/d compared to controls on day 105, while the rest of the cytokines did not show any significant differences at any time points. In saliva

6.3. Cytokine profiles

samples, the levels of TNF, TIMP-1 and MIP-1 α were significantly higher for 1 fr/d compared to 2 fr/d on day 5/12 after the onset of irradiation. However, the tendency changed by day 105 with an increase in all saliva cytokine levels for the mice irradiated with 2 fr/d compared to 1 fr/d and controls. TNF showed the same trend, but the difference was not significant. Furthermore, a discernible wave-like pattern in cytokine response was observed for 1 fr/d, with alternating low and high levels at each consecutive timepoint, while no such pattern was observed in the cytokine response for 2 fr/d.

Chapter 6. Comparing X-ray fractionation schedules

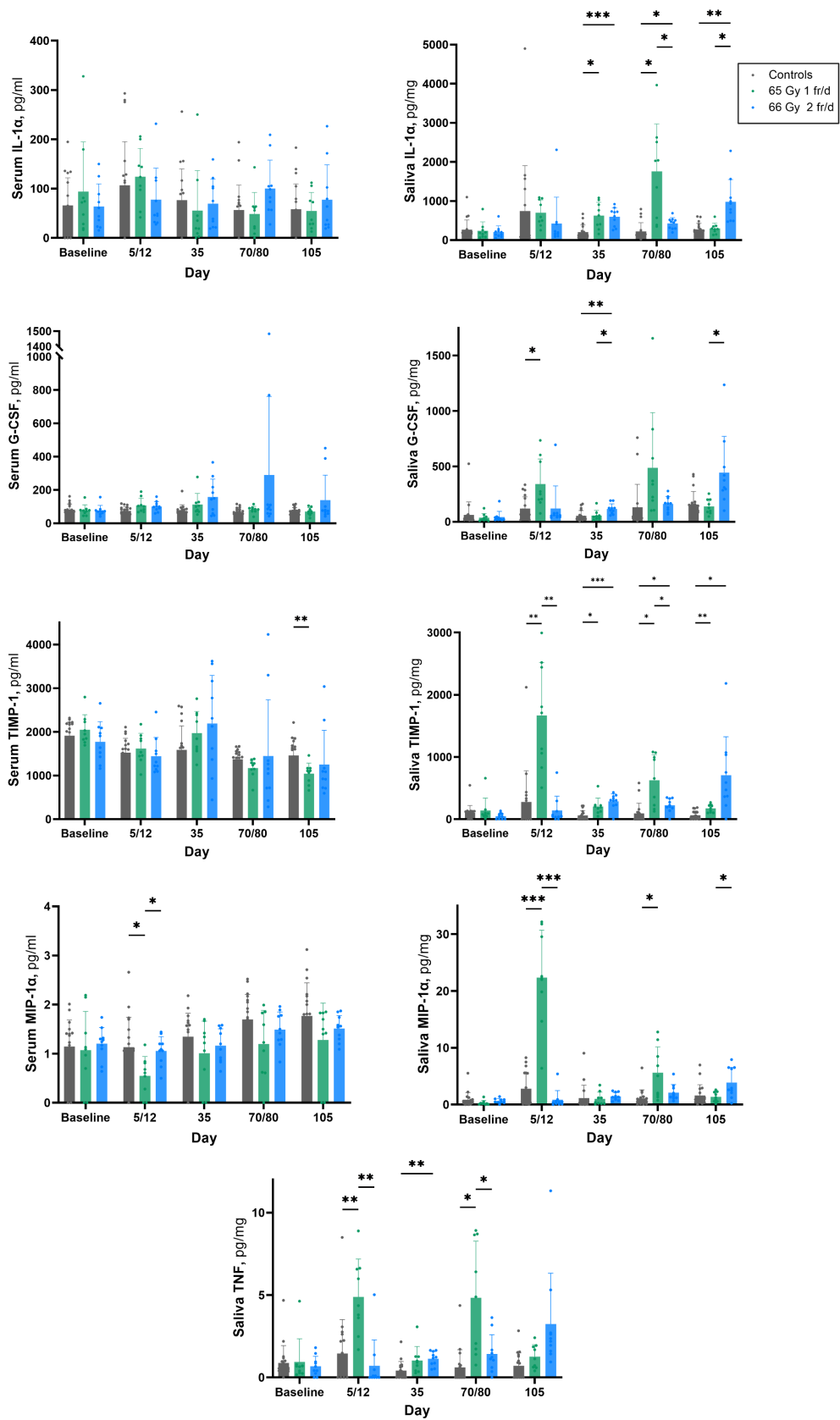


Figure 6.12: Levels of serum and salivary cytokines before and after fractionated irradiation. Data are presented as mean \pm SD pg/ml cytokine per total protein mg/ml for saliva and as pg/ml cytokine for serum (* p <0.05, ** p <0.01, *** p <0.001).

Discussion

Chapter 7

Discussion

7.1 Methodological considerations

Mouse model

Although in vitro experiments are very useful in radiation research, in vivo animal models are essential to understand the systemic response and mechanisms of radiation-induced normal tissue side effects as well as to obtain longitudinal data of the progression of the effects. In addition, all potential drug agents must be extensively tested using animal models to prove efficacy and safety before becoming a candidate for early clinical trials [82]. It has also been shown that animal models help to validate the RBE models in terms of tolerance doses and fractionation effects when it comes to different types of radiation [71]. A wide range of animal model species has been studied for use as preclinical models of normal tissue side effects of H&N SCC including rodents, domestic animals, and zebrafish [83]. However, rodents including mice, rats and hamsters are the most used animals in H&N tumor or normal tissue experiments. Our main goal was to study several H&N radiation-induced effects including oral mucositis and salivary gland dysfunction. For oral mucositis induction in animal models, the protocols described in the literature differ in the animal species chosen for the experiments, site of exposure, source, and total radiation dose and fractionation scheme. These factors directly interfere with the intensity and speed of the oral mucositis development and hinder the standardization of clinical analysis [84]. The hamster model has greatly contributed to the understanding of the mechanisms of oral mucositis and allowed formulating the current working five-phase hypothesis of mucositis that was presented in the section *Background*. However, to induce oral mucositis in hamster model, the cheek pouch needs to be “mechanically” scratched or irritated, which differs from the clinical setting in humans [82]. Rats were also demonstrated to be a difficult model for induction of oral mucositis because of the highly keratinized epithelium nature [82]. Advantages of using mice are small animal size, standardized and easy handling and care procedures, extensive physiological and molecular similarities to humans, and extended use in research. A mouse model was therefore chosen for our experiments.

As discussed in paper I, the mouse strain-specific variations may affect the normal tissue response to radiation in terms of the development of oral mucositis and SG damage [85, 86]. It is also important to be able to use the potential of modified models including immunodeficient mice or genetically engineered mice in future experiments. The C57BL/6J mouse strain is widely used in radiation research and is regarded as a “standard” inbred line. In addition, it is the first mouse strain to have its complete genome sequenced and is therefore widely used as a transgenic mouse model [87]. In addition, C57BL/6 mice have been used as syngeneic models for oral SCC or HPV-related mouse oral cancer [87]. Another advantage of this mouse strain is that C57BL/6J is relatively radioresistant compared to other strains, which allowed us to induce both early and late radiation-induced effects in the same model. The challenge though was the number of experiments that was performed to find the optimal dose to induce similar effects as cancer patients develop after RT, for example oral mucositis. However, the project was designed to maximize data extraction per mouse including minimally invasive sampling of blood and saliva, visual oral examinations, imaging, cytokine screening and, histological assessments, which increases the efficiency and reduce the total number of animals needed.

Irradiation procedure

Radiation delivery to the H&N area of mice requires careful planning. It is challenging to reproduce or compare results to other published studies because of the variety of radiation fields, doses and dose delivery settings. There is no standard on performance of irradiation and/or dosimetry in H&N mice models or in radiobiology models in general.

To study oral mucositis on lip, tongue or mucosa, different research groups have irradiated tongue, mouth, snout or the whole head of mice with various single doses or fractionations while shielding the rest of the body (see overview of doses in the General discussion below) [82, 88, 89, 90]. The well-known group of Wolfgang Dörr who studied oral mucositis in tongue mucosa used a combination of irradiation techniques including irradiation of either the entire snout or only the tongue followed by local “top-up” irradiation of the lower tongue to precipitate the subclinical mucosal damage into a clinically symptomatic effect [82]. The advantage of external snout irradiation is that no repeated manipulations of the tongue is required that could cause mechanical irritation or trauma and influence the tissue response [91].

To study salivary gland dysfunction, most of the published studies used irradiation of the whole H&N region with a SD or fractionations while shielding the rest of the body [92, 93, 94, 95]. Some groups collimated the local irradiation field with up to 1 cm slits or with apertures to target only the SG areas [86, 96]. One group reported that the precise field extended from the foreleg to 20 mm below the lower lip confirmed by CT scanning, such that the position of all SG was within the 95% isodose [97]. It was pointed out that to explore the mechanisms of radiation-induced SG damage, the reduction of saliva volume must be fully attributed to the direct SG irradiation and not to effects caused by non-glandular

tissue within the radiation field [98]. However, in studies where the whole H&N region is exposed to radiation, the animals demonstrated clear signs of indirect effects [98]. Such inconsistencies in the delivery of radiation doses contribute to variations in the induced effects, and poor description of the dosimetry adds even more uncertainties.

In our study, mice were positioned on the side, and a local field of $15 \times 25 \text{ mm}^2$ was used, which only exposed the oral cavity and area of SG confirmed by the in-built X-ray imaging system. The advantage of our set-up was the high reproducibility which led to consistent biological effects in mice. However, we cannot claim that our observed effects were not influenced by indirect effects as the excretory ducts and oral cavity were irradiated as well, but the contribution of indirect effects is diminished compared to studies with the whole H&N irradiation.

Most of the published studies aimed to test various radioprotective agents and therefore chose SD irradiations instead of fractionation, which is more time and human resources demanding. However, the standard clinical X-ray or proton treatment of HNC is fractionation treatment, and the mechanisms behind the normal tissue responses should be studied following similar clinical regimes. Although it is challenging to mimic these regimes in animal experiments, we managed to induce the clinically relevant effects using fractionated irradiation with 10 fractions given as 1 or 2 fr/d. Another quality of our experiments is the extensive dosimetry that was conducted to confirm the delivered doses using both an ionization chamber, Gafchromic EBT3 dosimeter films, and alanine pellets. Initially the dosimetry for X-ray experiments was conducted only for open field without the lead collimator because of the risk of partial volume effect in the ionization chamber leading to false results. However, the dosimetry with alanine pellets showed decreased doses in the collimated case and the dosimetry was revised using EBT3 films. The results showed that the actual dose with the use of the lead collimator was 12% lower, and the impact of the collimator was underestimated. Therefore, the doses in paper I were corrected through a correction note that was published by the journal [99].

Anesthesia and analgesia

Immobilization and fixation of mice in jigs during irradiation are often used. Anesthesia might change blood flow and temperature of animals, which might affect the radiosensitivity, so an advantage of using physical restraint is to reduce uncontrollable irradiation conditions. Gas anesthesia is less stressful for animals because it is non-invasive, and the time that the animal needs to wake up and function normally is some minutes compared to injection anesthesia where the recovery may take hours. In our study, we were aiming to minimize the stress for the animals by using gas anesthesia during irradiation. In addition, the fixation and positioning of unanesthetized mice in our setup would be challenging and might increase the risk of irradiation of unnecessary parts with high doses in case of the accidental escape of the animal. A weakness in our study is the requisite use of analgesia during the acute side effect phase. Pronounced effects such as oral mucositis caused extensive weight loss, and the mice required pain

alleviation in combination with saline injections to avoid dehydration. Analgesia treatment is a minor invasive procedure for mice, although it is stressful and includes frequent handling. Consequently, the sampling days were scheduled either before the initiation of the pain treatment or more than 2 weeks post-treatment, minimizing potential impact on the cytokine analyses. In addition, control groups in all experiments were treated in the same way as irradiated groups and received the same analgesia treatment.

Cytokine analysis and sampling protocol design

In addition to strain-specific individual variations, factors that may contribute to differences in reported cytokine levels include varying experimental design for sampling. In our experiments, blood and saliva samples were taken from the same mice at all time points. This allowed monitoring the cytokine expression from all mice individually as well as to have a reliable baseline which many studies do not have because of the use of terminal sampling techniques. Moreover, this experimental design included sampling the control mice at the same time points as the mice from the irradiated groups, which can show whether cytokine expression was affected by the radiation treatment, age, or stress from procedures as controls undergo the same “sham” procedures including the positioning in the foam restraint equipment for irradiation, gas anaesthesia, injections, and handling. The sampling of saliva was done at the same time of the day for all time points which ensures similar conditions for cytokines presented in saliva as there is a risk for cytokines being washed out after food intake. One limitation of our cytokine analysis is the use of cytokine kits that were originally designed for blood samples. This limitation might explain the low detected expression levels as well as the low number of detected cytokines in saliva.

Clinical endpoints

The visual changes of the tongue and lip mucosa were inspected and scored during daily examinations and used as endpoints for oral mucositis which is the common way to score in many studies. To assess the SG changes after RT, the saliva volume and fibrotic area in the glands were used as endpoints. Saliva volume has been widely used as an indicator of xerostomia in clinical studies with cancer patients [40]. For accurate measurement of saliva volume, it is recommended to refrain laboratory animals from eating and drinking for several hours before the sampling [40]. In our experiment, the saliva samples were not only used for measuring the saliva volume but also for cytokine analysis. Therefore, we decided not to follow the recommendation regarding food and water because it would require additional handling and stress to the animals, which might affect the cytokine levels in the collected samples. Instead, the sampling of saliva was performed at the same time of the day at all time points as mentioned above.

Logistical issues

Our original plan was to compare X-ray versus proton-induced effects in the H&N region using 2 fr/d. Several reference X-ray experiments were conducted in Norway to find the optimal radiation dose to induce relevant early and late effects. However, the proton experiments at our collaborator's facility in Denmark were postponed because of COVID-19 pandemic which affected the treatment schedule of the patients there. Because of the design of our setup with a vertical beam, our proton experiments could only be conducted in the clinical room with gantry. With the new treatment schedule and the estimated time needed for irradiations, the only feasible fractionation regime at the proton facility was 1 fr/d after the patients. Therefore, we needed to change the fractionation regime and conducted several additional X-ray experiments using 1 fr/d in Norway before the proton experiments.

In conclusion, none of the experimental limitations were critical for the validity of the study, but all the mentioned limitations were taken into account in the analyses of the results.

7.2 General discussion

To achieve the main goal of the project and to study the differences in normal tissue effects in H&N after X-ray versus proton irradiation, we established a mouse model where a certain radiation dose gives reproducible reactions in oral mucosa and salivary glands corresponding to the clinical effects reported in patients. In the first X-ray experiments, we developed the experimental setup including the custom designed restraining equipment, the timeline for examination, sampling, termination and the methodology for all the other procedures. The original fractionation scheme represented irradiation with 2 fr/d with doses of 2.6 Gy, thus comparable to clinically applied doses. However, the applied doses did not induce oral mucositis and the experiments were repeated with a range of doses from 2.6 to 7.5 Gy/fraction until the optimal dose (6.6 Gy/fraction) for inducing oral mucositis, while still being tolerable for the mice, was determined. As was discussed in the previous section, the fractionation scheme had to be changed from 2 fr/d to 1 fr/d, and additional experiments were conducted to verify the optimal dose in the new fractionation scheme. Based on the results, the dose 6.6 Gy/fr was confirmed and employed for proton experiment that included two dose delivery plans with different dose distributions: Transmission mode and Bragg peak mode (see Figure 7.13 adapted from paper III and IV).

Collecting all the experimental results, our project serves as a first H&N mouse study that directly compared the radiation-induced normal tissue side effects following X-ray irradiation delivered as “accelerated” (2 fr/d) or “conventional” (1 fr/d) treatment as well as proton irradiation delivered in 1 fr/d but with the Bragg peak positions either in the middle of the H&N (BP) or on the other side of the animal (TM) using the same irradiation setup. The data extracted from the experiments allowed for studies of several early and late radiation-

Chapter 7. Discussion

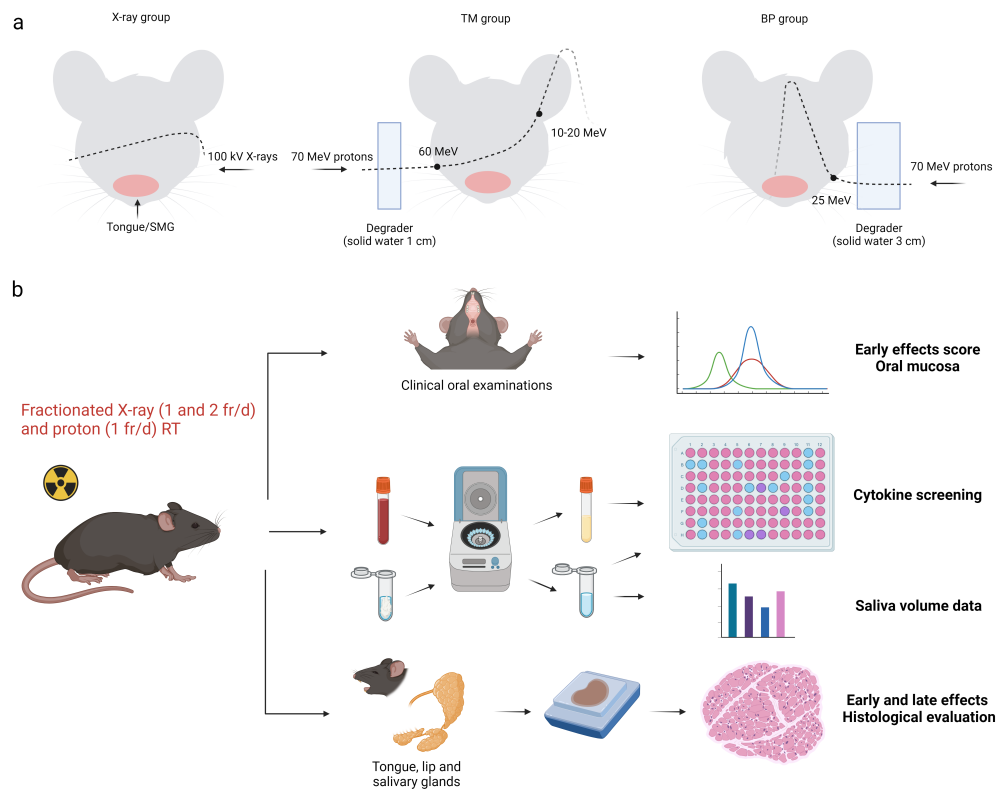


Figure 7.13: Graphical treatment plan (a) and graphical overview (b) of the X-ray and proton experiments. Created with BioRender.com.

induced effects and cytokine responses (Fig. 7.13). The first two papers present the methodology, the established setup, and the results including early and late effects and cytokine responses after “accelerated” X-ray irradiation. The last two papers focus on the comparison of early and late effects and cytokine responses after “conventional” fractionated X-ray and proton irradiation. In the section *Comparing X-ray fractionation schedules*, the effects and cytokine responses after X-ray irradiation with different fractionation schemes are compared. Early and late radiation-induced H&N effects have been studied by many groups through preclinical experiments using various animal models, doses, fractionation schemes and techniques. In order to compare our results with the literature, the most relevant studies of radiation-induced effects in oral mucosa and salivary glands were reviewed. The total radiation doses used in these studies, and our experiments were recalculated as BED and SFED using the equations 3.2 and 3.3 presented in the section *Background* using an α/β ratio for oral mucosa the same as for early responding tissues ($\alpha/\beta = 10$) and for salivary glands the same as for late responding tissues ($\alpha/\beta = 3$). The results are presented in Tables 7.1 and 7.2. The graphical summaries of doses used in other studies and our range of doses are presented in Figures 7.14 and 7.15.

Most of the analyzed studies focused on only one of the endpoints (oral mucositis or salivary gland dysfunction) while our study encompasses both critical endpoints (Fig. 7.13).

Table 7.1: Oral mucosa

Study	Fractionated (# of fr × dose)	Single dose (Gy)	BED (Gy)	SFED (Gy)
Mouse [91, 100]*	5×3, 10×3, 15×3	12-22	19.5, 39, 58.5	9.8, 15.4, 19.7
Mouse [88]	-	13-20	29.9-60	13-20
Mouse [89]	-	10-25	20-87.5	10-25
Mouse [101]	3×8	-	43.2	16.2
Mouse [102]	3×10	-	60	20
Hamster [103]	-	35, 40	157.5, 200	35, 40
Hamster [104]**	-	10, 20, 30, 35	20-157.5	10-35
Hamster [105]	-	20, 40, 60	60, 200, 420	20-60
Rat [84]	-	30	120	30
Rat [106]	-	13.5-18	31.7-50.4	13.5-18
Mouse - our	10×2.6-7.5 10×6.5 (X-rays) 6×6.4 (BP) 7×6.8 (TM)	-	32.8-131.3 107.3 64.4 75.1	13.8-31.6 28.1 20.9 22.9

The differences in energy of X-rays and the fractionated schemes (# fr/d) were not considered.

*Irradiation is followed by local top-up SD irradiation 2.5/5 Gy or with graded doses.

**Mucositis was induced using irradiation and scarification.

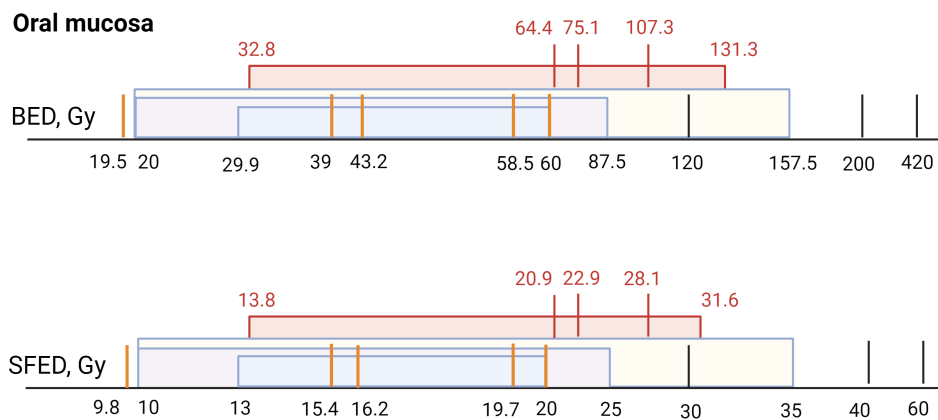


Figure 7.14: A graphical summary of doses used for studying radiation-induced effects in oral mucosa found from a literature search (SD in black, fractionated in orange) and our doses (in red). Created with BioRender.com.

As seen from Figures 7.14 and 7.15, our dose range overlaps with most of the applied doses in other studies. For oral mucositis, groups have employed fractionated irradiation and included more doses per experiment to study the dose-response relationship, while for SG most of the groups chose single dose irradiation with few studies using several doses. A probable reason is the location of the irradiated tissue/organ as oral mucosa can be isolated and is easily accessible in rodents, while irradiation of salivary glands is more challenging and prone

to include other tissues in the irradiation field which can cause indirect effects and additional complications. In addition, the oral mucositis as an early effect is usually scored visually within the acute phase while salivary gland dysfunction as a late effect requires more complex methods for assessment. In addition, no studies including proton irradiation of normal tissues in the H&N area of mice were found. The radiation-induced effects observed in our study compared to the reviewed studies from other groups are discussed below.

Table 7.2: Salivary glands

Study	Fractionated (# of fr × dose)	Single dose (Gy)	BED (Gy)	SFED (Gy)
Mouse [107]*	-	10-20	43.3-153.3	10-20
Mouse [108, 109]	1-5×2	5	16.7 or 13.3	5.7 or 5
Mouse [92]	-	7.5, 15	26.3, 90	7.5, 15
Mouse [110]	-	15	90	15
Mouse [97]	-	10, 15	43.3, 90	10, 15
Mouse [86]	-	25	233.3	25
Mouse [94]	5×5.6	13	80.3 or 69.3	14.1 or 13
Rat [111]	16×2	15	53.3 or 90	11.2 or 15
Rat [112]*	-	10, 15, 20, 30, 40	43.3 – 573.3	10-40
Rat [113]	5×15	-	450	35.3
<hr style="border-top: 1px dashed black;"/>				
Mouse - our	10×2.6-7.5		48.5-262.5	10.7-26.6
	10×6.5 (X-rays)	-	205.8	23.4
	6×6.4 (BP)		123.5	17.8
	7×6.8 (TM)		144.1	19.3

The differences in energy of X-rays and the fractionated schemes (# fr/d) were not considered.

*SD 10-30 Gy were applied for both 100% and 50% volume and SD of 40 Gy for 50% volume.

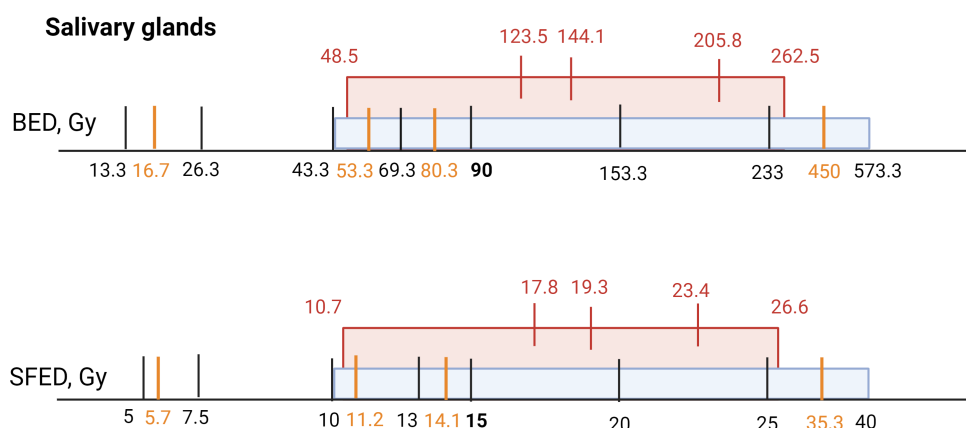


Figure 7.15: A graphical summary of doses used for studying radiation-induced effects in salivary glands found from a literature search (SD in black, fractionated in orange) and our doses (in red). Created with BioRender.com.

Early effects – lip dermatitis, oral mucositis, and cytokine expression

In our experiments, radiation-induced lip dermatitis and mucositis on the tongue were observed after both X-ray and proton irradiation. As presented in paper I, the severity of the lip skin toxicity was dependent on X-ray irradiation dose, and higher doses induced an earlier onset of lip dermatitis. Changing the fractionation to once daily or to irradiation with protons did not affect the lip dermatitis onset or severity score (see paper III). Similar lip epidermal score, onset and duration were also observed in another mouse model after SD X-ray irradiation with similar BED (see [88] in Table 7.1). These findings suggest that a potential threshold dose might exist beyond which the score for lip skin toxicity remains unchanged, even with further increases in dose, changes in fractionation, or in radiation type.

Most of the studies propose to use the mouse tongue as a model for oral mucositis because of the homogeneous epithelial structure that is similar to human [91]. A few studies have observed oral mucositis in mouse tongue following SD or fractionated X-ray irradiation with a latent time, defined as time from the onset of irradiation to the first diagnosis of oral mucositis of around 8-12 days with resolution within 3-6 days [88, 89, 106]. Interestingly, in our studies oral mucositis was induced only with X-ray doses more than 6.5 Gy per fraction twice daily with similar latent time (12 days) but much longer duration in 40 % of the mice. The increase in dose per fraction to 7.5 Gy induced earlier onset of oral mucositis (day 9) in 60 % of the mice and its severity was not tolerable for the animals. Changing the fractionation scheme to once daily and keeping the dose of 6.5 Gy per fraction as a reference to proton experiments led to the oral mucositis induction in 80 % of the mice with the same latent time (day 12) and duration (20 days). For comparison, another mouse study on wild-type mice with 3 fractions of 8 Gy reported oral mucositis and ulcers on the tongue at day 9 [101]. The BEDs that were sufficient to induce oral mucositis in mice in the SD and fractionation studies included in the literature review were lower than the BEDs employed in our study (Table 7.1). In contrast, much higher BEDs were used to induce oral mucositis in hamster models with similar latent time (day 12) and longer duration. These findings indicate that several parameters influence the induction of oral mucositis in animal models such as animal species and strain, radiation field (head, snout or tongue), dose per fraction and fractionation scheme, and despite the successful induction of oral mucositis with SD irradiation, it might be challenging to translate this knowledge to clinics. Therefore, the fractionated experiments are more appropriate to study the mechanisms of oral mucositis and potential drug interventions.

Mucositis originates from the inflammation and epithelial and endothelial cells death, followed by the sterilization of stem cells in the germinative layer of the epithelium which results in a deficit of cellular supply for the functional layers [91]. As these superficial layers naturally undergo shedding due to mechanical wear and tear, hypoplasia of the epithelium develops, ultimately leading to ulcerative mucositis. Therefore, the response of the mucosa is significantly influenced by the dynamics of compensatory repopulation during the treatment period. One explanation for more severe oral mucositis after irradiation with 1 fr/d compared

to 2 fr/d in our experiments might be the cellular repopulation that was adjusted to the level of damage. Dörr's group suggested that the higher weekly dose during the first treatment week is a higher stimulus to repopulation [114, 115]. In addition, a reduction of oral mucositis severity in clinical trials was found after an accelerated fractionated RT, but not after conventional protocols [115].

In order to achieve the main goal of the project, the proton experiments were designed to reproduce similar dose distributions for the low LET TM plan to the reference X-ray experiment and included high LET BP plan to study the effects of LET (Fig. 7.13). The similarity of the dose distributions were confirmed by alanine dosimetry (paper III). The proton irradiation resulted in induction of oral mucositis in 100 % of the mice with minimal variation of latent time and severity in both proton plans. Moreover, the radiation treatment had to be stopped as oral mucositis developed earlier (day 8-9) and was more severe, and the mice showed a large weight loss already in the beginning of the second treatment week. Compared to X-rays, proton irradiation with lower total dose induced more severe oral mucositis with earlier onset, which indicates an RBE higher than 1.1 of protons for this effect. Our study is the first direct comparison of early and late normal tissue effects in H&N region following X-ray and proton irradiation. Another mouse study focused on early effects of intestinal crypt regeneration after X-ray and proton irradiation and showed that proton irradiation may be more effective in inducing severe gastrointestinal tract toxicity [73]. In that study, mice were placed in the middle of the SOBP, which is more common for the tumor position rather than for the normal tissue. In contrast, our study encompasses low and high LET regions of the proton path which is more clinically relevant for normal tissue effects as described in paper III. However, for early effects both proton plans with different irradiation volume and LET employed in our study induced similar severity of oral mucositis.

Our experimental design was tailored for cytokine screening of serum and saliva samples collected at different time points before and after radiotherapy to obtain molecular insights to the induced effects. We hypothesized that saliva is more sensitive for cytokine changes driven by local radiation damage because serum might reflect various systematic changes. Indeed, in paper II we demonstrated a stronger correlation between salivary cytokine levels from a pro-inflammatory cytokine panel and late endpoints compared to serum cytokines. Therefore, the further focus was on salivary cytokines from the mice irradiated with different fractionation schemes and radiation types. The results showed that the majority of the detected cytokine levels were significantly increased in the mice X-irradiated with 1 fr/d compared to controls and the mice irradiated with 2 fr/d at day 5/12 (the day after the last fraction), including the pro-inflammatory cytokines. The group of mice irradiated with 1 fr/d, which developed more severe early effects, also showed increased cytokine response. The cytokine release might act as signal transducers to amplify the damage response, and pro-inflammatory cytokines that contributes to early inflammation have been reported to be an essential component of early radiogenic oral mucositis [116].

However, the analysis comparing early cytokine response by X-rays with that of proton irradiation showed surprising results (paper IV). The levels of pro-

inflammatory cytokines IL-1 α in serum and saliva, and TNF in saliva showed significant increase at day 9/12 after the onset of X-ray irradiation compared to proton irradiation and controls. All other detected cytokines in saliva also showed increased levels after X-ray compared to proton irradiation at day 9/12. Here, the groups of mice irradiated with protons, who developed more severe early effects, did not show any increased cytokine response. This raises questions regarding the biological mechanisms of radiation-induced responses after protons versus X-rays including the contribution of pro-inflammatory cytokines. For the proton experiments, we included cytokines in serum as the knowledge about systemic responses after proton- compared to X-irradiation is limited. Interestingly, the G-CSF cytokine that plays a role in controlling the immune response showed different responses in serum and saliva being greatly increased in serum after proton- compared to X-irradiation at day 9/12. This might reflect a systemic inflammatory response caused by more severe radiation-induced early effects after proton irradiation.

Salivary gland hypofunction - saliva volume

Compared to oral mucositis, which can be visually observed and scored, SG dysfunction can be monitored through the saliva volume or histologically. The measurement of saliva parameters is frequently employed in the examination of radiation-induced damage to the SG. However, in many studies, various sampling time points are selected without explicit justification or rationale. As we aimed to study cytokine response in serum and saliva, the sampling points in our experiments were chosen to encompass both early and late phases while satisfying the regulatory requirements for frequency of blood sampling in mice.

Our experiments with 6.6 Gy per fraction twice daily showed significant saliva reduction on day 35, 80 and 105 after onset of irradiation, while no significant decrease was observed for lower doses (paper I and II). Surprisingly, in another study, reduction of saliva was observed 30, 60 and 90 days after 1-2 Gy per fraction once daily for 5 days meaning much lower BED compared to our study [108]. This may perhaps be explained by the difference in radiosensitivity of different mouse strains as C57Bl/6 mouse strain, chosen for our experiments, is considered to be more radioresistant than the FVB mouse strain used in this study. Change of fractionation scheme to once daily led to a reduction of saliva volume already on day 12 (the day after the last fraction), 35, 70 and 105 (paper III and IV). Since the sampling for X-ray experiments was carried out the day after the last fraction, the sampling days differ for the different fractionation schemes (day 5 for 2 fr/d and day 12 for 1 fr/d). Therefore, the different time points of sampling may potentially influence the results, primarily due to the progression of damage over time rather than the alteration in the scheme itself. Studies in rats showed that the late effects in the SMG following fractionated X-ray irradiation exceeds that of the damage induced by a single dose, while no differences in effects were observed after conventional versus accelerated irradiation [111]. Salivary glands are expected to be late responding tissue (>60 days) because their excretory cells have a slow turnover (60–120 days) [117]. However, the changes in saliva volume and

composition occurring shortly after RT indicate that salivary glands also belong to the acutely responding tissues [117, 98]. This has been termed the enigmatic radiosensitivity of the SG in the literature [98]. The mechanisms of early and late irradiation damage of SG have been reported to differ from each other [92, 38]. There are some discrepancies in the mechanism of early effects presented in the literature. Some studies report apoptosis of salivary acinar cells occurring at 8–72 h after irradiation in mice as one of the factors contributing to the acute decrease of function post-RT [37], while most other studies did not find acinar cell loss at the early stages [92, 38, 98]. The possible mechanisms of early SG damage may include failure of vasculature function, acinar cell signal transduction, inflammation, and damage to the plasma membrane [38, 98]. In addition, the process of activating a cell death program in limited number of acinar cells may serve as a stimulus for the secretion of signaling factors to the surrounding cells that potentially contributes to a chronic loss of function [118]. As we aimed to study primarily the late effects of SG, no histological evidence was collected at early time points to explore the potential mechanism of reduced saliva secretion after the termination of RT.

After proton irradiation, saliva volume was significantly reduced compared to controls at the same time points as after X-ray irradiation with 1 fr/d (day 9/12, day 35, 70, and 105). For the BP group, the plan was to irradiate half of the mouse H&N and salivary glands to spare their function, and this group indeed showed a tendency to a higher saliva volume compared to the TM group at every time point after irradiation. Here, the volume effect might explain the better recovery tendency of saliva volume in the BP group. Nevertheless, the BP group showed significant decrease of saliva volume compared to controls, which might be explained by the high LET effect compensating for the lower irradiated volume. In addition, we cannot know which part of each salivary gland was irradiated on the hind side of the intended position of the Bragg peak because of the millimeter extension of the proton Bragg peak and possible uncertainties with positioning, etc. The TM group showed saliva levels similar to the X-ray group except on day 105, where the latter showed significantly higher levels. The TM group was irradiated with low LET protons, and the dose distribution throughout the whole mouse head was comparable to X-rays, while the total BED was lower compared to the X-ray irradiations. It is challenging to calculate RBE *in vivo* because the mouse H&N thickness is approximately 10–13 mm, and the range of LETs across the system especially for the BP plan is broad. Still, the developed early and late effects clearly indicated that protons are biologically more effective than X-rays. However, some morphological recovery was observed in both proton groups as a higher appearance of acinar cell clusters compared to X-ray group, which points to mechanistic differences between different radiation types and emphasizes the requirement for additional studies.

Late effects - fibrosis, acinar atrophy, and cytokine expression

For later time points, our histological data showed a reduction of total gland area, increased fibrotic area, and loss of acinar cells at day 105 in all irradiated groups following X-ray and proton irradiation. Acinar cell loss and fibrosis are considered

one of the main contributors to the mechanism of late damage of salivary glands. Therefore, our findings align with other studies in the field [92, 38, 98].

Comparing the different fractionation schemes, the group irradiated with 2 fr/d demonstrated significantly higher fibrotic area compared to 1 fr/d (section *Comparing X-ray fractionation schedules*). Interestingly, most of the cytokines in saliva also showed significantly increased levels at day 35, 80 and 105 in the group irradiated with 2 fr/d (paper II), while a wave-like increase of salivary cytokines was observed for the mice irradiated with 1 fr/d on day 12 and 70 (paper IV). The overview of detected cytokines is presented in the Discussion section in paper II. On day 105, IL-1 α , G-CSF and MIP-1 α cytokine levels from the mice irradiated with 2 fr/d were significantly higher compared to those with 1 fr/d. TIMP-1 and TNF cytokines showed the same tendency, but the increases were not significant.

Cytokine biomarkers may contribute to predicting or monitoring the response of normal tissues following radiotherapy. For identification of potential biomarkers of late effects, we used a decision tree regression model for the cytokine levels at day 35 to predict the combined late effect score including both fibrotic area and saliva volume in a leave-one-out-cross-validation procedure. The model gave a clear separation between the irradiated group and the control group. The feature importance analysis showed that IL-1 α levels on day 35 were by far the strongest contributor to the prediction model which indicates that IL-1 α might be highly involved in the pathological processes leading to fibrosis and hyposalivation. IL-1 α is a macrophage product reported to activate the inflammatory process after irradiation as well as to contribute to fibrosis under chronic inflammation by stimulation of fibroblast proliferation [119, 29]. Therefore, inhibition of IL-1 α might be considered as potential intervention strategy to mitigate radiation-induced fibrosis.

Comparing proton and X-ray tissue effects, the fibrotic area showed an increase (not significant) in the SMG for both proton groups compared to X-rays (paper IV). Analysis of acinar cell density demonstrated a significant reduction of acinar cells from both proton groups compared to the X-ray group. Despite the increased late damage of the salivary glands after proton irradiation, this was not reflected in the cytokine expression in neither saliva nor serum. Most of the detected cytokines in saliva showed increased levels after X-rays compared to protons at day 70. At day 105, TIMP-1 in saliva showed an increase in all irradiated groups compared to controls, with higher levels in the TM group compared to the X-ray group. TIMP-1 has been reported to suppress profibrotic matrix metalloproteinases and its levels have been found to be elevated under chronic inflammation [120]. The TM group indeed demonstrated a larger replacement of gland tissue with fibrous connective tissue at day 105 compared to the BP and X-ray groups. As discussed in paper IV, our results might be explained by a different contribution of pro-inflammatory cytokines in the development of effects induced by protons vs X-rays. The studies on cytokine response after proton and X-ray irradiation are limited. Another preclinical study with foot irradiation also demonstrated different pro-inflammatory cytokine response with lower expression levels in plasma both in the early and late phase after proton irradiation compared to X-rays [121]. Additional research is required to clarify the mechanisms underlying the cytokine regulation

Chapter 7. Discussion

in radiation-induced normal tissue toxicities. This might facilitate the discovery of new prognostic biomarkers and devise new strategies for mitigating these effects.

Conclusions and perspectives

Chapter 8

Conclusions and perspectives

8.1 Conclusions

A preclinical model was established to study early and late radiation-induced effects in the H&N region. The chosen normal tissue side effects represent clinically relevant endpoints such as oral mucositis and salivary gland dysfunction. The developed model and the experimental protocol are an optimal compromise with respect to ease of use and possibilities for short-term and long-term studies with tissue collection and body fluids sampling for cytokine monitoring.

To our knowledge, our work is the first H&N mouse study that directly compare radiation-induced normal tissue effects following X-ray and proton RT using the same irradiation setup to reproduce similar dose distributions with X-rays and low LET protons (before the Bragg peak, TM). In addition, a high LET proton plan (placing the pristine Bragg peak in the middle of the mouse, BP) was included. The observations of oral mucositis in the tongue and measurements of acinar atrophy, fibrosis and saliva volume showed much larger normal tissue effects after proton irradiation than after X-ray irradiation, despite the proton doses being 40.8 Gy (BP) and 44.8 Gy (TM), while the X-ray dose was 65 Gy. The results of our study indicate that the relative biological effectiveness of protons in normal tissue is considerably larger than the current clinical standard of 1.1, which should be considered in the future proton clinical trials of RT of HNC.

In addition, this was the first study monitoring both salivary and serum cytokines after H&N irradiation in mice. We observed differential secretion of cytokines in saliva from all the irradiated groups compared to the controls. A strong correlation between salivary cytokine levels and late endpoints was found, while cytokines from serum were only weakly correlated with the endpoints. This pointed towards a higher potential for saliva cytokines to be used as biomarkers of local radiation-induced damage of SG. Even though the correlation of saliva cytokine levels to late effects was similar, the cytokine response from X-rays showed much higher values, while the proton irradiated mice showed a relatively 'cold' cytokine response despite having more severe early and late effects. This highlights the importance of studying the mechanistic pathways with respect to the immune system, inflammatory response, and the development of tissue toxicities

after proton versus X-ray irradiation.

8.2 Perspectives

Norway will get its first operational proton therapy center in Oslo and Bergen in 2025. The preclinical model established in this PhD project might be further employed to:

- obtain more dose response data for protons to estimate RBE;
- study the normal tissue toxicity after combinations of chemo- or immunotherapy with radiation;
- study the mitigation strategies targeting normal tissue toxicities;
- study the cytokine response, molecular mechanisms and contribution of inflammation to the development of normal tissue toxicities;
- study orthotopic tumor response and the effect of tumor microenvironment on normal tissue toxicity.

References

- [1] Mark Gormley et al. 'Reviewing the epidemiology of head and neck cancer: definitions, trends and risk factors'. In: *British Dental Journal* 233.9 (2022), pp. 780–786.
- [2] Farzan Siddiqui and Benjamin Movsas. 'Management of radiation toxicity in head and neck cancers'. In: *Seminars in Radiation Oncology*. Vol. 27. 4. Elsevier. 2017, pp. 340–349.
- [3] Alejandro M Chibly et al. 'Salivary gland function, development, and regeneration'. In: *Physiological Reviews* 102.3 (2022), pp. 1495–1552.
- [4] Maddison Hunter et al. 'Toxicities caused by head and neck cancer treatments and their influence on the development of malnutrition: Review of the literature'. In: *European Journal of Investigation in Health, Psychology and Education* 10.4 (2020), pp. 935–949.
- [5] Rajamanickam Baskar et al. 'Cancer and radiation therapy: current advances and future directions'. In: *International journal of medical sciences* 9.3 (2012), p. 193.
- [6] Tara A Water et al. 'The potential benefit of radiotherapy with protons in head and neck cancer with respect to normal tissue sparing: a systematic review of literature'. In: *The oncologist* 16.3 (2011), pp. 366–377.
- [7] Michael Baumann et al. 'Radiation oncology in the era of precision medicine'. In: *Nature Reviews Cancer* 16.4 (2016), pp. 234–249.
- [8] Man Hu et al. 'Proton beam therapy for cancer in the era of precision medicine'. In: *Journal of hematology & oncology* 11.1 (2018), pp. 1–16.
- [9] Harald Paganetti et al. 'Relative biological effectiveness (RBE) values for proton beam therapy'. In: *International Journal of Radiation Oncology* Biology* Physics* 53.2 (2002), pp. 407–421.
- [10] Shanthi Marur and Arlene A Forastiere. 'Head and neck cancer: changing epidemiology, diagnosis, and treatment'. In: *Mayo Clinic Proceedings*. Vol. 83. 4. Elsevier. 2008, pp. 489–501.
- [11] John Andrew Ridge et al. 'Head and neck tumors'. In: *Cancer management: a multidisciplinary approach* 11.3 (2008), p. 369.

References

- [12] J-P Machiels et al. ‘Squamous cell carcinoma of the oral cavity, larynx, oropharynx and hypopharynx: EHNS–ESMO–ESTRO Clinical Practice Guidelines for diagnosis, treatment and follow-up’. In: *Annals of Oncology* 31.11 (2020), pp. 1462–1475.
- [13] P Bossi et al. ‘Nasopharyngeal carcinoma: ESMO-EURACAN Clinical Practice Guidelines for diagnosis, treatment and follow-up’. In: *Annals of Oncology* 32.4 (2021), pp. 452–465.
- [14] Carla van Herpen et al. ‘Salivary gland cancer: ESMO–European Reference Network on Rare Adult Solid Cancers (EURACAN) clinical practice guideline for diagnosis, treatment and follow-up’. In: *ESMO open* 7.6 (2022).
- [15] Christian Rønn Hansen et al. ‘Evaluation of decentralised model-based selection of head and neck cancer patients for a proton treatment study. DAHANCA 35’. In: *Radiotherapy and Oncology* (2023), p. 109812.
- [16] Alexander Lin et al. ‘PTCOG head and neck subcommittee consensus guidelines on particle therapy for the management of head and neck tumors’. In: *International journal of particle therapy* 8.1 (2021), pp. 84–94.
- [17] Kenneth Jensen et al. ‘The danish head and neck cancer group (dahanca) 2020 radiotherapy guidelines’. In: *Radiotherapy and Oncology* 151 (2020), pp. 149–151.
- [18] Helsedirektoratet. *Hode-/halskreft – handlingsprogram. Nasjonal faglig retningslinje*. 2020. URL: <https://www.helsedirektoratet.no/retningslinjer/hode-hals-kreft-handlingsprogram> (visited on 15/09/2023).
- [19] Francesco Tommasino and Marco Durante. ‘Proton radiobiology’. In: *Cancers* 7.1 (2015), pp. 353–381.
- [20] David S Chang et al. *Basic radiotherapy physics and biology*. Tech. rep. Springer, 2014.
- [21] Sarah Baatout. *Radiobiology Textbook*. 2023.
- [22] Harald Paganetti. ‘Proton relative biological effectiveness–uncertainties and opportunities’. In: *International journal of particle therapy* 5.1 (2018), pp. 2–14.
- [23] J Donald Chapman and Colin J Gillespie. ‘Radiation-induced events and their time scale in mammalian cells’. In: *Advances in radiation biology* 9 (1981), pp. 143–198.
- [24] Harald Paganetti. ‘Relative biological effectiveness (RBE) values for proton beam therapy. Variations as a function of biological endpoint, dose, and linear energy transfer’. In: *Physics in Medicine & Biology* 59.22 (2014), R419.
- [25] Bleddyn Jones. ‘Why RBE must be a variable and not a constant in proton therapy’. In: *The British journal of radiology* 89.1063 (2016), p. 20160116.
- [26] A Vissink et al. ‘Oral sequelae of head and neck radiotherapy’. In: *Critical Reviews in Oral Biology & Medicine* 14.3 (2003), pp. 199–212.

- [27] Linda S Elting et al. 'Risk, outcomes, and costs of radiation-induced oral mucositis among patients with head-and-neck malignancies'. In: *International Journal of Radiation Oncology* Biology* Physics* 68.4 (2007), pp. 1110–1120.
- [28] Aishan Shih et al. 'Mechanisms for radiation-induced oral mucositis and the consequences'. In: *Cancer nursing* 26.3 (2003), pp. 222–229.
- [29] Jay S Cooper et al. 'Late effects of radiation therapy in the head and neck region'. In: *International Journal of Radiation Oncology* Biology* Physics* 31.5 (1995), pp. 1141–1164.
- [30] Charles T Lee and Thomas J Galloway. 'Pathogenesis and amelioration of radiation-induced oral mucositis'. In: *Current Treatment Options in Oncology* 23.3 (2022), pp. 311–324.
- [31] Shiyu Liu et al. 'Status of treatment and prophylaxis for radiation-induced oral mucositis in patients with head and neck cancer'. In: *Frontiers in Oncology* 11 (2021), p. 642575.
- [32] Rajesh V Lalla et al. 'Oral mucositis due to high-dose chemotherapy and/or head and neck radiation therapy'. In: *JNCI Monographs* 2019.53 (2019), lgz011.
- [33] Osama Muhammad Maria, Nicoletta Eliopoulos and Thierry Muanza. 'Radiation-induced oral mucositis'. In: *Frontiers in oncology* 7 (2017), p. 89.
- [34] Adriana Blakaj et al. 'Oral mucositis in head and neck cancer: Evidence-based management and review of clinical trial data'. In: *Oral oncology* 95 (2019), pp. 29–34.
- [35] Tomiko Sunaga et al. 'The association between cumulative radiation dose and the incidence of severe oral mucositis in head and neck cancers during radiotherapy'. In: *Cancer Reports* 4.2 (2021), e1317.
- [36] Shreerang A Bhide et al. 'Dose–response analysis of acute oral mucositis and pharyngeal dysphagia in patients receiving induction chemotherapy followed by concomitant chemo-IMRT for head and neck cancer'. In: *Radiotherapy and Oncology* 103.1 (2012), pp. 88–91.
- [37] Kimberly J Jasmer et al. 'Radiation-induced salivary gland dysfunction: mechanisms, therapeutics and future directions'. In: *Journal of clinical medicine* 9.12 (2020), p. 4095.
- [38] Lara Barazzuol, Rob P Coppes and Peter van Luijk. 'Prevention and treatment of radiotherapy-induced side effects'. In: *Molecular oncology* 14.7 (2020), pp. 1538–1554.
- [39] Siri Beier Jensen et al. 'Salivary gland hypofunction and xerostomia in head and neck radiation patients'. In: *JNCI Monographs* 2019.53 (2019), lgz016.
- [40] Vincent WC Wu and Kit Yee Leung. 'A review on the assessment of radiation induced salivary gland damage after radiotherapy'. In: *Frontiers in oncology* 9 (2019), p. 1090.

References

- [41] Joseph O Deasy et al. ‘Radiotherapy dose–volume effects on salivary gland function’. In: *International Journal of Radiation Oncology* Biology* Physics* 76.3 (2010), S58–S63.
- [42] Judith M Roesink et al. ‘Quantitative dose-volume response analysis of changes in parotid gland function after radiotherapy in the head-and-neck region’. In: *International Journal of Radiation Oncology* Biology* Physics* 51.4 (2001), pp. 938–946.
- [43] Bo Zhu et al. ‘Accelerated hyperfractionated radiotherapy versus conventional fractionation radiotherapy for head and neck cancer: a meta-analysis of randomized controlled trials’. In: *Journal of Oncology* 2019 (2019).
- [44] Karen K Fu et al. ‘A Radiation Therapy Oncology Group (RTOG) phase III randomized study to compare hyperfractionation and two variants of accelerated fractionation to standard fractionation radiotherapy for head and neck squamous cell carcinomas: first report of RTOG 9003’. In: *International Journal of Radiation Oncology* Biology* Physics* 48.1 (2000), pp. 7–16.
- [45] J Bernier and SM Bentzen. ‘Altered fractionation and combined radio-chemotherapy approaches: pioneering new opportunities in head and neck oncology’. In: *European Journal of cancer* 39.5 (2003), pp. 560–571.
- [46] Jean Bourhis et al. ‘Hyperfractionated or accelerated radiotherapy in head and neck cancer: a meta-analysis’. In: *The Lancet* 368.9538 (2006), pp. 843–854.
- [47] Andrew J Boria and Carlos J Perez-Torres. ‘Minimal difference between fractionated and single-fraction exposure in a murine model of radiation necrosis’. In: *Radiation Oncology* 14 (2019), pp. 1–5.
- [48] Søren M Bentzen et al. ‘Biomarkers and surrogate endpoints for normal-tissue effects of radiation therapy: the importance of dose–volume effects’. In: *International Journal of Radiation Oncology* Biology* Physics* 76.3 (2010), S145–S150.
- [49] Claudio Pulito et al. ‘Oral mucositis: the hidden side of cancer therapy’. In: *Journal of experimental & clinical cancer research* 39 (2020), pp. 1–15.
- [50] Elena Ferrari et al. ‘Salivary cytokines as biomarkers for oral squamous cell carcinoma: a systematic review’. In: *International journal of molecular sciences* 22.13 (2021), p. 6795.
- [51] Martha M Matuszak et al. ‘Functional adaptation in radiation therapy’. In: *Seminars in radiation oncology*. Vol. 29. 3. Elsevier. 2019, pp. 236–244.
- [52] Ondrej Palata et al. ‘Radiotherapy in combination with cytokine treatment’. In: *Frontiers in Oncology* 9 (2019), p. 367.
- [53] Tamara Diesch et al. ‘Cytokines in saliva as biomarkers of oral and systemic oncological or infectious diseases: A systematic review’. In: *Cytokine* 143 (2021), p. 155506.

- [54] Paolo Bossi et al. ‘Salivary cytokine levels and oral mucositis in head and neck cancer patients treated with chemotherapy and radiation therapy’. In: *International Journal of Radiation Oncology* Biology* Physics* 96.5 (2016), pp. 959–966.
- [55] Thuy-Tien Maria Huynh et al. ‘Associations between patient-reported late effects and systemic cytokines in long-term survivors of head and neck cancer treated with radiotherapy’. In: *Journal of Cancer Survivorship* 17.4 (2023), pp. 1082–1093.
- [56] Sandra Nuyts et al. ‘Proton therapy for squamous cell carcinoma of the head and neck: early clinical experience and current challenges’. In: *Cancers* 14.11 (2022), p. 2587.
- [57] William M Mendenhall et al. ‘Proton Beam Radiation Therapy for Oropharyngeal Squamous Cell Carcinoma’. In: *International Journal of Particle Therapy* 9.4 (2023), pp. 243–252.
- [58] Terence T Sio et al. ‘Intensity modulated proton therapy versus intensity modulated photon radiation therapy for oropharyngeal cancer: first comparative results of patient-reported outcomes’. In: *International Journal of Radiation Oncology* Biology* Physics* 95.4 (2016), pp. 1107–1114.
- [59] Pierre Blanchard et al. ‘Intensity-modulated proton beam therapy (IMPT) versus intensity-modulated photon therapy (IMRT) for patients with oropharynx cancer—a case matched analysis’. In: *Radiotherapy and Oncology* 120.1 (2016), pp. 48–55.
- [60] Pierre Blanchard et al. ‘Proton therapy for head and neck cancers’. In: *Seminars in radiation oncology*. Vol. 28. 1. Elsevier. 2018, pp. 53–63.
- [61] Zhe Chen et al. ‘Proton versus photon radiation therapy: A clinical review’. In: *Frontiers in Oncology* 13 (2023), p. 1133909.
- [62] Noorazrul Yahya and Hanani Abdul Manan. ‘Quality of life and patient-reported outcomes following proton therapy for oropharyngeal carcinoma: a systematic review’. In: *Cancers* 15.8 (2023), p. 2252.
- [63] N Patrik Brodin et al. ‘Systematic review of normal tissue complication models relevant to standard fractionation radiation therapy of the head and neck region published after the QUANTEC reports’. In: *International Journal of Radiation Oncology* Biology* Physics* 100.2 (2018), pp. 391–407.
- [64] Angel I Blanco et al. ‘Dose–volume modeling of salivary function in patients with head-and-neck cancer receiving radiotherapy’. In: *International Journal of Radiation Oncology* Biology* Physics* 62.4 (2005), pp. 1055–1069.
- [65] Hubert Szymon Gabryś et al. ‘Parotid gland mean dose as a xerostomia predictor in low-dose domains’. In: *Acta Oncologica* 56.9 (2017), pp. 1197–1203.
- [66] Radhe Mohan. ‘A review of proton therapy—Current status and future directions’. In: *Precision Radiation Oncology* 6.2 (2022), pp. 164–176.

References

- [67] Brita Singers Sørensen et al. ‘Relative biological effectiveness (RBE) and distal edge effects of proton radiation on early damage in vivo’. In: *Acta Oncologica* 56.11 (2017), pp. 1387–1391.
- [68] Harald Paganetti. ‘Significance and implementation of RBE variations in proton beam therapy’. In: *Technology in cancer research & treatment* 2.5 (2003), pp. 413–426.
- [69] Emilia Rita Szabo et al. ‘Radiobiological effects and proton RBE determined by wildtype zebrafish embryos’. In: *PLoS One* 13.11 (2018), e0206879.
- [70] Brita Singers Sørensen. ‘Commentary: RBE in proton therapy—where is the experimental in vivo data?’ In: *Acta Oncologica* 58.10 (2019), pp. 1337–1339.
- [71] Tracy SA Underwood and Stephen J McMahon. ‘Proton relative biological effectiveness (RBE): a multiscale problem’. In: *The British Journal of Radiology* 92.1093 (2018), p. 20180004.
- [72] John Gueulette et al. ‘Proton RBE for early intestinal tolerance in mice after fractionated irradiation’. In: *Radiotherapy and oncology* 61.2 (2001), pp. 177–184.
- [73] Changhoon Choi et al. ‘Comparison of proton and photon beam irradiation in radiation-induced intestinal injury using a mouse model’. In: *International journal of molecular sciences* 20.8 (2019), p. 1894.
- [74] John Gueulette et al. ‘Proton relative biological effectiveness (RBE) for survival in mice after thoracic irradiation with fractionated doses’. In: *International Journal of Radiation Oncology* Biology* Physics* 47.4 (2000), pp. 1051–1058.
- [75] Maria Saager et al. ‘Determination of the proton RBE in the rat spinal cord: Is there an increase towards the end of the spread-out Bragg peak?’ In: *Radiotherapy and Oncology* 128.1 (2018), pp. 115–120.
- [76] Henning Willers et al. ‘Toward A variable RBE for proton beam therapy’. In: *Radiotherapy and Oncology* 128.1 (2018), pp. 68–75.
- [77] *Absorbed Dose Determination in Photon and Electron Beams*. Technical Reports Series 277. Vienna: INTERNATIONAL ATOMIC ENERGY AGENCY. ISBN: 92-0-100597-0. URL: <https://www.iaea.org/publications/5693/absorbed-dose-determination-in-photon-and-electron-beams>.
- [78] Azam Niroomand-Rad et al. ‘Report of AAPM task group 235 radiochromic film dosimetry: an update to TG-55’. In: *Medical physics* 47.12 (2020), pp. 5986–6025.
- [79] C Ankjærgaard et al. ‘Irradiation of subcutaneous mouse tumors with a clinical linear accelerator validated by alanine dosimetry’. In: *Radiation Measurements* 147 (2021), p. 106636.
- [80] Harini Bagavant et al. ‘A method for the measurement of salivary gland function in mice’. In: *JoVE (Journal of Visualized Experiments)* 131 (2018), e57203.

- [81] Supriya Mallick, Rony Benson and GK Rath. ‘Radiation induced oral mucositis: a review of current literature on prevention and management’. In: *European Archives of Oto-Rhino-Laryngology* 273 (2016), pp. 2285–2293.
- [82] Joanne M Bowen, Rachel J Gibson and Dorothy MK Keefe. ‘Animal models of mucositis: implications for therapy’. In: *The journal of supportive oncology* 9.5 (2011), pp. 161–168.
- [83] Patricia Chaves et al. ‘Preclinical models in head and neck squamous cell carcinoma’. In: *British Journal of Cancer* 128.10 (2023), pp. 1819–1827.
- [84] Juliana Jasper et al. ‘Effect of G-CSF on oral mucositis and traumatic ulcers produced in the tongue of rats undergoing radiotherapy: clinical and histologic evaluation’. In: *Oral surgery, oral medicine, oral pathology and oral radiology* 122.5 (2016), pp. 587–596.
- [85] W Dörr, K Spekl and M Martin. ‘Radiation-induced oral mucositis in mice: strain differences’. In: *Cell proliferation* 35 (2002), pp. 60–67.
- [86] Mana Kamiya et al. ‘X-ray-induced damage to the submandibular salivary glands in mice: an analysis of strain-specific responses’. In: *BioResearch Open Access* 4.1 (2015), pp. 307–318.
- [87] Qiang Li et al. ‘Mouse tumor-bearing models as preclinical study platforms for oral squamous cell carcinoma’. In: *Frontiers in oncology* 10 (2020), p. 212.
- [88] Charles S Parkins, Jack F Fowler and Shen Yu. ‘A murine model of lip epidermal/mucosal reactions to X-irradiation’. In: *Radiotherapy and oncology* 1.2 (1983), pp. 159–165.
- [89] Osama Muhammad Maria et al. ‘Single-dose radiation-induced oral mucositis mouse model’. In: *Frontiers in oncology* 6 (2016), p. 154.
- [90] Fu-Xi Xu, Emmanuel van der Schueren and K Kian Ang. ‘Acute reactions of the lip mucosa of mice to fractionated irradiations’. In: *Radiotherapy and Oncology* 1.4 (1984), pp. 369–374.
- [91] W Dörr and J Kummermehr. ‘Accelerated repopulation of mouse tongue epithelium during fractionated irradiations or following single doses’. In: *Radiotherapy and Oncology* 17.3 (1990), pp. 249–259.
- [92] Miranda Muhvic Urek et al. ‘Early and late effects of X-irradiation on submandibular gland: a morphological study in mice’. In: *Archives of medical research* 36.4 (2005), pp. 339–343.
- [93] Jennifer L Avila et al. ‘Radiation-induced salivary gland dysfunction results from p53-dependent apoptosis’. In: *International Journal of Radiation Oncology* Biology* Physics* 73.2 (2009), pp. 523–529.
- [94] Yitzhak Marmary et al. ‘Radiation-induced loss of salivary gland function is driven by cellular senescence and prevented by IL6 modulation’. In: *Cancer research* 76.5 (2016), pp. 1170–1180.
- [95] Liping Xu et al. ‘Resveratrol attenuates radiation-induced salivary gland dysfunction in mice’. In: *The Laryngoscope* 123.11 (2013), E23–E29.

References

- [96] Xibao Liu et al. ‘Loss of TRPM2 function protects against irradiation-induced salivary gland dysfunction’. In: *Nature communications* 4.1 (2013), p. 1515.
- [97] Ienaka Takeda et al. ‘Possible role of nitric oxide in radiation-induced salivary gland dysfunction’. In: *Radiation research* 159.4 (2003), pp. 465–470.
- [98] Antonius WT Konings, Rob P Coppes and Arjan Vissink. ‘On the mechanism of salivary gland radiosensitivity’. In: *International Journal of Radiation Oncology* Biology* Physics* 62.4 (2005), pp. 1187–1194.
- [99] Inga Solgård Juvkam et al. ‘A preclinical model to investigate normal tissue damage following fractionated radiotherapy to the head and neck’. In: *Journal of radiation research* 64.1 (2023), pp. 44–52.
- [100] Stefanie Pabst, Kathrin Spekl and Wolfgang Dörr. ‘Changes in the effect of dose fractionation during daily fractionated irradiation: studies in mouse oral mucosa’. In: *International Journal of Radiation Oncology* Biology* Physics* 58.2 (2004), pp. 485–492.
- [101] Gangwen Han et al. ‘Preventive and therapeutic effects of Smad7 on radiation-induced oral mucositis’. In: *Nature medicine* 19.4 (2013), pp. 421–428.
- [102] Lyudmila G Burdelya et al. ‘Toll-like receptor 5 agonist protects mice from dermatitis and oral mucositis caused by local radiation: implications for head-and-neck cancer radiotherapy’. In: *International Journal of Radiation Oncology* Biology* Physics* 83.1 (2012), pp. 228–234.
- [103] ST Sonis et al. ‘Defining mechanisms of action of interleukin-11 on the progression of radiation-induced oral mucositis in hamsters’. In: *Oral oncology* 36.4 (2000), pp. 373–381.
- [104] Jose Fernando Bastos Moura et al. ‘A novel model of megavoltage radiation-induced oral mucositis in hamsters: Role of inflammatory cytokines and nitric oxide’. In: *International journal of radiation biology* 91.6 (2015), pp. 500–509.
- [105] Carolyn T Jordan et al. ‘Radiation-induced oral mucositis hamster model using a linear accelerator enhances clinical relevance of preclinical studies for treatment strategy investigation’. In: *Animal Models and Experimental Medicine* 4.1 (2021), pp. 47–53.
- [106] MaGAR Rezvani and GA Ross. ‘Modification of radiation-induced acute oral mucositis in the rat’. In: *International journal of radiation biology* 80.2 (2004), pp. 177–182.
- [107] Isabelle MA Lombaert et al. ‘Keratinocyte growth factor prevents radiation damage to salivary glands by expansion of the stem/progenitor pool’. In: *Stem cells* 26.10 (2008), pp. 2595–2601.
- [108] Kirsten H Limesand et al. ‘Insulin-like growth factor-1 preserves salivary gland function after fractionated radiation’. In: *International Journal of Radiation Oncology* Biology* Physics* 78.2 (2010), pp. 579–586.

- [109] Katie L Martin et al. ‘Prevention of radiation-induced salivary gland dysfunction utilizing a CDK inhibitor in a mouse model’. In: *PLoS One* 7.12 (2012), e51363.
- [110] Aviram Mizrachi et al. ‘Radiation-induced microvascular injury as a mechanism of salivary gland hypofunction and potential target for radioprotectors’. In: *Radiation research* 186.2 (2016), pp. 189–195.
- [111] Rob P Coppes, Arjan Vissink and Antonius WT Konings. ‘Comparison of radiosensitivity of rat parotid and submandibular glands after different radiation schedules’. In: *Radiotherapy and Oncology* 63.3 (2002), pp. 321–328.
- [112] Antonius WT Konings et al. ‘Volume effects and region-dependent radiosensitivity of the parotid gland’. In: *International Journal of Radiation Oncology* Biology* Physics* 62.4 (2005), pp. 1090–1095.
- [113] Tonje Sønstevold, Anne Christine Johannessen and Linda Stuhr. ‘A rat model of radiation injury in the mandibular area’. In: *Radiation Oncology* 10.1 (2015), pp. 1–11.
- [114] Wolfgang Dörr and Marion Weber-Frisch. ‘Repopulation response of mouse oral mucosa during unconventional radiotherapy protocols’. In: *Radiotherapy and Oncology* 37.3 (1995), pp. 230–236.
- [115] W Dörr. ‘Modulation of repopulation processes in oral mucosa: experimental results’. In: *International journal of radiation biology* 79.7 (2003), pp. 531–537.
- [116] Sylvia Gruber et al. ‘Early inflammatory changes in radiation-induced oral mucositis: effect of pentoxifylline in a mouse model’. In: *Strahlentherapie und Onkologie* 193.6 (2017), p. 499.
- [117] Arjan Vissink et al. ‘Clinical management of salivary gland hypofunction and xerostomia in head-and-neck cancer patients: successes and barriers’. In: *International Journal of Radiation Oncology* Biology* Physics* 78.4 (2010), pp. 983–991.
- [118] O Grundmann, GC Mitchell and KH Limesand. ‘Sensitivity of salivary glands to radiation: from animal models to therapies’. In: *Journal of dental research* 88.10 (2009), pp. 894–903.
- [119] Jae Ho Kim, Kenneth A Jenrow and Stephen L Brown. ‘Mechanisms of radiation-induced normal tissue toxicity and implications for future clinical trials’. In: *Radiation oncology journal* 32.3 (2014), p. 103.
- [120] Shankar Siva et al. ‘A pattern of early radiation-induced inflammatory cytokine expression is associated with lung toxicity in patients with non-small cell lung cancer’. In: *PloS one* 9.10 (2014), e109560.
- [121] Steffen Nielsen et al. ‘Proton scanning and X-ray beam irradiation induce distinct regulation of inflammatory cytokines in a preclinical mouse model’. In: *International Journal of Radiation Biology* 96.10 (2020), pp. 1238–1244.

References

Paper I

**A preclinical model to investigate
normal tissue damage following
fractionated radiotherapy to the head
and neck**

I

A preclinical model to investigate normal tissue damage following fractionated radiotherapy to the head and neck

Inga Solgård Juvkam^{1,†}, Olga Zlygosteva^{2,†}, Delmon Arous^{2,3},
Hilde Kanli Galtung¹, Eirik Malinen^{2,3}, Tine Merete Søland^{1,4,‡} and
Nina Jeppesen Edin^{2,‡,*}

¹Institute of Oral Biology, Faculty of Dentistry, University of Oslo, 0372 Oslo, Norway

²Department of Physics, Faculty of Mathematics and Natural Sciences, University of Oslo, 0371 Oslo, Norway

³Department of Medical Physics, Cancer Clinic, Oslo University Hospital, 0379 Oslo, Norway

⁴Department of Pathology, Oslo University Hospital, 0372 Oslo, Norway

*Corresponding author. Department of Physics, Faculty of Mathematics and Natural Sciences, University of Oslo, Oslo, Norway. E-mail: n.f.j.edin@fys.uio.no

[†]Joint first authors.

[‡]Joint senior authors.

(Received 19 May 2022; revised 9 August 2022; editorial decision 6 September 2022)

ABSTRACT

Radiotherapy (RT) of head and neck (H&N) cancer is known to cause both early- and late-occurring toxicities. To better appraise normal tissue responses and their dependence on treatment parameters such as radiation field and type, as well as dose and fractionation scheme, a preclinical model with relevant endpoints is required. 12-week old female C57BL/6 J mice were irradiated with 100 or 180 kV X-rays to total doses ranging from 30 to 85 Gy, given in 10 fractions over 5 days. The radiation field covered the oral cavity, swallowing structures and salivary glands. Monte Carlo simulations were employed to estimate tissue dose distribution. The follow-up period was 35 days, in order to study the early radiation-induced effects. Baseline and post irradiation investigations included macroscopic and microscopic examinations of the skin, lips, salivary glands and oral mucosa. Saliva sampling was performed to assess the salivary gland function following radiation exposure. A dose dependent radiation dermatitis in the skin was observed for doses above 30 Gy. Oral mucositis in the tongue appeared as ulcerations on the ventral surface of the tongue for doses of 75–85 Gy. The irradiated mice showed significantly reduced saliva production compared to controls. In summary, a preclinical model to investigate a broad panel of normal tissue responses following fractionated irradiation of the H&N region was established. The optimal dose to study early radiation-induced effects was found to be around 75 Gy, as this was the highest tolerated dose that gave acute effects similar to that observed in cancer patients.

Keywords: Radiotherapy (RT); fractionation; early effects; head and neck (H&N); mice; histology

INTRODUCTION

Head and neck (H&N) cancer patients who receive radiotherapy (RT) as part of their treatment may be severely affected by radiation-induced damages to normal tissue. RT can result in early side effects such as dermatitis and oral mucositis, which may occur during or soon after RT and could potentially lead to interruption of the treatment. Furthermore, RT can also produce late side effects that may severely reduce the patient's quality of life, such as salivary gland hypofunction, tissue fibrosis and osteoradionecrosis [1, 2]. Generally,

clinical symptoms of side effects following RT are well documented. However, preclinical models are essential to investigate radiation-induced early and late side effects in normal tissues of the H&N region and their dependence on RT-related factors such as radiation field and type (e.g. X-rays and protons) as well as dose and fractionation scheme. A better appraisal of these effects and underlying biological processes may aid the development of new methods and strategies for mitigating or eliminating such tissue damage and subsequent clinical symptoms [3].

Current radical RT of H&N cancer is delivered as fractionated treatment, normally in fractions of 2 Gy to a total dose of typically 70 Gy [4]. Still, most previous studies investigating the side effects of RT in the H&N region of murine model systems have used either single dose (SD) irradiation or extremely hypofractionated schedules with few fractions of very high doses [5–10]. Some studies have used fractionation for H&N experiments [11–14], but without any justification for the choice of dose. Also, the radiation field(s) employed in previous studies did not cover the typical region as seen in patients, which should encompass areas such as the oral cavity, the oropharynx and the laryngopharynx. Examples from the literature encompass large radiation fields including the entire head or upper body of the animal [5, 8, 10] or small radiation fields only covering, e.g. the tongue or snout of the animal [9, 11–13], which differ from radiation fields used in the clinic. Thus, preclinical studies employing more clinically relevant radiation fields and fractionated radiation delivery are highly needed. Also, as a broad spectrum of tissue responses may occur after irradiation of the H&N area, the selected preclinical model should be an optimal compromise with respect to ease of use and possibilities for long term follow-up with tissue and liquid sampling.

The aim of the present investigation was to establish a preclinical model employing a clinically relevant radiation field and careful assessment of radiation dose distribution to study various early radiation-induced effects in the H&N region induced by different dose deliveries.

MATERIALS AND METHODS

Animals

Nine-week-old C57BL/6J male and female mice were purchased from Janvier (France), kept in a 12-h light/12-h dark cycle under pathogen-free conditions and fed a standard commercial fodder with water given ad libitum. Standard housing with nesting material and refuge was provided. All experiments were approved by the Norwegian Food Safety Authority (ID 20889, 26 246 and 27 931) and performed in accordance with directive 2010/63/EU on the protection of animals used for scientific purposes. At the onset of experiments, animals were 12 weeks old.

Irradiation procedure

RT was delivered in 10 fractions over 5 days (8 am and 4 pm) with a Faxitron Multirad225 irradiation system (Faxitron Bioptics, Tucson, AZ, USA). Four sets of experiments were performed with two different X-ray settings: (i) 180 kV X-ray potential, 10 mA current, 0.3 mm Cu filter and 0.65 Gy/min dose rate, and (ii) 100 kV, 15 mA, 2.0 mm Al and 0.75 Gy/min. Absolute calibration of the X-ray system was conducted using an FC65-G ionization chamber (IBA Dosimetry, Germany) together with a MAX-4000 electrometer (Standard Imaging, USA) according to standards for absorbed dose to water. For all fractions, animals were anesthetized using gas anesthesia with Sevoflurane 4% in O₂. The anesthetized mice were positioned on their right side in a custom-made foam holder with the beam entering on the left side. A lead collimator was custom built to define a radiation field of 25 × 20 mm covering the oral cavity, pharynx and major salivary glands and placed on top of the foam holder. The radiation field was carefully planned to only irradiate the tissues of interest and avoid

exposure of the eyes and brain. A built-in X-ray imaging system was used to verify the anatomical location of the radiation field (Fig. 1A). In the following, day 0 is the time point where the first irradiation was performed.

MRI

Magnetic Resonance Imaging (MRI) of the H&N region was performed using a 7.05 T Biospec scanner (Bruker Medical systems, Germany) on the same days as the saliva sampling. A fast T2 weighted spin-echo sequence, TurboRARE, with TE = 31 ms and TR = 3100 ms was employed. Body temperature was monitored and maintained at 37°C by a feedback-regulated heating fan. Respiration rate was monitored by a respiration probe. The MR image was used to show the radiation field in relation to the anatomical structures of the mouse (Fig. 1B). For MRI, animals were anesthetized using gas anesthesia with Sevoflurane 4% in O₂.

Monte Carlo simulations

Monte Carlo simulations of the dose distribution in mice were conducted in FLUKA 4–1.1 [15] (see supplementary file for details). Briefly, the simulations were performed in computed tomography (CT) images of one euthanized male mouse (10–11 weeks of age). Both X-ray setting 1 and 2 were simulated, providing 3D dose distributions for 100 kV and 180 kV X-ray spectra, respectively. A rectangular irradiation field was used which covered the same regions as defined experimentally. The transport and production cutoff of photons and electrons was set to 1 keV. The treatment field was simulated for 5×10^7 primary X-ray photons. The absorbed dose was scored on a voxel-by-voxel basis, providing tissue-specific dose estimates where mean and ranges are reported.

Experimental protocol

Altogether, four sets of experiments were accomplished. First, two pilot experiments (experiment 1 and 2) were performed to establish procedures and appropriate X-ray voltages and doses. Then, two main experiments (experiment 3 and 4) were conducted with a larger number of animals in each treatment group to further assess the early radiation-induced effects. Experiment 1 employed both male and female mice, randomly assigned to either sham treatment, 10×3 Gy, or 10×4.4 Gy irradiation ($n = 3$ for each gender and dose group). Here, X-ray setting 1 (see *Irradiation Procedure* above) was used. An aggressive behavior was observed in the male group that led to loss of several mice during experiment 1. Because possible gender difference in response to radiation was not the aim of the current study, we decided to include only female mice in the further experiments. Therefore, experiment 2 used only female mice, randomly assigned to either sham treatment, 10×5 Gy, 10×5.75 Gy, or 10×6.5 Gy irradiation ($n = 4$ for each treatment group) with a shorter follow-up period to ensure documentation of histological effects. As will become evident, pilot experiment 1 and 2 gave rather mild symptoms and experiment 3 was therefore conducted with increased doses. Experiment 3 used only female mice, randomly assigned to either sham treatment or 10×8.5 Gy ($n = 10$ for each treatment group). However, the dose of 10×8.5 Gy was not well tolerated by the mice and experiment 3 was terminated on day 14 due

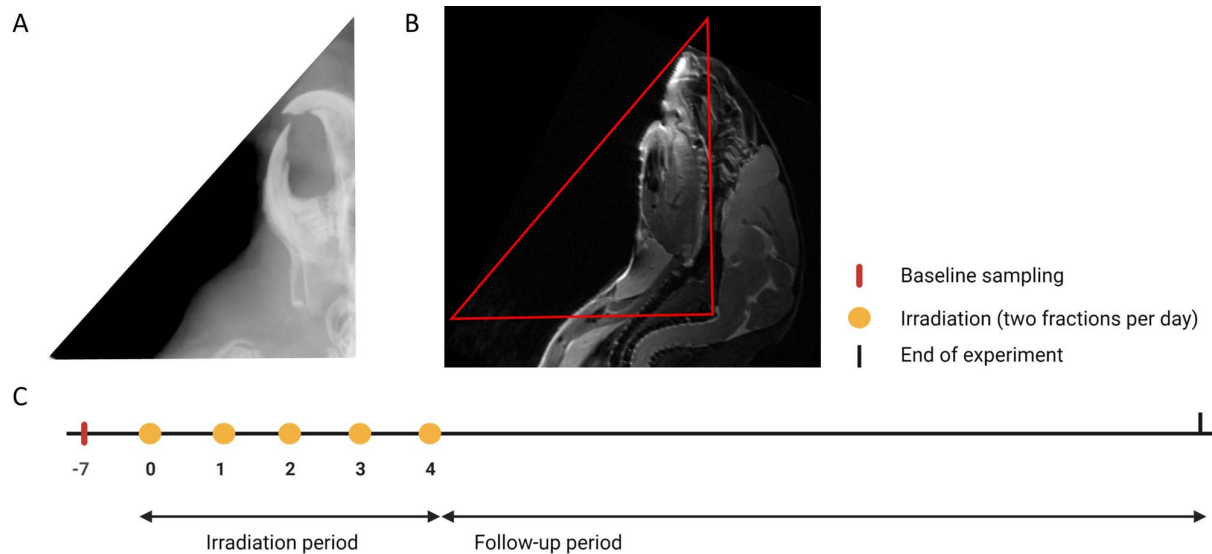


Fig. 1. Experimental design. (A) X-ray image of the radiation field used. (B) MR image of the H&N region. The red triangle shows the approximate radiation field. (C) Experimental protocol timeline. Irradiation was given twice a day for 5 days (days 0–4) as 10 fractions of 3, 4.4, 5, 5.75, 6.5, 7.5 and 8.5 Gy. Examinations of the oral cavity and saliva sampling were performed throughout the follow-up period.

to unacceptable weight loss (> 20%). Based on experiments 1–3, the optimal dose was determined to be between 6.5 and 8.5 Gy per fraction (Gy/f). Therefore, experiment 4 was conducted with female mice, randomly assigned to either sham treatment or 10×7.5 Gy ($n = 10$ for each treatment group). In experiment 2–4, X-ray setting 2 was used because of a more clinically relevant dose distribution (presented in Results). All reported tissue doses are mean doses at the midpoint in the X-ray path through the mouse.

On day -7, baseline body weight was determined and saliva sampling was performed in all animals. On days 0–4, fractionated irradiation was given twice a day to the irradiation groups, as explained above (see also Fig. 1C). The maximum follow-up period in this study was 35 days to fully cover the early radiation-induced effect. During the follow-up period, the animals were monitored frequently. Examinations of the oral cavity were performed every second day and weighing was done daily. Macroscopic examinations of the oral cavity were performed using magnifying glasses ($\times 3.5$) and a light source, while the mice were under anesthesia. Subcutaneous injection of anesthesia was used (Zoletil-mix: Zoletil-mix: 10 ml Narcoxyl or Rompun® [xylasin 20 mg/ml] + 0.5 ml Torbugesic® [butorphanol 10 mg/ml] + Zoletil® [zolazepam 125 mg and tiletamin 125 mg]). Assessment of overall activity and body weight (less than 20% body weight loss was considered acceptable) were also performed. Presence of oral mucositis was monitored and scored as present/not present, while skin toxicity was graded using a modified scoring scheme based on the Radiation Therapy Oncology Group (RTOG) developed scoring criteria [16–18]. Euthanasia was performed through overdose of anesthetic (Pentobarbitol, Exagon® Vet) by intraperitoneal injection under terminal anesthesia to prevent tissue damage from cervical dislocation.

Histological evaluations

At the time of euthanasia, the tongue, mucosa and skin of the lower lips, left and right buccal mucosa and the major salivary glands (parotid, submandibular and sublingual glands) were collected and fixated for 24 hours in 10% formalin, dehydrated in ethanol and embedded in paraffin. Tissue sections of $4 \mu\text{m}$ were cut (Leica RM2155 microtome) and stained with hematoxylin and eosin (HE) and various antibodies by immunohistochemical method (see supplementary material). Histological examinations of the oral tissues were performed in a Nikon E90i microscope, and histological images were acquired using a Nikon DS-Ri1 camera with a CFI Plan Fluor $\times 10$ (NA 0.30), $\times 20$ (NA 0.50) or $\times 40$ objective (NA 0.75).

Saliva sampling

Saliva collection was performed before RT (day -7), immediately after (day 5), and at a later time point during the follow-up period (day 35). Mice were anesthetized with subcutaneous injection of Zoletil-mix (see *Experimental Protocol* above). The saliva sampling procedure was performed as previously described [19]. Briefly, 0.375 mg/kg of pilocarpine (Pilocarpine hydrochloride, Sigma) was intraperitoneally administered to the mice under anesthesia. Saliva was collected into a cotton swab for 15 minutes, which was then centrifuged at 7500 g and 4°C for 2 minutes, and the obtained volume was measured and stored at -80°C . Saliva production was calculated as saliva volume (μl) per saliva collection time (15 min).

Statistical analyses

Statistical analyses were performed in Prism 8 for Windows (Version 8.3.0, GraphPad Software, LLC) and in RStudio (Version 4.1.1).

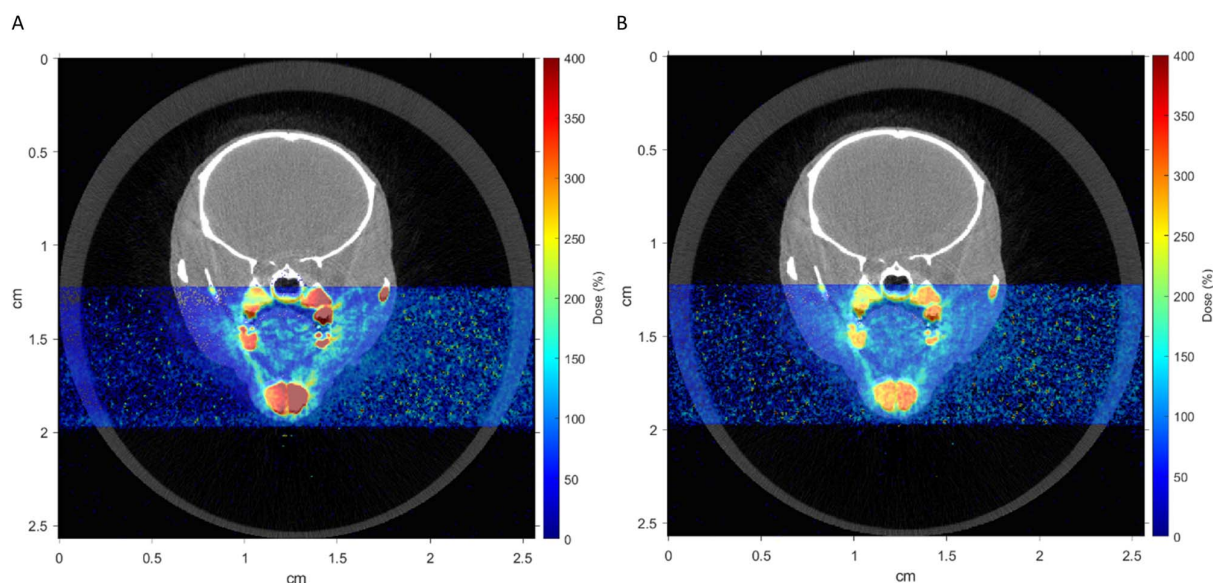


Fig. 2. Monte Carlo simulated dose distributions relative to the prescribed dose for (A) 100 kV and (B) 180 kV in a transverse CT image of a mouse.

Correlation between body weight loss and oral mucositis was analyzed using a linear regression model. Saliva production was analyzed using a mixed-effects analysis and Sidak's multiple comparison test. A significance level of 0.05 was used for all comparisons.

RESULTS

Monte Carlo simulations

Figure 2 shows normalized dose maps for 100 and 180 kV X-ray voltages superimposed onto the same CT slice, which is central to the beam axis. The dose distribution is almost constant throughout the animal for 180 kV X-rays, whereas 100 kV X-rays give a gradual decline in dose. For 180 kV, the oral cavity, lip, skin and submandibular gland received on average (range) 102% (91, 111), 85% (73, 98), 80% (74, 86) and 79% (74, 84) of the prescribed dose, respectively. For 100 kV, the same structures received an average (range) of 93% (75, 108), 93% (79, 101), 71% (61, 79) and 70% (64, 74), respectively.

Macroscopic changes

Early radiation-induced effects were observed macroscopically in the lower lip, on the ventral surface of the tongue and on the skin of the upper chest. Radiation dermatitis of the lower lip was observed in all mice exposed to more than 3 Gy/f and was graded using RTOG-based score schemes (Fig. 3A–B). Mice exposed to 4.4 Gy/f developed mild radiation dermatitis with faint erythema, mild edema and dry desquamation, while mice exposed to 5–6.5 Gy/f developed moderate radiation dermatitis with bright erythema, moderate edema and patchy moist desquamation. Mice exposed to 7.5 Gy/f experienced severe radiation dermatitis with confluent moist desquamation that not only affected the skin of the lower lip as in the other RT groups, but also (affected) the skin of the upper chest. Radiation dermatitis of the lower lip was first observed on day 12 and peaked about day 21 (Fig. 3C–D).

LD₅₀ for skin toxicity grade 1, 2 and 3 was 4.4 Gy/f, 4.7 Gy/f and 7.5 Gy/f, respectively. Skin toxicity was not fully assessed in mice exposed to 8.5 Gy/f as this group was terminated before reaching the peak of skin toxicity. Fur loss localized to the upper chest inside the radiation field was observed in all irradiation groups receiving 4.4 Gy/f or more. Areas with complete fur loss was observed typically from day 17.

Oral mucositis was observed on the ventral surface of the tongue only in mice exposed to 7.5 and 8.5 Gy/f (Fig. 3E–F), and was first observed on day 9 and 12, respectively. By day 18, oral mucositis was completely resolved in the mice exposed to 7.5 Gy/f. Weight loss above 10% was only observed in RT groups exposed to 7.5 and 8.5 Gy/f (Supplementary Fig. 1). Weight loss was significantly correlated with development of oral mucositis ($P = 0.007$). Mice exposed to 8.5 Gy/f experienced more than 20% weight loss during the first 14 days of the experiment. Analgesia treatment (Temgesic injections) did not help, thus this group was terminated at an earlier time point than planned (day 14), and 8.5 Gy/f was considered too high for this mouse strain. By termination day 14, oral mucositis was still present on the ventral tongue of mice exposed to 8.5 Gy/f. For the present fractionation scheme and irradiation set-up, 7.5 Gy/f was thus found to be the optimal dose.

Histological changes

Early radiation-induced effects were also present in histologically examined tissues. Large morphological differences were seen in the lower lip between irradiated and control mice (Fig. 4A). Increased keratin thickness of the epidermis and desquamation of keratin, in addition to atrophy of sebaceous glands and hair follicles was observed in the irradiated mice (Fig. 4A). Moreover, an increased amount of cells, including neutrophils, Vimentin⁺-cells and F4/80⁺-cells were seen in the connective tissue both in the skin of the lip and

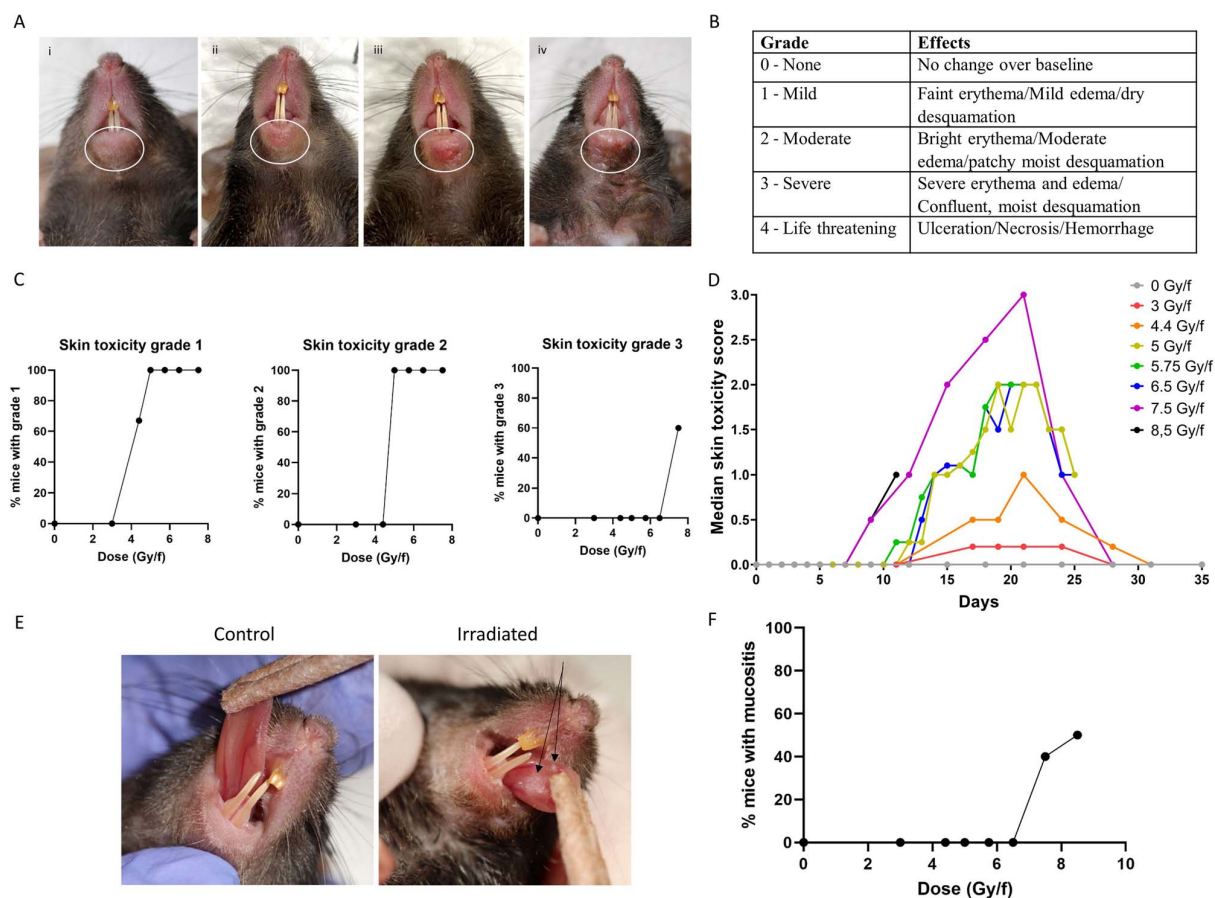


Fig. 3. Skin toxicity effects and oral mucositis observed after fractionated irradiation with different doses per fraction. (A) Example images of different skin toxicity grades observed in the lower lip of irradiated mice; (i) grade 0, (ii) grade 1 (iii) grade 2, and (iv) grade 3. White circles show the area of interest. (B) Skin toxicity scoring scheme based on RTOG. (C) Dose response curves for different skin toxicity grades observed in different doses per fraction. (D) Timeline of median skin toxicity score observed in the skin of the lower lip of irradiated mice for different doses per fraction. The number of animals used in each group varied as following 0 Gy/f ($n=9$), 3 Gy/f ($n=3$), 4.4 Gy/f ($n=3$), 5 Gy/f ($n=4$), 5.75 Gy/f ($n=4$), 6.5 Gy/f ($n=4$), 7.5 Gy/f ($n=10$), 8.5 Gy/f ($n=10$). (E) Example images of macroscopically visible mucositis (black arrows) on the ventral tongue of mice exposed to 7.5 and 8.5 Gy/f compared to control. (F) Dose response curves for oral mucositis observed in different doses per fraction.

in the oral mucosa (Fig. 4B and Supplementary Fig. 3). Fibroblasts as well as neutrophils and lymphocytes are positive for Vimentin while macrophages in mice are F4/80⁺ (Supplementary Fig. 3). Macroscopically observed oral mucositis on the ventral tongue of mice exposed to 7.5 and 8.5 Gy/f coincided with histological findings of mucosal ulcerations (Fig. 4C). Additionally, histological examinations of the parotid glands showed acinar vacuolization on day 14 in 4 of 10 mice exposed to 8.5 Gy/f (Fig. 4D). In the submandibular and sublingual glands however, no histological differences were seen on day 14 (not shown).

Saliva production

Significantly reduced saliva production ($P < 0.0001$) was found in mice exposed to 7.5 Gy/f ($3.6 \pm 1.4 \mu\text{L}/15 \text{ min}$) compared to controls

($13.1 \pm 1.9 \mu\text{L}/15 \text{ min}$) on day 35 (Fig. 5). Compared to controls, there was a tendency towards reduced saliva production in the other RT groups as well (3–6.5 Gy/f), albeit not statistically significant due to large inter-individual variations and a somewhat small number of animals per group (Supplementary Fig. 4). The average coefficient of variation (CV) for saliva production was 59%.

DISCUSSION

In the current work, we show early radiation-induced effects using our preclinical model in which mice are exposed to fractionated radiation in the H&N region. In the present study, we have tested doses per fraction ranging from 3–8.5 Gy \times 10 (30–85 Gy total dose) and have found that for the current fractionation scheme and irradiation setup, the optimal

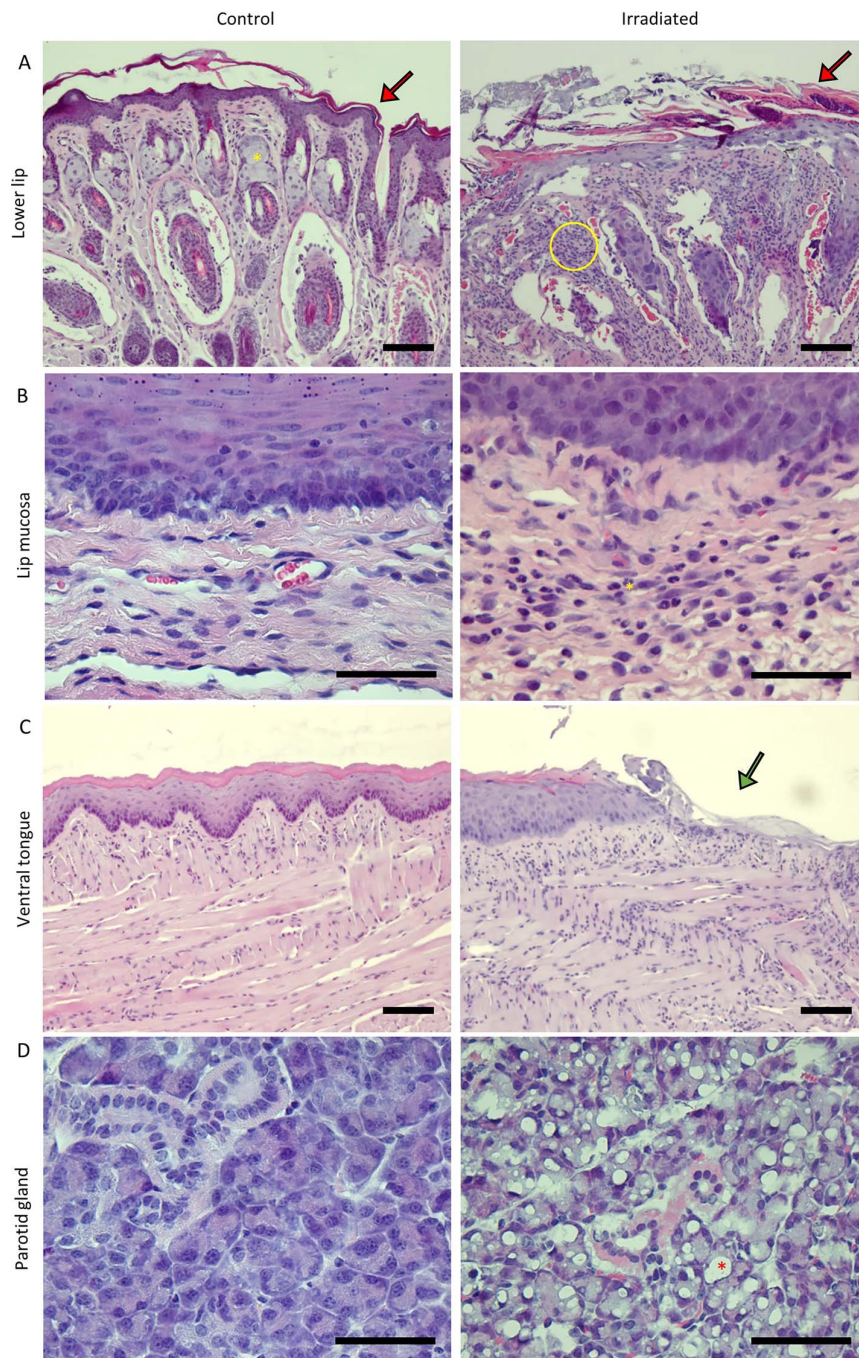


Fig. 4. Representative images of HE stained sections of oral tissues in mice after exposure to fractionated irradiation. (A) HE sections of the skin of the lower lip showed increased keratin layer (red arrow), atrophy of sebaceous glands (yellow asterisk = presence of sebaceous gland in control) and increased amount of cells in the connective tissue (yellow circle) in irradiated (8.5 Gy/f on day 14) compared to control mice. The image was taken at $\times 10$ magnification and the scale bar is $100\ \mu\text{m}$. (B) HE sections of lip mucosa showed increased amount of cells in the connective tissue, including neutrophils (yellow asterisk), in irradiated (8.5 Gy/f on day 14) compared to control mice. The image was taken at $\times 40$ magnification and the scale bar is $50\ \mu\text{m}$. (C) HE sections of the ventral tongue showed epithelial ulceration (green arrow) of the mucosa of irradiated (8.5 Gy/f on day 14) compared to control mice. The image was taken at $\times 10$ magnification and the scale bar is $100\ \mu\text{m}$. (D) HE sections of the parotid gland showed acinar vacuolization (red asterisk) in irradiated (8.5 Gy/f on day 14) compared to control mice. The image was taken at $\times 40$ magnification and the scale bar is $50\ \mu\text{m}$.

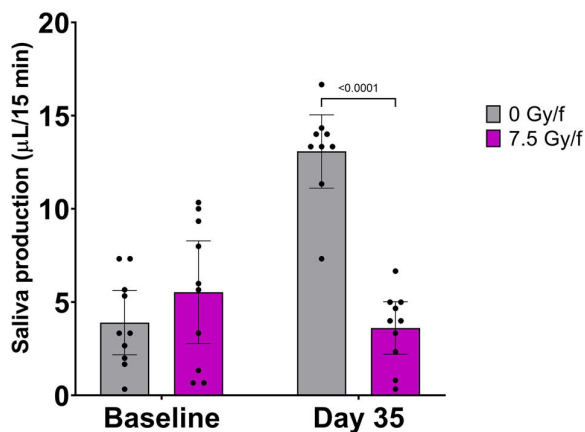


Fig. 5. Significantly lower saliva production was found in irradiated mice compared to controls at day 35 after exposure to fractionated irradiation. Saliva production was measured as $\mu\text{L}/15\text{ min}$ in 7.5 Gy/f and controls. Data is represented as mean \pm 95% CI. Each black dot represents an animal.

dose to obtain clinically relevant normal tissue response is 7.5 Gy/f. After exposure to 7.5 Gy/f mice experienced radiation dermatitis in the skin of the lip and upper chest, oral mucositis on the ventral surface of the tongue, acinar vacuolization in the parotid glands and significantly reduced saliva production compared to control mice.

Early radiation-induced effects in the H&N region depend on various parameters including type of radiation, dose, radiation field configuration and irradiation protocol (SD or fractionation). In preclinical research, the selection of different rodent strains for such studies also influences the results due to strain-specific variations in response to radiation-induced damage such as oral mucositis [20] and morphological and functional changes of the salivary glands [21]. Radiation-induced side effects of the H&N have previously been studied in hamsters [22, 23], rats [24–26], and mice [7, 8, 10, 13, 27]. Due to the lack of assay reagents available for hamsters, and that it is easier to keep a larger number of mice than hamsters or rats, mice were chosen for the present preclinical model. It is important to use a model that can cover both tumor and normal tissue effects in order to estimate the therapeutic ratio (tumor vs normal tissue effects) and to measure the effect of mitigators on late effects. We therefore selected C57BL/6 mice as this mouse strain has a large panel of syngeneic tumors. Compared to other mouse strains, C57BL/6 is relatively radioresistant [28–30] and is therefore a suitable strain for studying both early and late radiation-induced effects in the same model, as the mice will tolerate high doses of radiation. It is also the most widespread sub-strain used for studying genetically engineered mice [31] and has been recommended for studies with radioprotectors and mitigators [32]. It is well known that inbred mice are roughly half as sensitive to radiation as humans [30]. However, relevant exposures and regimens can be found by comparing effects seen in mice with effects observed in humans.

With the selected mouse strain, we established a setup including clinically applicable radiation fields with added imaging and Monte Carlo simulations to estimate local radiation doses to relevant tissues.

Compared to 180 kV X-rays, the simulations showed that 100 kV X-rays produced a more relevant, heterogeneous dose distribution, similar to clinical RT focusing on one part of the H&N region. In addition, fractionated irradiation was employed because of higher clinical relevance compared to SD. Dose fractionation in preclinical studies has not been extensively reported in the literature. Moreover, previous studies have either focused on early or late effects, while we believe that studying both early and late phases of the different tissue reactions could show the possible relationship between these effects and the influence of systemic processes (e.g. cytokine expression). In the present study we only focused on early radiation-induced effects, however the preclinical model presented here will be included in experiments with longer follow-up periods to study late radiation-induced effects.

In our study, the rate and severity of the skin toxicity was dependent on radiation dose, as evident from dose response curves and LD₅₀ values. The RTOG-based skin toxicity scoring table employed was not sufficiently sensitive to distinguish between all the tested doses per fraction. However, it could distinguish between three different groups: low dose (3 and 4.4 Gy/f), intermediate dose (5–6.5 Gy/f) and high dose (7.5 and 8.5 Gy/f). The macroscopic and microscopic changes seen in the skin of the lower lip were compatible with radiation dermatitis reported in mouse skin after SD [33] and fractionated irradiation with fewer fractions than we used [7, 14, 34, 35]. Even though the irradiation protocol and doses differ between the present work and earlier studies, the histological changes in the skin are similar. This might indicate that radiation-induced dermatitis occurs independent of irradiation protocol and dose, as long as the dose is above a certain threshold level.

Oral mucositis was observed macroscopically and histologically on the ventral surface of the tongue of mice exposed to 7.5 and 8.5 Gy/f. This is similar to what has been reported 8 days after SD irradiation of 18–25 Gy [8, 36], 10 days after fractionated irradiation given as 10 Gy/f over 3 days (30 Gy in total dose) [7] and as 3 Gy/f over 5 days (15 Gy in total dose) [37]. However, not all studies on oral mucositis in rodents observe oral mucosal ulcers. In other studies using SD irradiation, the authors state that rodents do not develop oral mucositis in the same manner as humans, but progress towards weight loss and death before ulcerative lesions appear [9, 10]. This is in contrast to the ulcerative lesions we observe in the ventral tongue together with weight loss in mice after exposure to 7.5 Gy/f. Both these effects were non-lethal and temporary for the given dose level. We found a significant correlation between oral mucositis and weight loss, which corresponds well with what is observed in H&N cancer patients experiencing oral mucositis, where the need of a feeding tube is frequent [38–40].

Saliva production was significantly lower in irradiated mice (7.5 Gy/f) compared to controls at day 35, which is consistent with previous reports after SD irradiation in mice [41–44] and fractionated irradiation in mice and rats [6, 25]. Interestingly, at day 35 saliva production in controls increased significantly from baseline, which might indicate that saliva production increases with age in normal salivary glands. Indeed, it has been shown that C57BL/6 mice increase their saliva production as they age from 10- to 30-weeks-old [45], which is in line with our results. In irradiated salivary glands however, the saliva production at day 35 was slightly lower compared to baseline values, implying that salivary gland function was compromised. The observed saliva levels in the present experiments varied considerably

between animals and time points and decreased with increasing dose (average CV of 59%). Additionally, we observed acinar vacuolization in the parotid glands in mice exposed to 8.5 Gy/f, which is consistent with previous reports after SD irradiation in mice [5, 6, 46]. The damages in the parotid glands may be parts of the explanation of the reduced saliva production in irradiated mice compared to controls.

In conclusion, the proposed preclinical model allows for the study of early radiation-induced effects in the H&N region. We observed both macroscopic and microscopic changes in skin, oral mucosa of the tongue and lip and salivary glands, as well as a significantly reduced saliva production in irradiated mice compared to controls. The present preclinical model is an optimal compromise with respect to ease of use and possibilities for short-term studies and for future long-term follow-up with tissue collection and liquid sampling that can allow for cytokine analysis in blood and/or saliva. Regarding the X-ray energies used, our Monte Carlo simulations show that 100 kV X-rays provide a more relevant and heterogeneous dose distribution compared to 180 kV, which will provide a better basis for future studies comparing side effects from X-rays and ions such as protons. In the present study, we have tested doses per fraction ranging from 3–8.5 Gy and have found that for the current fractionation scheme and irradiation setup, the optimal dose is 7.5 Gy/f. This dose is well tolerated in this mouse strain and results in similar early radiation-induced effects as in H&N cancer patients.

CONFLICT OF INTEREST

The authors declare no conflicts of interest.

FUNDING

This work was supported by UiO Life Science at the University of Oslo under grant reference 2018/10221 and South-Eastern Norway Regional Health Authority under grant number 2019050.

REFERENCES

- Siddiqui F, Movsas B. Management of radiation toxicity in head and neck cancers. *Semin Radiat Oncol* 2017;27:340–9.
- Sroussi HY, Epstein JB, Bensadoun RJ et al. Common oral complications of head and neck cancer radiation therapy: mucositis, infections, saliva change, fibrosis, sensory dysfunctions, dental caries, periodontal disease, and osteoradionecrosis. *Cancer Med* 2017;6:2918–31.
- Barazzuol L, Coppes RP, van Luijk P. Prevention and treatment of radiotherapy-induced side effects. *Mol Oncol* 2020;14:1538–54.
- Alterio D, Marvaso G, Ferrari A et al. Modern radiotherapy for head and neck cancer. *Semin Oncol* 2019;46:233–45.
- Urek MM, Bralic M, Tomac J et al. Early and late effects of X-irradiation on submandibular gland: a morphological study in mice. *Arch Med Res* 2005;36:339–43.
- Limesand KH, Said S, Anderson SM. Suppression of radiation-induced salivary gland dysfunction by IGF-1. *PLoS One* 2009;4:e4663.
- Burdelya LG, Gleiberman AS, Toshkov I et al. Toll-like receptor 5 agonist protects mice from dermatitis and oral mucositis caused by local radiation: implications for head-and-neck cancer radiotherapy. *Int J Radiat Oncol Biol Phys* 2012;83:228–34.
- Maria OM, Syme A, Eliopoulos N et al. Single-dose radiation-induced oral mucositis mouse model. *Front Oncol* 2016;6:154.
- Nolan MW, Long CT, Marcus KL et al. Nocifensive Behaviors in mice with radiation-induced oral mucositis. *Radiat Res* 2017;187:397–403.
- Chen J, Bekale LA, Khomtchouk KM et al. Locally administered heparin-binding epidermal growth factor-like growth factor reduces radiation-induced oral mucositis in mice. *Sci Rep* 2020;10:17327.
- Cini N, Gruber S, Arican Alicikus Z et al. Modulation of radiation-induced oral mucositis (mouse) by dermatan sulfate: effects on differentiation processes. *Strahlenther Onkol* 2020;196:85–94.
- Gruber S, Frings K, Kuess P et al. Protective effects of systemic dermatan sulfate treatment in a preclinical model of radiation-induced oral mucositis. *Strahlenther Onkol* 2018;194:675–85.
- Gruber S, Arnold M, Cini N et al. Radioprotective effects of dermatan Sulfate in a preclinical model of oral mucositis-targeting inflammation, hypoxia and junction proteins without stimulating proliferation. *Int J Mol Sci* 2018;19.
- Ang KK, Xu FX, Vanuytsel L et al. Repopulation kinetics in irradiated mouse lip mucosa: the relative importance of treatment protraction and time distribution of irradiations. *Radiat Res* 1985;101:162–9.
- Böhlen TT, Cerutti F, Chin MPW et al. The FLUKA code: developments and challenges for high energy and medical applications. *Nuclear Data Sheets* 2014;120:211–4.
- Trotti A, Byhardt R, Stetz J et al. Common toxicity criteria: version 2.0. An improved reference for grading the acute effects of cancer treatment: impact on radiotherapy. *Int J Radiat Oncol Biol Phys* 2000;47:13–47.
- Mallick S, Benson R, Rath GK. Radiation induced oral mucositis: a review of current literature on prevention and management. *Eur Arch Otorhinolaryngol* 2016;273:2285–93.
- Sonis ST, Elting LS, Keefe D et al. Perspectives on cancer therapy-induced mucosal injury: pathogenesis, measurement, epidemiology, and consequences for patients. *Cancer* 2004;100:1995–2025.
- Bagavant H, Trzeciak M, Papinska J et al. A method for the measurement of salivary gland function in mice. *J Vis Exp* 2018;131.
- Dorr W, Spekl K, Martin M. Radiation-induced oral mucositis in mice: strain differences. *Cell Prolif* 2002;35:60–7.
- Kamiya M, Kawase T, Hayama K et al. X-ray-induced damage to the submandibular salivary glands in mice: an analysis of strain-specific responses. *Biores Open Access* 2015;4:307–18.
- Watanabe S, Suemaru K, Nakanishi M et al. Assessment of the hamster cheek pouch as a model for radiation-induced oral mucositis, and evaluation of the protective effects of keratinocyte growth factor using this model. *Int J Radiat Biol* 2014;90:884–91.
- Jordan CT, Bradford EM, Cheek DC et al. Radiation-induced oral mucositis hamster model using a linear accelerator enhances clinical relevance of preclinical studies for treatment strategy investigation. *Animal Model Exp Med* 2021;4:47–53.

24. Li CY, Chen XH, Tao XA et al. The development and inflammatory features of radiotherapy-induced glossitis in rats. *Med Oral Patol Oral Cir Bucal* 2011;16:e348–53.
25. Sonstevold T, Johannessen AC, Stuhr L. A rat model of radiation injury in the mandibular area. *Radiat Oncol* 2015;10:129.
26. Nakashima T, Uematsu N, Shibamori M et al. Establishment of an X-ray irradiation-induced glossitis model in rats: biphasic elevation of proinflammatory cytokines and chemokines. *J Pharmacol Exp Ther* 2013;347:660–8.
27. Yang C, Tang H, Wang L et al. Dimethyl sulfoxide prevents radiation-induced oral mucositis through facilitating DNA double-strand break repair in epithelial stem cells. *Int J Radiat Oncol Biol Phys* 2018;102:1577–89.
28. Singh VK, Newman VL, Berg AN et al. Animal models for acute radiation syndrome drug discovery. *Expert Opin Drug Discov* 2015;10:497–517.
29. Boria AJ, Perez-Torres CJ. Impact of mouse strain and sex when modeling radiation necrosis. *Radiat Oncol* 2020;15:141.
30. Plett PA, Sampson CH, Chua HL et al. Establishing a murine model of the hematopoietic syndrome of the acute radiation syndrome. *Health Phys* 2012;103:343–55.
31. Wang Q, Du L, Wang Y et al. The development and biological characteristics of a novel potentially radioresistant inbred mouse strain. *Mol Med Rep* 2017;15:759–67.
32. Williams JP, Brown SL, Georges GE et al. Animal models for medical countermeasures to radiation exposure. *Radiat Res* 2010;173:557–78.
33. Fallah M, Shen Y, Broden J et al. Plasminogen activation is required for the development of radiation-induced dermatitis. *Cell Death Dis* 2018;9:1051.
34. Yang K, Kim SY, Park JH et al. Topical application of phlorotannins from Brown seaweed mitigates radiation dermatitis in a mouse model. *Mar Drugs* 2020;18:377.
35. Park JH, Byun HJ, Kim HJ et al. Effect of photobiomodulation therapy on radiodermatitis in a mouse model: an experimental animal study. *Lasers Med Sci* 2021;36:843–53.
36. Saul-McBeth J, Dillon J, Lee A et al. Tissue damage in radiation-induced oral mucositis is mitigated by IL-17 receptor Signaling. *Front Immunol* 2021;12:687627.
37. Dorr W, Spekl K, Farrell CL. Amelioration of acute oral mucositis by keratinocyte growth factor: fractionated irradiation. *Int J Radiat Oncol Biol Phys* 2002;54:245–51.
38. Davy C, Heathcote S. A systematic review of interventions to mitigate radiotherapy-induced oral mucositis in head and neck cancer patients. *Support Care Cancer* 2021;29:2187–202.
39. Sanguinetti G, Gunn GB, Parker BC et al. Weekly dose-volume parameters of mucosa and constrictor muscles predict the use of percutaneous endoscopic gastrostomy during exclusive intensity-modulated radiotherapy for oropharyngeal cancer. *Int J Radiat Oncol Biol Phys* 2011;79:52–9.
40. Shu Z, Zeng Z, Yu B et al. Nutritional status and its association with radiation-induced oral mucositis in patients with nasopharyngeal carcinoma during radiotherapy: a prospective study. *Front Oncol* 2020;10:594687.
41. Lin AL, Johnson DA, Wu Y et al. Measuring short-term gamma-irradiation effects on mouse salivary gland function using a new saliva collection device. *Arch Oral Biol* 2001;46:1085–9.
42. Takeda I, Kizu Y, Yoshitaka O et al. Possible role of nitric oxide in radiation-induced salivary gland dysfunction. *Radiat Res* 2003;159:465–70.
43. Martin KL, Hill GA, Klein RR et al. Prevention of radiation-induced salivary gland dysfunction utilizing a CDK inhibitor in a mouse model. *PLoS One* 2012;7:e51363.
44. Mizrachi A, Cotrim AP, Katabi N et al. Radiation-induced microvascular injury as a mechanism of salivary gland hypofunction and potential target for Radioprotectors. *Radiat Res* 2016;186:189–95.
45. Choi JS, Park IS, Kim SK et al. Analysis of age-related changes in the functional morphologies of salivary glands in mice. *Arch Oral Biol* 2013;58:1635–42.
46. Xu L, Yang X, Chen J et al. Simvastatin attenuates radiation-induced salivary gland dysfunction in mice. *Drug Des Devel Ther* 2016;10:2271–8.

Correction to: A preclinical model to investigate normal tissue damage following fractionated radiotherapy to the head and neck

This is a correction to: Inga Solgård Juvkam, Olga Zlygosteva, Delmon Arous, Hilde Kanli Galtung, Eirik Malinen, Tine Merete Søland, Nina Jeppesen Edin, A preclinical model to investigate normal tissue damage following fractionated radiotherapy to the head and neck, *Journal of Radiation Research*, Volume 64, Issue 1, January 2023, Pages 44–52, <https://doi.org/10.1093/jrr/rrac066>

In this work, we used a lead collimator to limit the radiation field to certain parts of the mouse head, as described in the original manuscript. The original dosimetry was performed without the lead shield, as we were concerned that the resulting collimation would lead to partial volume effects, and thus systematic errors, in the ion chamber measurements. However, the impact of the lead plate on the dose to the irradiated area was underestimated. This was evident from additional dosimetry of the irradiation setup with and without the plate performed after the original work was published. This revised dosimetry is given below.

The absorbed dose rate to water of the X-ray system was measured to be 0.63 ± 0.02 Gy/min for an unshielded beam using a FC65-G Farmer type ionization chamber (IBA Dosimetry, Germany) together with a MAX-4000 electrometer (Standard Imaging, USA) according to IAEA report TRS-277 [1-2]. To measure the dose in the collimated case, we employed Gafchromic™ EBT3 dosimeter films at a source-surface distance representing sagittal skin entrance of the mouse. Calibration was done using an unshielded beam. EBT3 films (lot No. 02122001) were irradiated and processed according to the recommended protocols specified for radiochromic film dosimetry in the report of AAPM Task Group 235 [3]. The results showed that the actual dose with the use of the collimator lead plate was 12% lower than the dose reported in the original manuscript. Therefore, all the doses in the manuscript should be corrected accordingly: 3 Gy to 2.6 Gy, 4.4 Gy to 3.9 Gy, 5 Gy to 4.4 Gy, 5.75 Gy to 5.1 Gy, 6.5 Gy to 5.7 Gy, 7.5 Gy to 6.6 Gy, 8.5 Gy to 7.5 Gy.

The authors apologize for any inconvenience this might have caused.

[1]: IAEA, Report No. ISBN 92-0-115 087-3, 1987.

[2]: IAEA, Report No. ISSN 1011-4289, 1996.

[3]: Niroomand-Rad A, Chiu-Isao S-T, Grams M P, Lewis D F, Soares C G, Van Battum L J, Das I J, Trichter S, Kissick M W and Massillon-JL G 2020 Report of AAPM task group 235 radiochromic film dosimetry: an update to TG-55 *Med. Phys* **47**:S 986-6025.

NB: the error in dosimetry is emended in this correction notice alone. The errors have not been emended throughout the paper online.

Supplementary file

Supplementary Materials and Methods

Monte Carlo simulations

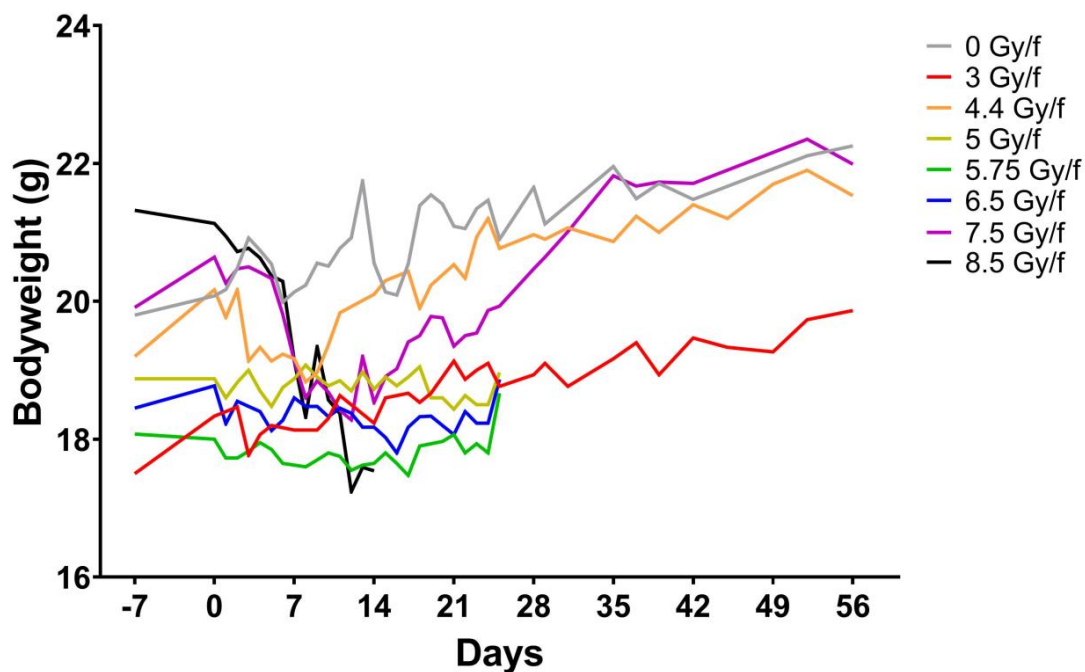
DICOM computed tomography (CT) images of one euthanized male mouse (10-11 weeks of age) with isotropic voxel sizes of $0.02 \times 0.02 \times 0.02 \text{ mm}^3$ were imported into Matlab R2020b (MathWorks, Natick, MA, USA) and co-registered to diagnostic DICOM magnetic resonance (MR) images of voxel sizes $0.12 \times 0.12 \times 0.70 \text{ mm}^3$ in the sagittal, coronal and axial plane of the animal, respectively, using an in-house developed software. Registration-based interpolation was performed in order to spatially align the axial CT stack to the axial MR images (fixed, reference) when equivalent posture and positioning of the mouse between the CT-MR image scanning acquisitions was accomplished. The interpolated CT images were subsequently imported into FLUKA 4-1.1 [1-3], where the geometrical scheme of the irradiation setup was defined using DICOM tools in Flair v3.1-13 (FLUKA Advanced Interface) [4]. Herewith, FLUKA Monte Carlo (MC) simulations allowed for exploration of the tissue dose distribution following different applied X-ray voltages. The absorbed dose distributions were simulated for 100 kV and 180 kV X-ray spectra attenuated by 2.0 mm Al and 0.3 mm Cu filters, respectively. For both energies, a rectangular irradiation field of size $1.5 \times 0.75 \text{ cm}^2$ was focused sagittally to the neck region of the mouse from a 52.0 cm source to sample distance (SSD), providing salivary gland area coverage and other normal tissue structures.

For the voxelized CT-based geometry, the FLUKA MC system was calibrated to match tissue mass densities and stopping powers with correlating CT numbers by a published stoichiometric calibration procedure [5]. Moreover, the MC simulations were run using PRECISIO defaults to guarantee reliable accuracy without increasing the simulation time significantly, where the transport and production cutoff of photons and electrons was set to 1 keV. The treatment field was simulated for 5×10^7 primary X-ray photons. Furthermore, dose scoring was performed using the USRBIN card in FLUKA. The dose quantities were scored on a voxel-by-voxel basis using the grid specified by the aforementioned MR images, wherefore the scoring region was defined to encompass all relevant volumes.

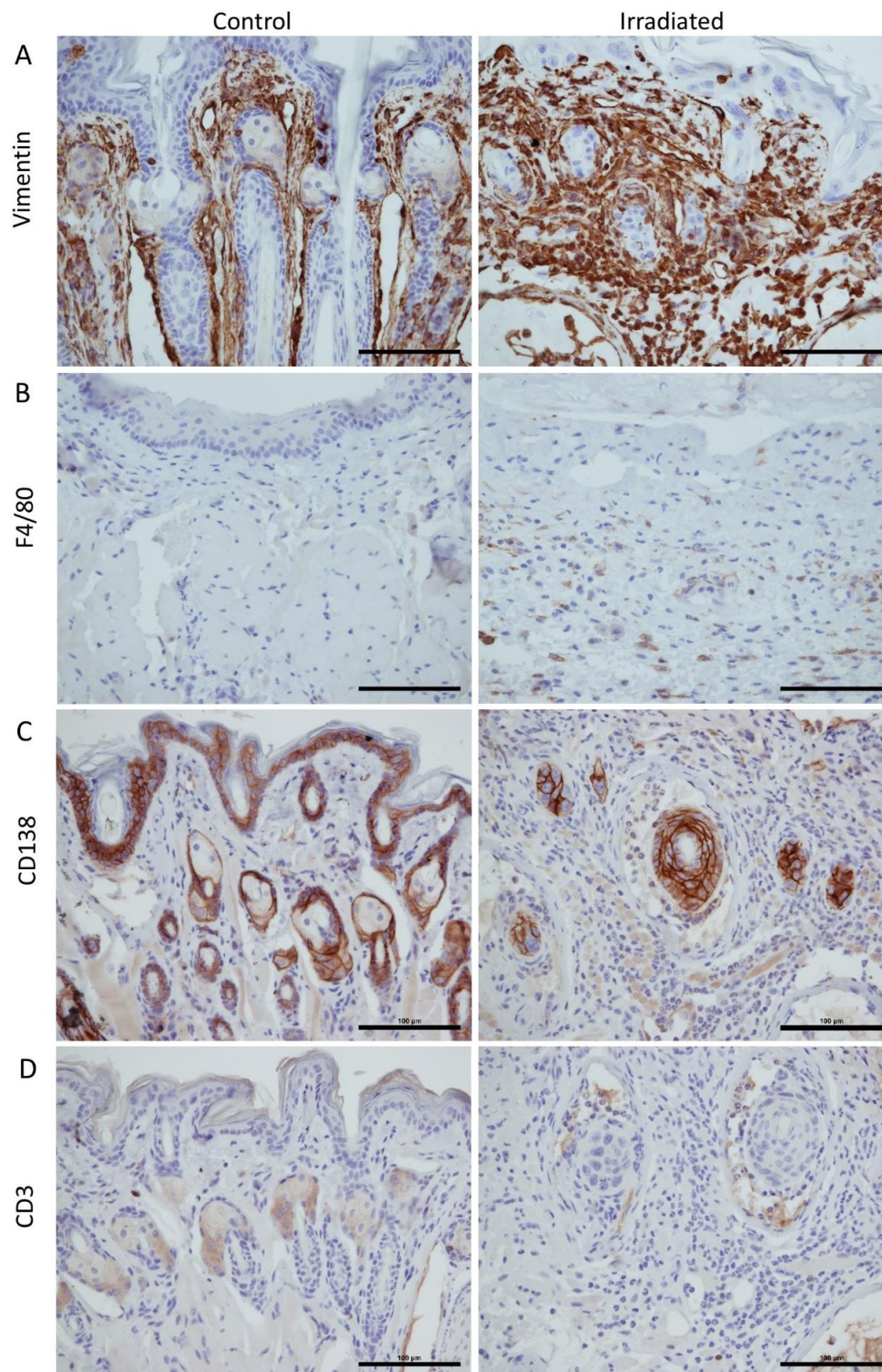
Immunohistochemistry

For immunohistochemistry, tissue sections of $4 \mu\text{m}$ were cut (Leica RM2155 microtome) and placed on microscopy glass slides (Superfrost Plus, Thermo Fisher). Following deparaffination and hydration, heat-induced antigen retrieval was performed using citraconic anhydride pH 7.4, for 15 minutes at 100°C . Primary antibodies against CD138/Syndecan-1 (Rat IgG2a, 1:450), CD3 (Rat IgG1, 1:450), Vimentin (clone EPR3776, Rabbit IgG, 1:500) and F4/80 (clone BM8, Rat IgG2a, #123101, BioLegend) were used. Before incubation with primary antibodies, blocking was performed for 60 minutes at room temperature using Normal Rabbit Serum 5 % (CD138, CD3, F4/80) and Normal Goat Serum 5 % (Vimentin). Next, sections were incubated with primary antibodies over night at 4°C . Negative control was PBS instead of primary antibody. Positive controls were sections of mouse spleen (CD3, CD138, F4/80), plasmacytoma (CD3, CD138) and blood vessels (Vimentin). Furthermore, the sections were washed in PBS for 2×10 minutes and incubated with secondary antibodies for 40 minutes at room temperature. Secondary antibodies used were Rabbit-a-Rat IgG (CD3, CD138, F4/80) and Goat-a-Rabbit IgG (Vimentin). Next, the slides were washed with PBS 2×10 minutes, incubated with biotinylated streptavidin (ABC^{HRP}) for 30 minutes at room temperature, incubated with DAB for 10 minutes at room temperature and washed with PBS. Finally, the slides were stained with Hematoxylin for 30 seconds, dehydrated and mounted with synthetic resin.

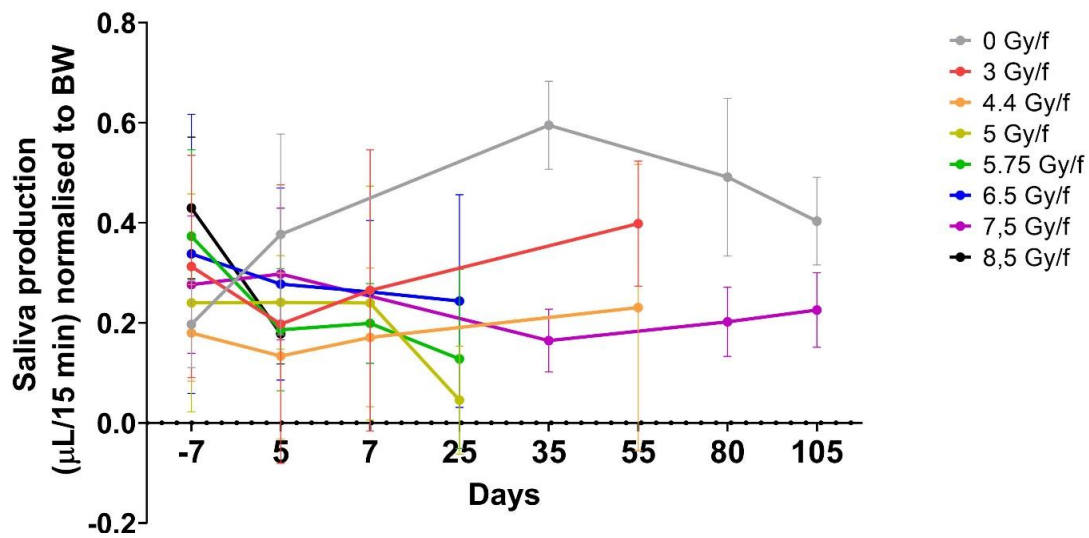
Histological images were acquired using a Nikon DS-Ri1 camera with a CFI Plan Fluor 20x objective (NA 0.5).



Supplementary figure 1. Bodyweight loss greater than 10 % was only seen in the mice exposed to 7.5 and 8.5 Gy/f (black and purple group). Mice receiving 7.5 Gy/f increased in weight and recovered around day 14, while mice receiving 8.5 Gy/f did not recover and was euthanised at day 14. The graphs show mean bodyweight in each group. The number of animals used in each group varied as following 0 Gy/f (n = 9), 3 Gy/f (n = 3), 4.4 Gy/f (n = 3), 5 Gy/f (n = 4), 5.75 Gy/f (n = 4), 6.5 Gy/f (n = 4), 7.5 Gy/f (n = 10), 8.5 Gy/f (n = 10). The black vertical line on the X-axis represent each day of radiation, giving 2 fractions per day.



Supplementary figure 2. **Representative images of immunohistochemically labelled sections of the lower lip in mice after exposure to fractionated irradiation.** (A-B) Irradiated sections showed an increase in Vimentin⁺ cells and F4/80⁺ cells. Fibroblasts as well as neutrophils and lymphocytes are positive for Vimentin, while macrophages in mice are F4/80⁺. (C) CD138 labeled epithelial cells, but showed no increase of plasma cells in the irradiated sections. (D) CD3 labelled the sebaceous glands, but showed no obvious increase of T cells in the irradiated sections. Scale bar is 100 μ m.



Supplementary figure 3. Saliva production measured as μL saliva/15 minutes normalised to bodyweight. Data is represented as mean \pm 95% CI. The number of animals used in each group varied as following 0 Gy/f (n = 9), 3 Gy/f (n = 3), 4.4 Gy/f (n = 3), 5 Gy/f (n = 4), 5.75 Gy/f (n = 4), 6.5 Gy/f (n = 4), 7.5 Gy/f (n = 10), 8.5 Gy/f (n = 10).

References

1. Battistoni G, Boehlen T, Cerutti F *et al.* Overview of the FLUKA code. *Annals of Nuclear Energy*. 2015; **82**: 10-8.
2. Böhlen TT, Cerutti F, Chin MPW *et al.* The FLUKA Code: Developments and Challenges for High Energy and Medical Applications. *Nuclear Data Sheets*. 2014; **120**: 211-4.
3. Battistoni G, Bauer J, Boehlen TT *et al.* The FLUKA Code: An Accurate Simulation Tool for Particle Therapy. *Frontiers in oncology*. 2016; **6**: 116-.
4. Vlachoudis V. *Flair: A powerful but user friendly graphical interface for FLUKA*. United States: American Nuclear Society - ANS; 2009.
5. Schneider W, Bortfeld T, Schlegel W. Correlation between CT numbers and tissue parameters needed for Monte Carlo simulations of clinical dose distributions. *Phys Med Biol*. 2000; **45**(2): 459-78.

Paper II

Cytokine Levels in Saliva Are Associated with Salivary Gland Fibrosis and Hyposalivation in Mice after Fractionated Radiotherapy of the Head and Neck

II

II



Article

Cytokine Levels in Saliva Are Associated with Salivary Gland Fibrosis and Hyposalivation in Mice after Fractionated Radiotherapy of the Head and Neck

Olga Zlygosteva ¹, Inga Solgård Juvkam ², Hans Christian D. Aass ³, Hilde K. Galtung ², Tine M. Søland ^{2,4}, Eirik Malinen ^{1,5,†} and Nina F. J. Edin ^{1,*,†}

¹ Department of Physics, University of Oslo, 0371 Oslo, Norway; olga.zlygosteva@fys.uio.no (O.Z.); eirik.malinen@fys.uio.no (E.M.)

² Institute of Oral Biology, University of Oslo, 0372 Oslo, Norway; i.s.juvkam@odont.uio.no (I.S.J.); hilde.galtung@odont.uio.no (H.K.G.); t.m.soland@odont.uio.no (T.M.S.)

³ The Blood Cell Research Group, Department of Medical Biochemistry, Oslo University Hospital, 0450 Oslo, Norway; h.c.aass@medisin.uio.no

⁴ Department of Pathology, Oslo University Hospital, 0372 Oslo, Norway

⁵ Department of Radiation Biology, Oslo University Hospital, 0379 Oslo, Norway

* Correspondence: n.f.j.edin@fys.uio.no

† These authors contributed equally to this work.

Abstract: Cytokines are mediators of inflammation that could lead to fibrosis. The aim was to monitor cytokine levels in saliva and serum after locally fractionated radiotherapy of the head and neck in mice and investigate associations with salivary gland fibrosis and hyposalivation. C57BL/6 mice were randomized to sham or X-ray irradiation of 66 Gy in 10 fractions over 5 days. Blood and saliva were collected on days −7, 5, 35, 80, and 105 following cytokine analysis. The harvested submandibular salivary gland was assessed for the presence of fibrosis. Decision tree regression analysis was used to investigate whether cytokine levels could predict late endpoints in terms of hyposalivation or fibrosis. Significant formation of fibrosis in gland tissue and reduced saliva production was found after irradiation. The pro-inflammatory cytokines IL-1 α , TNF, TIMP1, G-CSF, KC, and MIP-1 α showed increased levels in saliva in irradiated mice and a strong correlation with late endpoints. The decision tree analysis largely separated controls from irradiated animals, with IL-1 α being the strongest predictor. Pro-inflammatory cytokines in saliva, but not in serum, were associated with late endpoints. This indicates that cytokine expression in saliva is a good biomarker for local salivary gland damage with IL-1 α as the strongest single predictor.

Keywords: cytokines; X-rays; fractionated radiotherapy; normal tissue response; head and neck; salivary glands; fibrosis; mice



Citation: Zlygosteva, O.; Juvkam, I.S.; Aass, H.C.D.; Galtung, H.K.; Søland, T.M.; Malinen, E.; Edin, N.F.J. Cytokine Levels in Saliva Are Associated with Salivary Gland Fibrosis and Hyposalivation in Mice after Fractionated Radiotherapy of the Head and Neck. *Int. J. Mol. Sci.* **2023**, *24*, 15218. <https://doi.org/10.3390/ijms242015218>

Academic Editor: Tunde Szatmari

Received: 18 August 2023

Revised: 13 October 2023

Accepted: 14 October 2023

Published: 16 October 2023



Copyright: © 2023 by the authors. Licensee MDPI, Basel, Switzerland. This article is an open access article distributed under the terms and conditions of the Creative Commons Attribution (CC BY) license (<https://creativecommons.org/licenses/by/4.0/>).

1. Introduction

More than 60% of head and neck (H&N) cancer patients experience salivary gland hypofunction after radiotherapy (RT) [1]. In addition, RT can result in complications such as mucositis, chewing impairment, and oral infections. In general, this may lead to late effects such as pain, dysphagia, and decreased sense of taste, all of which substantially reduce quality of life [2]. Ionizing radiation triggers biological responses in malignant tumors as well as in normal tissues, which can influence the secretion of cytokines and growth factors. These molecules are involved in several processes such as cell–cell signaling and immunomodulation [3–5] and can function in a paracrine, autocrine, or endocrine manner [6,7]. Cytokines have been found to induce both local and systemic responses and are important mediators of both acute and chronic inflammation in normal tissue after irradiation [8]. Chronic inflammation is characterized by coexisting inflammation, tissue injury, and fibrosis [9]. In irradiated tissues, fibrosis is consequential late tissue damage [10–12]

and cytokines may play an important role in its development and manifestation. Therefore, cytokines could potentially be used as diagnostic biomarkers for tissue injuries following RT. Furthermore, they might function as therapeutic targets, or be used as monotherapy or a booster for other therapeutic agents to reduce radiation-induced tissue damage [7].

Modern laboratory techniques allow for measuring cytokines in tissues and various biological fluids at mRNA or protein levels [13]. As cytokines induced by RT are believed to be tissue-specific, several groups have studied various pro-inflammatory (IL-1 α , IL-2, IL-6, TNF, IFN- γ), pro-fibrotic (TGF- β 1), and stem-cell mobilizing (GM-CSF) cytokines in tissues and their correlation with cytokines in blood [14,15]. Biological fluids are generally more straightforward to collect than tissue biopsies and can be repeatedly sampled for screening. However, cytokine levels in fluids should correlate with relevant tissue processes or clinical endpoints in order to be used as surrogate biomarkers [16]. Some clinical and preclinical studies have shown changes in cytokine profiles in blood (serum or plasma) after total body irradiation or local radiation treatment [17–20]. However, only limited data exist on the association between cytokine levels in other biological fluids and clinical endpoints.

For local H&N irradiation, only a small number of clinical and preclinical studies have demonstrated elevated cytokine levels in blood and associations with inflammation and radiation-induced effects, especially salivary gland dysfunction [21,22]. Some clinical studies have reported dysregulated cytokine networks in saliva from H&N cancer patients after RT or in patients with hyposalivation as in Sjögren's syndrome [23–30]. To our knowledge, no studies have monitored cytokine expression in both saliva and blood after irradiation of the H&N region and compared their level of association with late endpoints. Here, we hypothesize that cytokines in saliva are more specific for salivary gland effects after local RT than those in blood. This is because the cytokine background in blood, which reflects normal physiological processes, is expected to dominate over a possible radiation-induced elevation of a limited set of cytokines released from a small irradiated area. Thus, salivary cytokines could be more precise and reliable biomarkers for salivary gland effects after H&N irradiation. Additionally, saliva would be advantageous in screening for irradiation effects due to reduced invasiveness, simplified logistics in sample collection, and higher acceptance by participants in potential clinical trials [31].

The aim of this work was to monitor salivary cytokine levels after local fractionated irradiation of the H&N area in mice and to compare these with cytokines in serum. Furthermore, we aimed to correlate the cytokines with late irradiation effects in salivary glands and to investigate the cytokine profiles as potential biomarkers of late effects in salivary glands.

2. Results

2.1. Cytokine Expression

From the panel of 12 cytokines, 6 were detected at measurable levels in the saliva and serum samples from both irradiated and control groups. The levels of the detected cytokines in saliva at different time points are presented in Figure 1, and all these cytokines showed differences between the irradiated and control groups. Typically, the first time point showing a significant increase in salivary cytokine levels for irradiated animals was day 35. The increase in levels was significant for IL-1 α , TNF, and TIMP-1 in irradiated mice compared to controls on days 35, 80, and 105 after the onset of irradiation. The levels of G-CSF and KC were only significantly higher in the irradiated group on days 35 and 80, while an increase in MIP-1 α was only observed on day 80. In contrast, there was a tendency towards a decrease in IL-1 α , TNF, MIP-1 α , and TIMP-1 levels in saliva from irradiated mice sampled on day 5 (24 h after the last fraction). In serum, only MIP-1 α was significantly decreased in the irradiated mice on days 35, 80, and 105 compared to controls, while the rest of the cytokines did not show any significant changes (Figure S1 in Supplementary Materials).

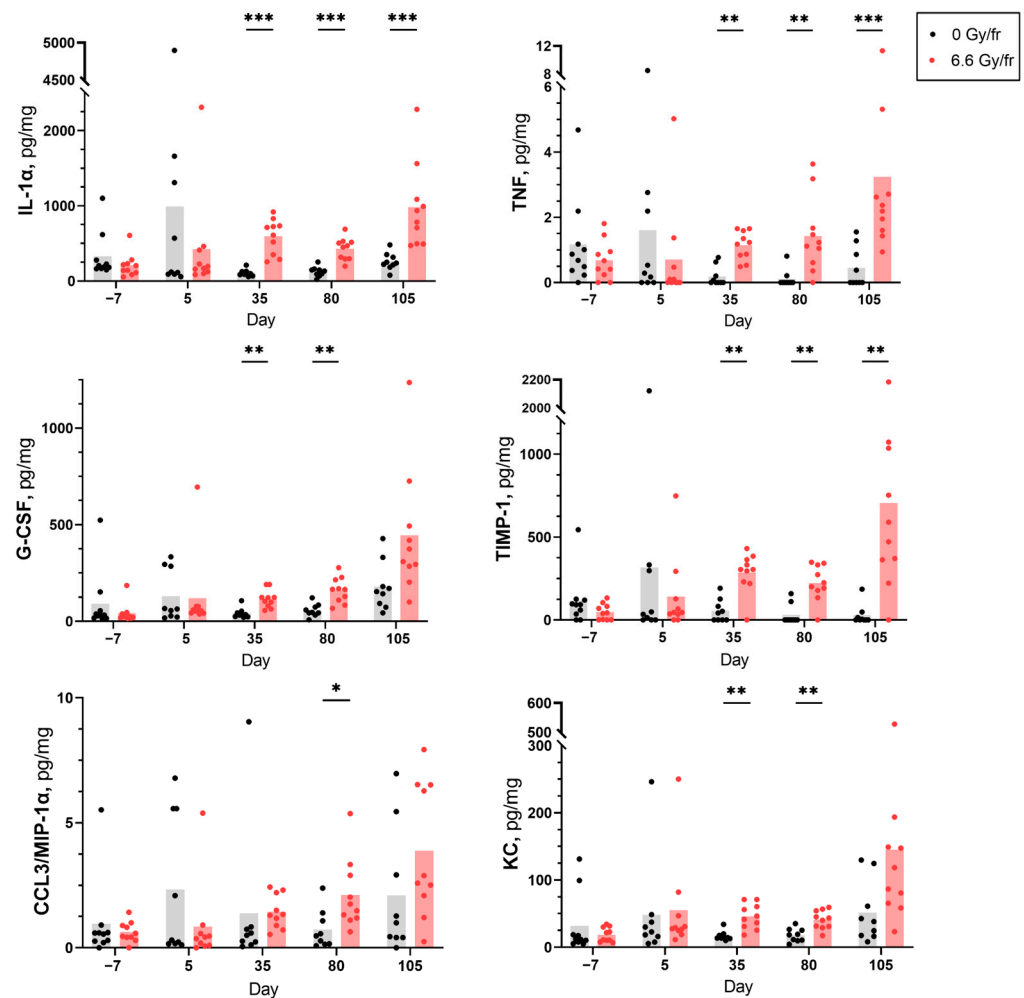


Figure 1. Levels of salivary cytokines IL-1 α , TNF, G-CSF, TIMP-1, MIP-1 α , and KC before and after fractionated irradiation at days -7, 5, 35, 80, and 105 ($n = 9$ in the control group, $n = 10$ in the irradiated group). Each dot represents an individual mouse. Data are presented as mean pg/mL cytokine per total protein mg/mL (* $p < 0.05$, ** $p < 0.01$, *** $p < 0.001$).

2.2. Fibrosis and Saliva Volume

The fraction of fibrotic area in the SMG and the saliva volume, as a measure of salivary gland function, were used as late endpoints (Figure 2). Increased connective tissue around some large SMG ducts and replacement of acinar cells by connective tissue were seen in histological sections (Figure 2a). The fraction of fibrotic area in the SMG was significantly higher in the irradiated mice compared to controls (Figure 2b). The irradiated mice also showed significantly decreased saliva production (Figure 2c).

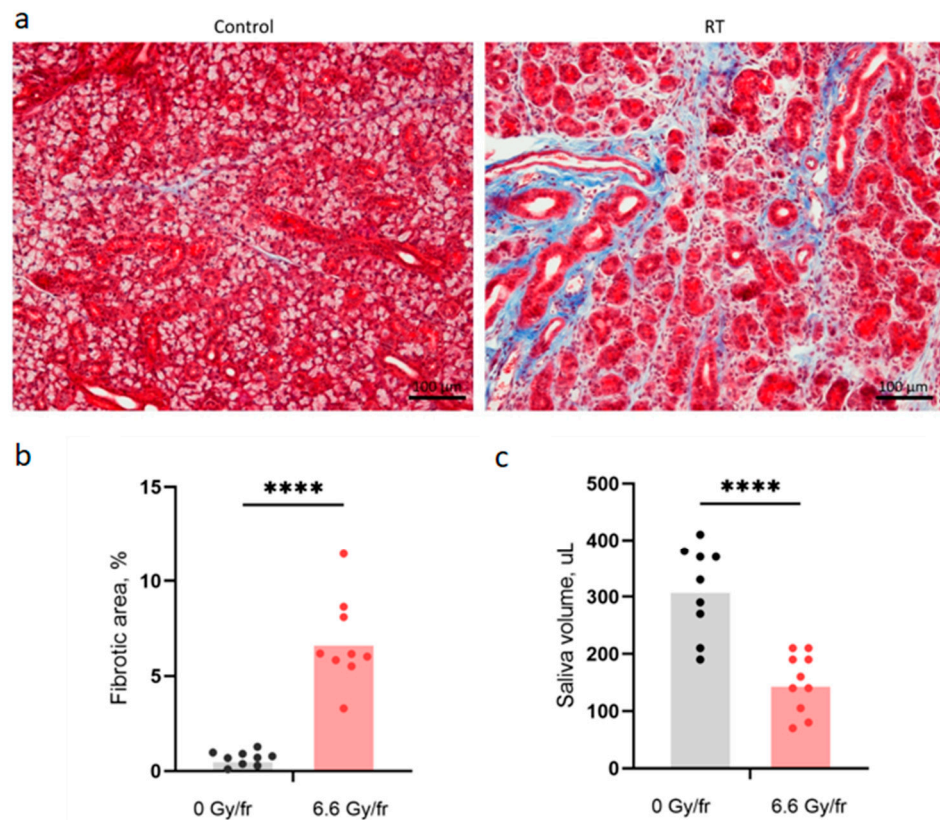


Figure 2. (a) Images of Masson Trichrome stained sections of the submandibular gland (SMG) in control and irradiated mice on day 105 with fibrotic regions in blue. (b) Fibrotic area fraction in SMG. (c) Pooled saliva volume. Each dot represents an individual mouse. Scale bar is 100 μm (**** $p < 0.0001$).

2.3. Correlations between Cytokines and Endpoints

Pearson's correlation between cytokine levels and endpoints (fibrotic area and saliva volume) for both groups was calculated for each time point. Correlation matrices for salivary cytokines at day 35 are shown in Figure 3a,b (correlation matrices for other time points are given in Figure S2 in the Supplementary Materials). At day 35, all cytokines in the control group were positively correlated to each other, while the cytokine levels in the irradiated group seemed to be more independent or weakly correlated. In the correlation matrix combining data from irradiated and control mice, a positive correlation of salivary cytokines with fibrotic area and a negative correlation with saliva volume was found (Figure 3c). For cytokines in serum, correlation matrix is given in Figure S3 in the Supplementary Materials. These correlations are generally lower than for cytokines in saliva.

The mean correlation of the whole cytokine panel with saliva volume and fibrosis for different time points is shown for salivary cytokines (Figure 4a) and serum cytokines (Figure 4b), respectively. As seen, the correlation between cytokines and endpoints is maximal ($r = 0.6$) around day 35. Moreover, correlation curves for fibrosis and hyposalivation are mirror images of each other, reflecting the difference in scoring (high and low levels indicate greater severity for respective endpoints) and that the endpoints are related. Importantly, there was a much stronger correlation between the salivary cytokines and endpoints than between the serum cytokines and endpoints.

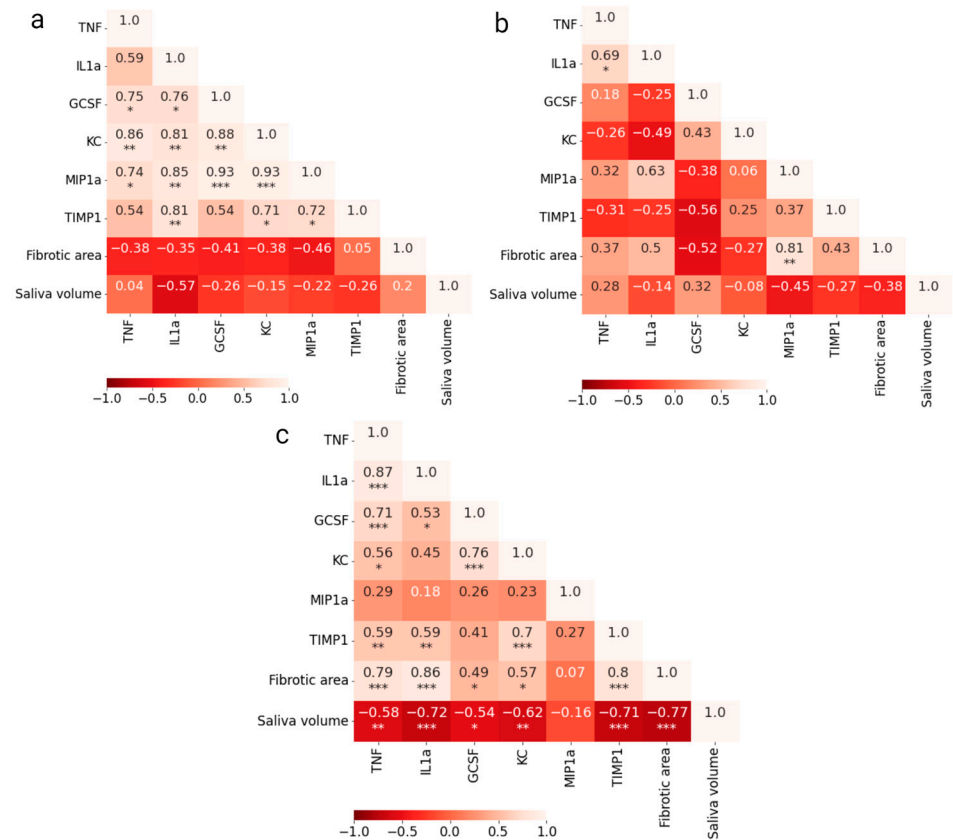


Figure 3. Pearson’s correlation matrix with significance for salivary cytokine levels at day 35 from (a) control mice; (b) irradiated mice; (c) both combined (* $p < 0.05$, ** $p < 0.01$, *** $p < 0.001$).

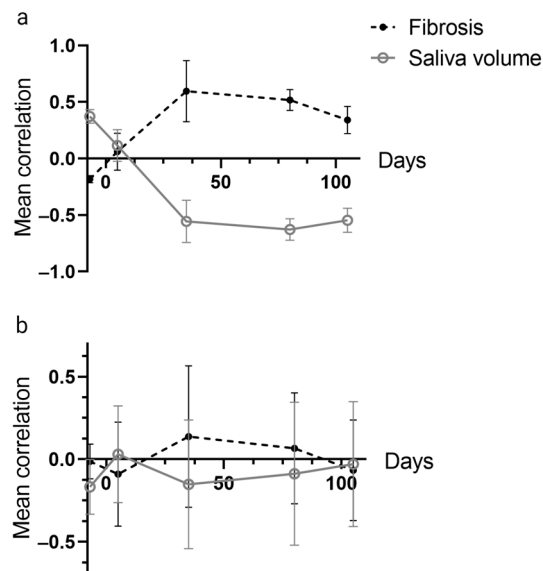


Figure 4. Mean correlation of (a) salivary and (b) serum cytokines with endpoints (fibrosis and saliva volume) at all time points.

2.4. Prediction of Late Effects Based on Early Cytokine Levels

Several of the salivary cytokines were associated with the two endpoints; fibrotic area and saliva volume. The decision tree regression model used all cytokine levels at a given time to predict the endpoints in a leave-one-out-cross-validation procedure. In a predictive assay, early assessment of predictors is pivotal, but cytokine levels at day -7

and day 5 showed no correlation with the endpoints (Figure 4). Thus, cytokines at day 35 were selected for the analysis. In Figure 5, the measured standard score (representing fibrotic area and saliva volume) is plotted against the predicted score. As seen, controls and irradiated animals are largely separated by the prediction model. The RMSE was in this case 0.75, compared to a baseline RMSE of 1.05 for a model where the mean measured overall score was used as the predictor. Separating the RMSEs for fibrotic area and saliva volume gave 0.76 and 0.8, respectively. The prediction using cytokine levels at day 80 or 105 was less good

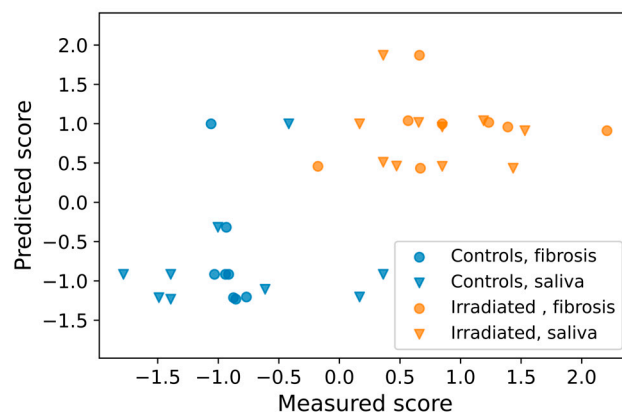


Figure 5. The decision tree prediction model for fibrosis and saliva volume, where the measured score is plotted against the predicted score.

The importance of each cytokine to the prediction model was 0.05, 16.5, 1.02, 1.50, 1.61, and 1.42 (relative units) for TNF, IL-1 α , GC-SF, KC, MIP-1 α , and TIMP1, respectively, indicating that IL-1 α is by far the strongest contributor to the prediction model.

3. Discussion

Irradiation initiates rapid molecular and cellular responses, which include activation of various repair and survival signaling pathways and cytokine secretion, leading to an acute inflammatory reaction in the affected tissues. In addition, radiation-induced changes in gene expression and dysregulated cytokine expression contribute to late tissue responses such as chronic inflammation and fibrosis [15,20]. Most of the cytokines have overlapping functions and can also recruit and activate other cytokines or cell types involved in the fibrotic process, which enhances and complicates the response [14,20].

In order to use cytokines as predictive biomarkers of late effects, it is important to appraise when and where the cytokines are released subsequent to irradiation. We monitored cytokine release into saliva as a function of time after irradiation and correlated the cytokine expression data to two late endpoints; saliva volume and salivary gland fibrosis. In addition, the experiments were designed specifically for studying relevant normal tissue effects after H&N RT using local field compared to other preclinical studies using total body irradiation. The latter might result in lower cytokine secretion, especially in the blood, which makes our approach more clinically relevant.

To our knowledge, this is the first study of changes in cytokine levels in mouse saliva after irradiation. Interestingly, the salivary cytokine levels in the first 24 h after the last fraction were not significantly changed. However, we found an increase in the levels of six salivary cytokines on day 35, and a further increase on days 80 and 105. This is in line with other studies showing persistent waves of cytokine secretion in lung tissue or blood for a prolonged time after partial irradiation [16]. The temporal pattern of cytokine secretion may be explained by the reactivate responses in the tissues to deal with induced damage [3]. For the potential use of cytokine levels as biomarkers for late effects, the early time points for sampling are most relevant (well before the clinical manifestation of endpoints) and we

have, therefore, focused on the salivary cytokine data from day 35 in the correlation and prediction models.

The formation of fibrosis in SMG tissue as well as reduced saliva production were used as endpoints for late effects after irradiation. The SMG was chosen for the assessment of fibrosis because it is the largest salivary gland in mice and, therefore, is easier to dissect in one piece for scoring the irradiated area. The early phases of radiation-induced fibrogenesis are similar to those of wound healing. However, while wound healing involves very early secretion of pro-inflammatory cytokines in blood or irradiated tissue [16,32], our experiments only showed increased levels of the investigated cytokines IL-1 α , TNF, TIMP1, G-CSF, KC, and MIP-1 α in the saliva from irradiated mice after day 35. All these cytokines have been reported to be highly involved in inflammatory responses and fibrosis formation, supporting the theory of cytokine-regulated development of radiation-induced late effects. For instance, IL-1 α and TNF may activate the inflammatory process after irradiation and contribute to fibrosis under chronic inflammation by stimulation of fibroblast proliferation [8,33]. IL-1 is also considered a pro-inflammatory senescence-associated secretory phenotype (SASP) factor [34]. A recent mouse study demonstrated that radiation-induced cellular senescence in the salivary gland stem/progenitor cell (SGSC) niche leads to the secretion of various SASP factors which can contribute to salivary gland dysfunction and fibrosis [34]. As with IL-1 α and TNF, TIMP-1 secretion levels have been found to be elevated in blood under chronic inflammation [35]. Additionally, TIMP-1 has been reported to be strongly associated with radiation-induced lung fibrosis by the induction of macrophage and neutrophil infiltration in lung tissue [36]. KC and MIP-1 α chemokines play a driving role in the inflammatory processes and wound healing by recruiting and activating various types of leukocytes and macrophages [29,37–39]. On the other hand, treatment with G-CSF, which is usually secreted in response to inflammatory stimuli, was found to increase the concentration of bone marrow-derived cells in irradiated salivary glands in mice and improve morphology and function of the salivary gland by reducing the loss of acinar cells [40].

Sjögren's syndrome is an autoimmune disease characterized by progressive destruction and dysfunction of salivary glands in many respects similar to the late effects in salivary glands after irradiation. It is believed that dysregulation of cytokine signaling plays a role in both systemic and exocrine gland manifestations of Sjögren's syndrome [24]. TNF levels in the blood and in lymphocytic infiltrates in salivary gland biopsies have been found to be increased in patients with Sjögren's syndrome compared to controls [41], which was associated with salivary gland hypofunction caused by inflammation [42]. Experiments in mice that mimicked the inflammatory conditions of swollen salivary glands showed that conditional overexpression of TNF levels in salivary gland biopsies led to acinar cell atrophy and hyposalivation [42], which is consistent with our findings but in saliva samples. It was also found that the biopsies from the salivary glands of patients with Sjögren's syndrome expressed higher concentrations of MIP-1 α [43].

The cytokines detected in this work (IL-1 α , TNF, G-CSF, KC, MIP-1 α , and TIMP1) have been found in other mouse studies, though in plasma and tissue samples after single or fractionated photon or proton irradiation [15,17–20]. However, only one study in rats reported a specific cytokine profile including IL-1 α , IL-2, IL-6, IL-10, TNF, IFN- γ , VEGF, and GM-CSF in association with late effects progressing after a 30 Gy single-dose irradiation [15]. In our study, we observed a positive correlation between all cytokines in the control group, while both positive and negative correlations were observed in the irradiated group. This most likely indicates that irradiation-induced processes have led to alterations in the regulation of cytokine secretion. The correlation matrices of salivary cytokines and the two endpoints showed a high mean correlation, although with different signs for the two endpoints (high degree of fibrotic area and low saliva volume indicate decreased salivary gland function). A much stronger correlation between the salivary cytokines with endpoints compared to the serum cytokines supported our hypothesis that serum cytokines are less specific and less sensitive to the local damage of salivary glands

than salivary cytokines. Therefore, saliva has a higher potential to be a reliable biomarker of local radiation-induced salivary gland damage.

Cytokine biomarkers may contribute to predicting or monitoring the response of normal tissues following radiotherapy and can also be of potential use for individualized *in vivo* dosimetry for biologically adaptive radiotherapy [44]. In addition, the biomarker can be employed during treatment to identify the need for preventive treatment of normal tissue toxicities or adjustment of the radiotherapy schedule. However, early prediction of late radiation effects using a panel of cytokines with multiple linear regression may be hampered by multicollinearity and a high risk of overfitting. For identification of potential biomarkers of late effects, we used a combined late effect score including both fibrotic area and saliva volume in a concatenated manner. By this, we generated a more robust endpoint series, which is better suited for a machine learning algorithm such as decision tree regression. Also, we used leave-one-out cross-validation, holding out one animal from the model training in each step. A feature vector based on all cytokines at day 35 was generated. The model gave a clear separation between the irradiated group and the control group but worked better for the fibrotic area than the saliva volume. This is not surprising since there was a larger spread in the saliva volume measurements within the groups and a smaller difference between controls and irradiated animals for saliva volume than for fibrosis. Also, fibrosis within the gland may be more directly linked to irradiation, while hyposalivation may also occur due to various direct and indirect radiation responses such as glandular, ductal, and nerve damage, acinar atrophy, and fibrosis. Notably, the feature importance analysis showed that IL-1 α levels on day 35 were by far the strongest contributor to the prediction model. In contrast, the prediction was poorer when cytokine expression at day 80 or 105 was used in the modeling. This indicates that IL-1 α expression around day 35 is highly involved in the pathological processes leading to fibrosis and hyposalivation. Therefore, inhibition of IL-1 α might be considered as potential intervention target to mitigate radiation-induced fibrosis, but more studies should be conducted to elucidate the mechanisms of cytokine regulation. Furthermore, in a human population, this time point might be different and must be identified using a similar methodology as in the current work.

4. Materials and Methods

The procedures, protocols, and set-up for local H&N irradiation of mice have previously been reported in detail [45].

4.1. Animals, Irradiation, and Follow-Up

C57BL/6J female mice from Janvier (France) were used. All experiments were performed in accordance with directive 2010/63/EU on the protection of animals used for scientific purposes and approved by the Norwegian Food Safety Authority (ID 27931). The animals were 12 weeks old at the onset of experiments.

X-ray treatment was given in 10 fractions over 5 days (twice a day with an 8 h difference) using a Faxitron Multirad225 irradiation system (Faxitron Bioptics, Tucson, AZ, USA) with the following settings: 100 kV X-ray voltage, 15 mA current, and 2.0 mm Al filter. The dose rate was 0.66 Gy/min. For irradiation, the mice were anesthetized using Sevoflurane 4% in O₂, positioned on the right side in a foam holder, and irradiated with the X-ray beam coming from the left. The radiation field included the oral cavity, pharynx, and major salivary glands and was defined by the lead collimator with a 25 × 20 mm opening to avoid the exposure of the eyes and brain.

Twenty female mice were randomly assigned to either sham treatment or 10 × 6.6 Gy ($n = 10$ for each treatment group). The reported tissue dose is the mean dose calculated at the midpoint of the X-ray path through the mouse. The experimental timeline with data collection and processing overview is presented in Figure 6. On day -7, blood and saliva sampling were performed in all animals as baseline measurements. On days 0–4, fractionated treatment was given twice a day to the irradiation group, as explained above.

Additional blood and saliva samplings were performed on days 5 (the day after the completion of irradiation), 35, 80, and 105 before termination. Blood and saliva samples were used for cytokine analysis (see below). The follow-up period in this study was 105 days to encompass the manifestation of both early and late radiation-induced tissue effects. During the follow-up period, the animal appearance (out-field), body weight loss (max 20% from baseline), and skin/oral mucosa (in-field) scores were used as humane endpoints. Upon the development of moderate to severe early effects, DietGel[®] (ClearH₂O, Westbrook, ME, USA) was provided to support the recovery, and analgesic treatment of buprenorphine (Temgesic, Indivior, Richmond, VA, USA) by subcutaneous injections was given to all mice for 4 days (day 12 to day 15, first injection after blood and saliva sampling) to alleviate the pain.

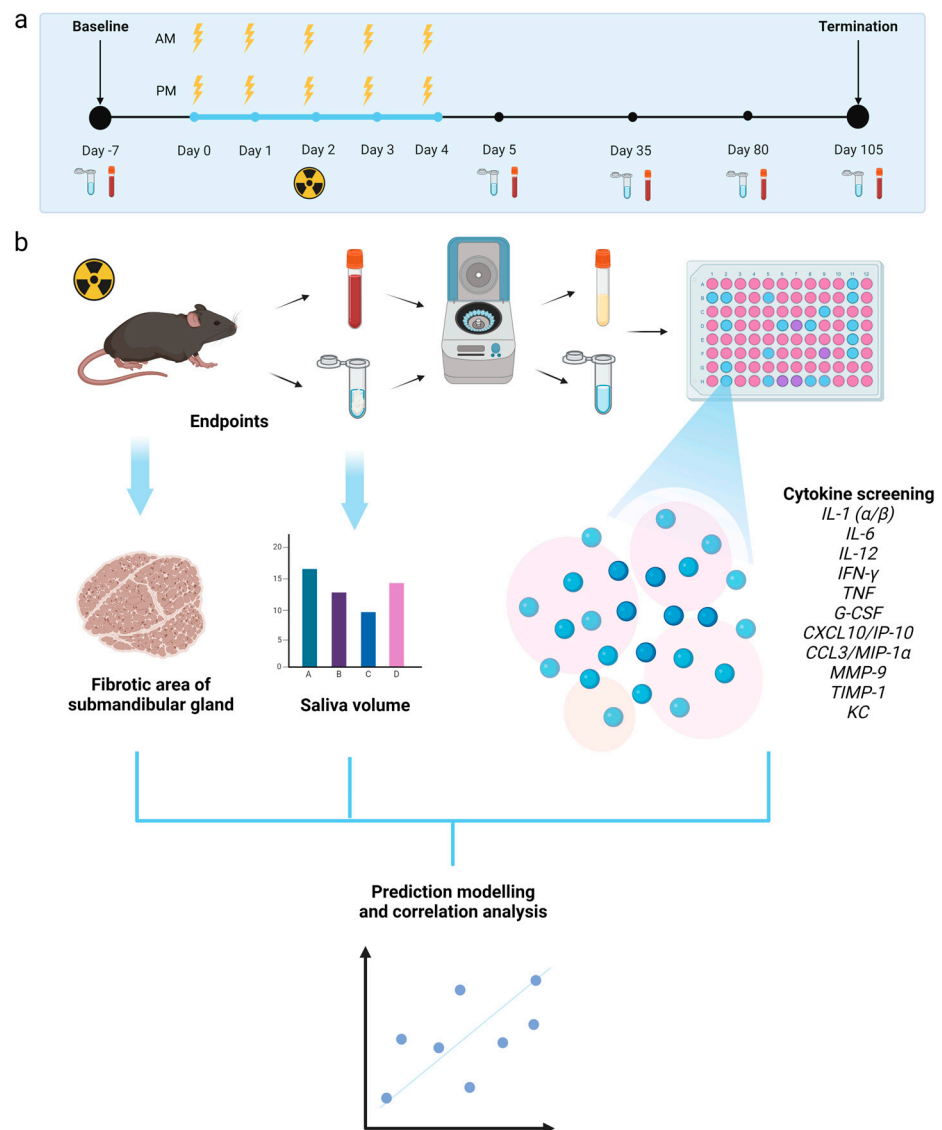


Figure 6. (a) Timeline of the experiment. (b) General overview of data collection and processing. Created with [BioRender.com](https://www.biorender.com) (accessed on 6 October 2023).

Mice were euthanized through an overdose of anesthetic (Pentobarbitol, Exagon[®] Vet, Richter Pharma AG, Wels, Austria) by intraperitoneal injection under terminal anesthesia to avoid H&N tissue damage from cervical dislocation. The left submandibular gland (SMG) in each animal was harvested and fixed in 10% formalin before undergoing dehydration and paraffin embedding. The SMG was used to quantify radiation-induced fibrosis since

this gland is the largest salivary gland in mice with a mixed serous and mucous secretion. Saliva volume and fibrotic area of SMG were used as endpoints of late effects in this study.

4.2. Blood and Saliva Sampling

Blood from the tail vein was collected into serum microvette tubes (Microvette, Sarstedt). The samples were centrifuged at $1000\times g$ and $4\text{ }^{\circ}\text{C}$ for 15 min, and the separated serum was stored at $-80\text{ }^{\circ}\text{C}$. Saliva collection was performed as previously described [46]. Briefly, 0.375 mg/kg of pilocarpine (Pilocarpine hydrochloride, Sigma-Aldrich Inc., St. Louis, MO, USA) was intraperitoneally administered to the mice under anesthesia to stimulate saliva production. Saliva was collected into a cotton swab for 15 min, which was then centrifuged at $7500\times g$ and $4\text{ }^{\circ}\text{C}$ for 2 min. The obtained volume was measured and stored at $-80\text{ }^{\circ}\text{C}$ until cytokine analysis. For saliva volume estimates, data from days 80 and 105 were pooled because of inter-animal variations due to the limited number of animals per group.

4.3. Cytokine and Chemokine Analysis

Serum and saliva samples were thawed on ice, vortexed, and spun down at $16,000\times g$ for 5 min at $4\text{ }^{\circ}\text{C}$. The samples were diluted (serum 1:1 and saliva 2:1) with the RD1-W buffer (R&D Systems, Abington, UK). All samples were analyzed with the custom-made 12-plex Luminex Mouse Discovery Assay kit (<http://www.biotechne.com/g8AnddcM> (accessed on 31 March 2022)) including CCL3/MIP-1 α , KC, IP-10, G-CSF, IFN- γ , IL-1 α , IL-1 β , IL-6, IL-12 p70, MMP-9, TIMP-1, and TNF (Bio-Techne Ltd., Abington, UK). The plates with saliva samples were incubated overnight. A Luminex IS 200 instrument (Bio-Rad, Hercules, CA, USA) was used to record data. IL-1 β , IL-6, IP-10, or IFN- γ were below the level of detection in saliva samples, while MMP-9 was excluded for both serum and saliva samples as the data were above the standard curve. Due to high background levels, IL-12 p70 was also excluded from the cytokine panel. Total protein concentrations in saliva samples were measured in mg/mL using spectrophotometry (Absorbance 280 nm, NanoDrop 2000c, Thermo Fisher Scientific, Waltham, MA, USA). The salivary cytokine levels were adjusted to total protein concentration and presented as (pg of cytokine)/(mg of total protein).

4.4. Quantitative Analysis of Fibrosis

A central section ($6\text{ }\mu\text{m}$) of each SMG was stained with Masson Trichrome (Trichrome Stain kit, abcam) according to the protocol from the manufacturer. Images of the stained sections were acquired using a Nikon DS-Ri1 camera with a CFI Plan Fluor $10\times$ objective (NA 0.30). The percentage of fibrotic area (blue area in Figure 3a) relative to the total area was extracted by thresholding in ImageJ based on 8–11 images of the SMG from each mouse. One irradiated SMG was excluded as the stained section did not encompass the entire gland tissue. The percentage of fibrotic area in each SMG was termed the fibrosis score.

4.5. Prediction of Late Effects Based on Cytokine Levels

Python (v3.9.13) together with scikit-learn [47] was used to investigate whether cytokine levels could predict late effects in terms of hyposalivation or fibrosis. A per-day feature matrix was generated, consisting of cytokine levels per mouse converted to a standard score with a mean of zero and a standard deviation of unity for each cytokine. An endpoint vector was generated by concatenating the standard score vector for fibrotic area and saliva volume. The saliva volume vector was negated in order to align this score with that of the fibrotic area (a high value means a worse outcome). Decision tree regression with three nodes was used with the feature matrix as the dependent variable and the concatenated endpoint vector as the independent variable. Leave-one-out-cross-validation with the calculation of root-mean-square error (RMSE) was used to evaluate the prediction performance. The contribution of each cytokine to the final model was evaluated in terms of Breiman's feature importance metric.

4.6. Statistical Analysis

Statistical analysis was performed using Prism 8 for Windows (Version 8.3.0, GraphPad Software, Boston, MA, USA) and Python 3.9.13. A significance level of 0.05 was used for all analyses. Pearson's correlation was used to measure the strength and direction of a linear relationship between cytokine concentrations and/or endpoints.

5. Conclusions

To our knowledge, this is the first study monitoring both salivary and serum cytokines after H&N irradiation. A differential secretion of cytokines was detected in saliva from irradiated mice compared to the controls. The majority of the investigated salivary cytokines showed increased levels from day 35 after irradiation. A strong correlation between salivary cytokine levels and late endpoints was found, while cytokines from serum were only weakly correlated with the endpoints. Decision tree regression identified IL-1 α as the strongest contributor with respect to the prediction of late endpoints, indicating that this cytokine might be a key in the pathological processes leading to fibrosis and hyposalivation.

Supplementary Materials: The following supporting information can be downloaded at: <https://www.mdpi.com/article/10.3390/ijms242015218/s1>.

Author Contributions: Conceptualization, H.K.G., T.M.S., N.F.J.E. and E.M.; methodology, O.Z., I.S.J. and E.M.; formal analysis, O.Z. and I.S.J.; investigation, O.Z., I.S.J. and H.C.D.A.; writing—original draft preparation, O.Z.; writing—review and editing, I.S.J., H.C.D.A., H.K.G., T.M.S., N.F.J.E. and E.M.; visualization, O.Z.; supervision, H.K.G., T.M.S., N.F.J.E. and E.M.; project administration, E.M.; funding acquisition, N.F.J.E. and E.M. All authors have read and agreed to the published version of the manuscript.

Funding: This research was funded by UiO: Life Science at the University of Oslo under grant reference 2018/10221 and South-Eastern Norway Regional Health Authority under grant number 2019050.

Institutional Review Board Statement: The animal study protocol was approved by the Norwegian Food Safety Authority (ID 27931, 9 July 2021).

Informed Consent Statement: Not applicable.

Data Availability Statement: The data presented in this study are available on request from the corresponding author.

Conflicts of Interest: The authors declare no conflict of interest. The funders had no role in the design of the study; in the collection, analyses, or interpretation of data; in the writing of the manuscript; or in the decision to publish the results.

References

1. Mercadante, V.; Al Hamad, A.; Lodi, G.; Porter, S.; Fedele, S. Interventions for the management of radiotherapy-induced xerostomia and hyposalivation: A systematic review and meta-analysis. *Oral Oncol.* **2017**, *66*, 64–74. [[CrossRef](#)]
2. Jasmer, K.J.; Gilman, K.E.; Munoz Forti, K.; Weisman, G.A.; Limesand, K.H. Radiation-Induced Salivary Gland Dysfunction: Mechanisms, Therapeutics and Future Directions. *J. Clin. Med.* **2020**, *9*, 4095. [[CrossRef](#)]
3. Schaeue, D.; Kachikwu, E.L.; McBride, W.H. Cytokines in radiobiological responses: A review. *Radiat. Res.* **2012**, *178*, 505–523. [[CrossRef](#)]
4. Di Maggio, F.M.; Minafra, L.; Forte, G.I.; Cammarata, F.P.; Lio, D.; Messa, C.; Gilardi, M.C.; Bravata, V. Portrait of inflammatory response to ionizing radiation treatment. *J. Inflamm.* **2015**, *12*, 14. [[CrossRef](#)]
5. Stewart, F.A.; Dorr, W. Milestones in normal tissue radiation biology over the past 50 years: From clonogenic cell survival to cytokine networks and back to stem cell recovery. *Int. J. Radiat. Biol.* **2009**, *85*, 574–586. [[CrossRef](#)]
6. Arango Duque, G.; Descoteaux, A. Macrophage cytokines: Involvement in immunity and infectious diseases. *Front. Immunol.* **2014**, *5*, 491. [[CrossRef](#)]
7. Palata, O.; Hradilova Podzimekova, N.; Nedvedova, E.; Umprecht, A.; Sadilkova, L.; Palova Jelinkova, L.; Spisek, R.; Adkins, I. Radiotherapy in Combination with Cytokine Treatment. *Front. Oncol.* **2019**, *9*, 367. [[CrossRef](#)]
8. Kim, J.H.; Jenrow, K.A.; Brown, S.L. Mechanisms of radiation-induced normal tissue toxicity and implications for future clinical trials. *Radiat. Oncol. J.* **2014**, *32*, 103–115. [[CrossRef](#)]
9. Hoda, S.A.; Cheng, E. Robbins Basic Pathology. *Am. J. Clin. Pathol.* **2017**, *148*, 557. [[CrossRef](#)]
10. McBride, W.H.; Schaeue, D. Radiation-induced tissue damage and response. *J. Pathol.* **2020**, *250*, 647–655. [[CrossRef](#)]

11. Westbury, C.B.; Yarnold, J.R. Radiation fibrosis—Current clinical and therapeutic perspectives. *Clin. Oncol.* **2012**, *24*, 657–672. [[CrossRef](#)] [[PubMed](#)]
12. Straub, J.M.; New, J.; Hamilton, C.D.; Lominska, C.; Shnyder, Y.; Thomas, S.M. Radiation-induced fibrosis: Mechanisms and implications for therapy. *J. Cancer Res. Clin. Oncol.* **2015**, *141*, 1985–1994. [[CrossRef](#)] [[PubMed](#)]
13. Tsang, M.L.; Weatherbee, J.A. Cytokine assays and their limitations. *Aliment. Pharmacol. Ther.* **1996**, *10* (Suppl. S2), 55–61; discussion 62. [[CrossRef](#)]
14. Stone, H.B.; Coleman, C.N.; Anscher, M.S.; McBride, W.H. Effects of radiation on normal tissue: Consequences and mechanisms. *Lancet Oncol.* **2003**, *4*, 529–536. [[CrossRef](#)] [[PubMed](#)]
15. Gallet, P.; Phulpin, B.; Merlin, J.L.; Leroux, A.; Bravetti, P.; Mecellem, H.; Tran, N.; Dolivet, G. Long-term alterations of cytokines and growth factors expression in irradiated tissues and relation with histological severity scoring. *PLoS ONE* **2011**, *6*, e29399. [[CrossRef](#)] [[PubMed](#)]
16. Lierova, A.; Jelicova, M.; Nemcova, M.; Proksova, M.; Pejchal, J.; Zarybnicka, L.; Sinkorova, Z. Cytokines and radiation-induced pulmonary injuries. *J. Radiat. Res.* **2018**, *59*, 709–753. [[CrossRef](#)]
17. Nielsen, S.; Bassler, N.; Grzanka, L.; Swakon, J.; Olko, P.; Horsman, M.R.; Sorensen, B.S. Proton scanning and X-ray beam irradiation induce distinct regulation of inflammatory cytokines in a preclinical mouse model. *Int. J. Radiat. Biol.* **2020**, *96*, 1238–1244. [[CrossRef](#)]
18. Cunningham, S.; McCauley, S.; Vairamani, K.; Speth, J.; Girdhani, S.; Abel, E.; Sharma, R.A.; Perentesis, J.P.; Wells, S.I.; Mascia, A.; et al. FLASH Proton Pencil Beam Scanning Irradiation Minimizes Radiation-Induced Leg Contracture and Skin Toxicity in Mice. *Cancers* **2021**, *13*, 1012. [[CrossRef](#)]
19. Ha, C.T.; Li, X.H.; Fu, D.; Moroni, M.; Fisher, C.; Arnott, R.; Srinivasan, V.; Xiao, M. Circulating interleukin-18 as a biomarker of total-body radiation exposure in mice, minipigs, and nonhuman primates (NHP). *PLoS ONE* **2014**, *9*, e109249. [[CrossRef](#)]
20. Ao, X.; Zhao, L.; Davis, M.A.; Lubman, D.M.; Lawrence, T.S.; Kong, F.M. Radiation produces differential changes in cytokine profiles in radiation lung fibrosis sensitive and resistant mice. *J. Hematol. Oncol.* **2009**, *2*, 6. [[CrossRef](#)]
21. Huynh, T.T.M.; Aass, H.C.D.; Falk, R.S.; Astrup, G.L.; Helland, A.; Bjoro, T.; Bjordal, K.; Dale, E.; Hellebust, T.P.; Herlofson, B.B.; et al. Associations between patient-reported late effects and systemic cytokines in long-term survivors of head and neck cancer treated with radiotherapy. *J. Cancer Surviv.* **2022**, *17*, 1082–1093. [[CrossRef](#)]
22. Gruber, S.; Bozsaky, E.; Roitinger, E.; Schwarz, K.; Schmidt, M.; Dorr, W. Early inflammatory changes in radiation-induced oral mucositis: Effect of pentoxifylline in a mouse model. *Strahlenther. Onkol.* **2017**, *193*, 499–507. [[CrossRef](#)]
23. Bossi, P.; Bergamini, C.; Miceli, R.; Cova, A.; Orlandi, E.; Resteghini, C.; Locati, L.; Alfieri, S.; Imbimbo, M.; Granata, R.; et al. Salivary Cytokine Levels and Oral Mucositis in Head and Neck Cancer Patients Treated with Chemotherapy and Radiation Therapy. *Int. J. Radiat. Oncol. Biol. Phys.* **2016**, *96*, 959–966. [[CrossRef](#)]
24. Roescher, N.; Tak, P.P.; Illei, G.G. Cytokines in Sjogren’s syndrome: Potential therapeutic targets. *Ann. Rheum. Dis.* **2010**, *69*, 945–948. [[CrossRef](#)]
25. Ohyama, K.; Moriyama, M.; Hayashida, J.N.; Tanaka, A.; Maehara, T.; Ieda, S.; Furukawa, S.; Ohta, M.; Imabayashi, Y.; Nakamura, S. Saliva as a potential tool for diagnosis of dry mouth including Sjogren’s syndrome. *Oral Dis.* **2015**, *21*, 224–231. [[CrossRef](#)]
26. Schapher, M.; Wendler, O.; Groschl, M. Salivary cytokines in cell proliferation and cancer. *Clin. Chim. Acta* **2011**, *412*, 1740–1748. [[CrossRef](#)]
27. Russo, N.; Bellile, E.; Murdoch-Kinch, C.A.; Liu, M.; Eisbruch, A.; Wolf, G.T.; D’Silva, N.J. Cytokines in saliva increase in head and neck cancer patients after treatment. *Oral Surg. Oral Med. Oral Pathol. Oral Radiol.* **2016**, *122*, 483–490 e481. [[CrossRef](#)]
28. Kang, E.H.; Lee, Y.J.; Hyon, J.Y.; Yun, P.Y.; Song, Y.W. Salivary cytokine profiles in primary Sjogren’s syndrome differ from those in non-Sjogren sicca in terms of TNF-alpha levels and Th-1/Th-2 ratios. *Clin. Exp. Rheumatol.* **2011**, *29*, 970–976.
29. Aqrabi, L.A.; Chen, X.; Hynne, H.; Amdal, C.; Reppe, S.; Aass, H.C.D.; Rykke, M.; Hove, L.H.; Young, A.; Herlofson, B.B.; et al. Cytokines Explored in Saliva and Tears from Radiated Cancer Patients Correlate with Clinical Manifestations, Influencing Important Immunoregulatory Cellular Pathways. *Cells* **2020**, *9*, 2050. [[CrossRef](#)]
30. Chen, X.; Aqrabi, L.A.; Utheim, T.P.; Tashbayev, B.; Utheim, Ø.A.; Reppe, S.; Hove, L.H.; Herlofson, B.B.; Singh, P.B.; Palm, Ø.; et al. Elevated cytokine levels in tears and saliva of patients with primary Sjögren’s syndrome correlate with clinical ocular and oral manifestations. *Sci. Rep.* **2019**, *9*, 7319. [[CrossRef](#)]
31. Pernot, E.; Cardis, E.; Badie, C. Usefulness of saliva samples for biomarker studies in radiation research. *Cancer Epidemiol. Biomark. Prev.* **2014**, *23*, 2673–2680. [[CrossRef](#)]
32. Bentzen, S.M. Preventing or reducing late side effects of radiation therapy: Radiobiology meets molecular pathology. *Nat. Rev. Cancer* **2006**, *6*, 702–713. [[CrossRef](#)]
33. Cooper, J.S.; Fu, K.; Marks, J.; Silverman, S. Late effects of radiation therapy in the head and neck region. *Int. J. Radiat. Oncol. Biol. Phys.* **1995**, *31*, 1141–1164. [[CrossRef](#)]
34. Peng, X.; Wu, Y.; Brouwer, U.; van Vliet, T.; Wang, B.; Demaria, M.; Barazzuol, L.; Coppes, R.P. Cellular senescence contributes to radiation-induced hyposalivation by affecting the stem/progenitor cell niche. *Cell Death Dis.* **2020**, *11*, 854. [[CrossRef](#)]
35. Siva, S.; MacManus, M.; Kron, T.; Best, N.; Smith, J.; Lobachevsky, P.; Ball, D.; Martin, O. A pattern of early radiation-induced inflammatory cytokine expression is associated with lung toxicity in patients with non-small cell lung cancer. *PLoS ONE* **2014**, *9*, e109560. [[CrossRef](#)]

36. Yu, H.H.; Chengchuan Ko, E.; Chang, C.L.; Yuan, K.S.; Wu, A.T.H.; Shan, Y.S.; Wu, S.Y. Fucoidan Inhibits Radiation-Induced Pneumonitis and Lung Fibrosis by Reducing Inflammatory Cytokine Expression in Lung Tissues. *Mar. Drugs* **2018**, *16*, 392. [[CrossRef](#)]
37. Cuello, C.; Palladinetti, P.; Tedla, N.; Di Girolamo, N.; Lloyd, A.R.; McCluskey, P.J.; Wakefield, D. Chemokine expression and leucocyte infiltration in Sjogren's syndrome. *Br. J. Rheumatol.* **1998**, *37*, 779–783. [[CrossRef](#)]
38. Schroder, S.; Kriesen, S.; Paape, D.; Hildebrandt, G.; Manda, K. Modulation of Inflammatory Reactions by Low-Dose Ionizing Radiation: Cytokine Release of Murine Endothelial Cells Is Dependent on Culture Conditions. *J. Immunol. Res.* **2018**, *2018*, 2856518. [[CrossRef](#)]
39. Son, D.S.; Parl, A.K.; Rice, V.M.; Khabele, D. Keratinocyte chemoattractant (KC)/human growth-regulated oncogene (GRO) chemokines and pro-inflammatory chemokine networks in mouse and human ovarian epithelial cancer cells. *Cancer Biol. Ther.* **2007**, *6*, 1302–1312. [[CrossRef](#)]
40. Lombaert, I.M.; Brunsting, J.F.; Wierenga, P.K.; Kampinga, H.H.; de Haan, G.; Coppes, R.P. Cytokine treatment improves parenchymal and vascular damage of salivary glands after irradiation. *Clin. Cancer Res.* **2008**, *14*, 7741–7750. [[CrossRef](#)]
41. Roescher, N.; Tak, P.P.; Illei, G.G. Cytokines in Sjogren's syndrome. *Oral Dis.* **2009**, *15*, 519–526. [[CrossRef](#)]
42. Limaye, A.; Hall, B.E.; Zhang, L.; Cho, A.; Prochazkova, M.; Zheng, C.; Walker, M.; Adewusi, F.; Burbelo, P.D.; Sun, Z.J.; et al. Targeted TNF-alpha Overexpression Drives Salivary Gland Inflammation. *J. Dent. Res.* **2019**, *98*, 713–719. [[CrossRef](#)]
43. Bhavsar, I.; Miller, C.S.; Al-Sabbagh, M. Macrophage Inflammatory Protein-1 Alpha (MIP-1 alpha)/CCL3: As a Biomarker. In *General Methods in Biomarker Research and Their Applications*; Springer: Berlin/Heidelberg, Germany, 2015; pp. 223–249. [[CrossRef](#)]
44. Bentzen, S.M.; Parliament, M.; Deasy, J.O.; Dicker, A.; Curran, W.J.; Williams, J.P.; Rosenstein, B.S. Biomarkers and surrogate endpoints for normal-tissue effects of radiation therapy: The importance of dose-volume effects. *Int. J. Radiat. Oncol. Biol. Phys.* **2010**, *76*, S145–S150. [[CrossRef](#)]
45. Juvkam, I.S.; Zlygosteva, O.; Arous, D.; Galtung, H.K.; Malinen, E.; Seland, T.M.; Edin, N.J. A preclinical model to investigate normal tissue damage following fractionated radiotherapy to the head and neck. *J. Radiat. Res.* **2022**, *64*, 44–52. [[CrossRef](#)]
46. Bagavant, H.; Trzeciak, M.; Papinska, J.; Biswas, I.; Dunkleberger, M.L.; Sosnowska, A.; Deshmukh, U.S. A Method for the Measurement of Salivary Gland Function in Mice. *J. Vis. Exp.* **2018**, *131*, e57203. [[CrossRef](#)]
47. Pedregosa, F.; Varoquaux, G.; Gramfort, A.; Michel, V.; Thirion, B.; Grisel, O.; Blondel, M.; Prettenhofer, P.; Weiss, R.; Dubourg, V.; et al. Scikit-learn: Machine learning in python. *J. Mach. Learn. Res.* **2011**, *12*, 2825–2830.

Disclaimer/Publisher's Note: The statements, opinions and data contained in all publications are solely those of the individual author(s) and contributor(s) and not of MDPI and/or the editor(s). MDPI and/or the editor(s) disclaim responsibility for any injury to people or property resulting from any ideas, methods, instructions or products referred to in the content.

Cytokine levels in saliva are associated with salivary gland fibrosis and hyposalivation in mice after fractionated radiotherapy of the head and neck

Supplementary figures

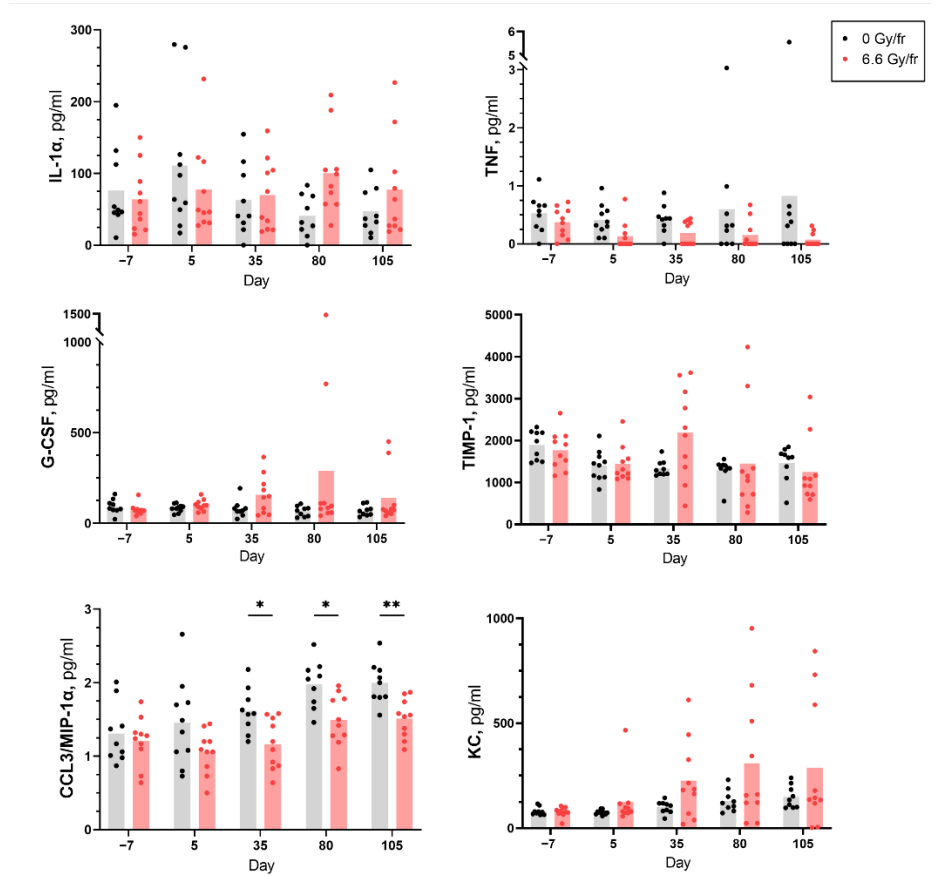


Figure S1. Levels of serum cytokines IL-1 α , TNF, G-CSF, TIMP-1, MIP-1 α and KC before and after fractionated irradiation at days -7, 5, 35, 80 and 105 (n = 9 in the control group, n = 10 in the irradiated group). Each dot represents an individual mouse. Data are presented as mean pg/mL cytokine (*p<0.05, **p<0.01).

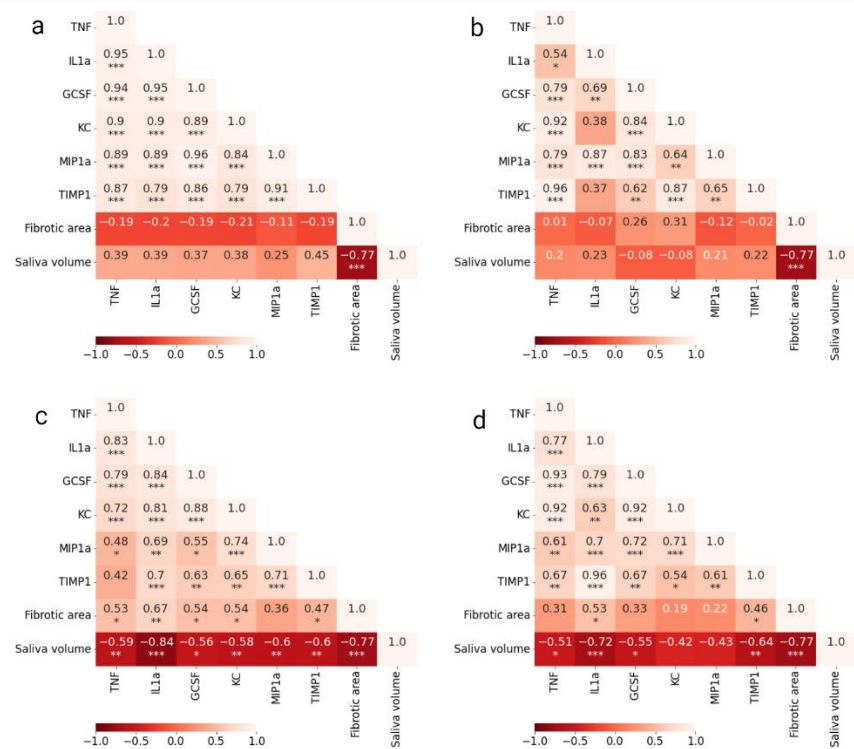


Figure S2. Pearson's correlation matrix with significance for combined (controls and irradiated) salivary cytokine expression on: (a) baseline, (b) day 5, (c) day 80, (d) day 105 (*p<0.05, **p<0.01, ***p<0.001).

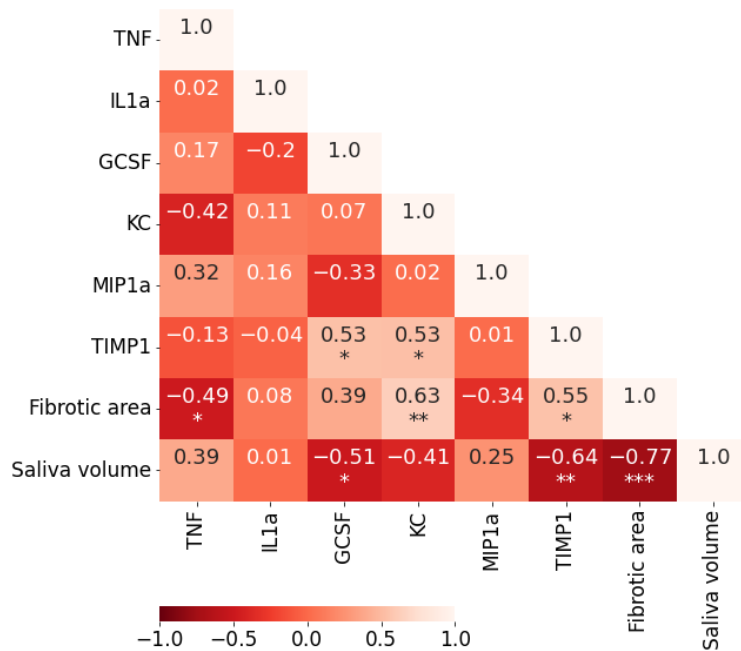


Figure S3. Pearson's correlation matrix with significance for combined cytokine levels in serum on day 35 (*p<0.05, **p<0.01, ***p<0.001).


Paper III

Acute normal tissue responses in a murine model following fractionated irradiation of the head and neck with protons or X-rays

III

III

Acute normal tissue responses in a murine model following fractionated irradiation of the head and neck with protons or X-rays

Olga Zlygosteva^{a*} , Inga Solgård Juvkam^{b*}, Delmon Arous^c, Mateusz Sitarz^d, Brita Singers Sørensen^{d,e}, Christina Ankjærgaard^f, Claus E. Andersen^f, Hilde Kanli Galtung^b, Tine Merete Søland^{b,g}, Nina Jeppesen Edin^{a†} and Eirik Malinen^{a,c†}

^aDepartment of Physics, Faculty of Mathematics and Natural Sciences, University of Oslo, Oslo, Norway; ^bInstitute of Oral Biology, Faculty of Dentistry, University of Oslo, Oslo, Norway; ^cDepartment of Medical Physics, Cancer Clinic, Oslo University Hospital, Oslo, Norway; ^dDanish Centre for Particle Therapy, Aarhus University Hospital, Aarhus, Denmark; ^eDepartment of Experimental Clinical Oncology, Aarhus University Hospital, Aarhus, Denmark; ^fDepartment of Health Technology, Technical University of Denmark, Roskilde, Denmark; ^gDepartment of Pathology, Oslo University Hospital, Oslo, Norway

ABSTRACT

Background: The purpose of this study was to investigate acute normal tissue responses in the head and neck region following proton- or X-irradiation of a murine model.

Materials and methods: Female C57BL/6J mice were irradiated with protons (25 or 60 MeV) or X-rays (100 kV). The radiation field covered the oral cavity and the major salivary glands. For protons, two different treatment plans were used, either with the Bragg Peak in the middle of the mouse (BP) or outside the mouse (transmission mode; TM). Delivered physical doses were 41, 45, and 65 Gy given in 6, 7, and 10 fractions for BP, TM, and X-rays, respectively. Alanine dosimetry was used to assess delivered doses. Oral mucositis and dermatitis were scored using CTC v.2.0-based tables. Saliva was collected at baseline, right after end of irradiation, and at day 35.

Results: The measured dose distribution for protons (TM) and X-rays was very similar. Oral mucositis appeared earlier, had a higher score and was found in a higher percentage of mice after proton irradiation compared to X-irradiation. Dermatitis, on the other hand, had a similar appearance after protons and X-rays. Compared to controls, saliva production was lower right after termination of proton- and X-irradiation. The BP group demonstrated saliva recovery compared to the TM and X-ray group at day 35.

Conclusion: With lower delivered doses, proton irradiation resulted in similar skin reactions and increased oral mucositis compared to X-irradiation. This indicates that the relative biological effectiveness of protons for acute tissue responses in the mouse head and neck is greater than the clinical standard of 1.1. Thus, there is a need for further investigations of the biological effect of protons in normal tissues.

ARTICLE HISTORY

Received 27 May 2023
Accepted 26 August 2023

KEYWORDS



Proton; X-rays; radiotherapy; mice; salivary glands; head and neck cancer

Background

Radiotherapy of head and neck (H&N) cancer may damage normal tissue surrounding the tumor, thereby causing detrimental acute and late side effects [1]. Acute side effects such as skin dermatitis and oral mucositis usually occur during or immediately after treatment and may cause an unfavorable treatment halt [2,3]. Therefore, approaches that can reduce normal tissue damage and thus decrease side effects from radiation therapy are warranted, and proton therapy has emerged as an important tissue-sparing approach.


Compared to conventional X-irradiation, proton irradiation has a more favorable dose distribution where a high dose is

deposited in the so-called Bragg peak with no dose deposited further into the tissue [4]. Thus, proton irradiation can reduce the radiation dose to normal tissues, especially behind the tumor. However, published studies point toward differences in biological responses between protons and X-rays, such as in DNA damage repair, gene expression modulation, and inflammatory regulation [5–10]. Relative biological effectiveness (RBE) is defined as the ratio of a reference X-ray dose to the proton dose that induce the same biological effect. It depends on several variables such as the dose per fraction, linear energy transfer (LET), tissue type, and biological endpoint [11–13]. Despite accumulated experimental

CONTACT Eirik Malinen  eirik.malinen@fys.uio.no  Department of Physics, Faculty of Mathematics and Natural Sciences, University of Oslo, Oslo, Norway; Department of Medical Physics, Cancer Clinic, Oslo University Hospital, Oslo, Norway

*Joint first authors

†Joint senior authors

 Supplemental data for this article can be accessed online at <https://doi.org/10.1080/0284186X.2023.2254481>.

© 2023 The Author(s). Published by Informa UK Limited, trading as Taylor & Francis Group. This is an Open Access article distributed under the terms of the Creative Commons Attribution-NonCommercial-NoDerivatives License (<http://creativecommons.org/licenses/by-nc-nd/4.0/>), which permits non-commercial re-use, distribution, and reproduction in any medium, provided the original work is properly cited, and is not altered, transformed, or built upon in any way. The terms on which this article has been published allow the posting of the Accepted Manuscript in a repository by the author(s) or with their consent.

data on the variability of proton RBE, a fixed standard value for RBE of 1.1 for protons is used at most treatment centers, but there is a growing awareness of RBE variation along the proton path [14–17].

Increasing clinical evidence shows that proton therapy is superior to X-ray therapy in lowering the radiation dose to normal tissue and thus reducing side effects [18–20]. Still, for H&N cancer, there is a scarcity of randomized clinical studies directly comparing acute or late side effects from proton and X-therapy, and more knowledge regarding the differences in normal tissue responses between X-ray and proton irradiation is needed. The purpose of this preclinical study was thus to investigate acute normal tissue responses following H&N proton- and X-irradiation to gain new knowledge on the differences in biological effects between the two radiation types.

Materials and methods

Animals

Female C57BL/6J mice purchased from Janvier (France) were used in this study. Mice were kept in a 12-h light/12-h dark cycle under pathogen-free conditions and fed standard commercial fodder with water given *ad libitum*. Standard housing with nesting material and refuge was provided. Animals were 12 weeks old at the onset of experiments. All animal experiments in Norway were performed in accordance with directive 2010/63/EU on the protection of animals used for scientific purposes and approved by the Norwegian Food Safety Authority (ID 27931). All animal experiments in Denmark were performed in accordance with the animal welfare policy of Aarhus University and approved by the Danish Animal Experiments Inspectorate.

Irradiation procedure

X-irradiation was performed with a Faxitron Multirad225 irradiation system (Faxitron Bioptics, Tucson, AZ, USA) at the Radium Hospital in Oslo, Norway. Mice in the X-ray group were irradiated with a total dose of 65 Gy given in 10 fractions over 10 days with the following settings: 100 kV X-ray potential, 15 mA current, 2.0 mm Al filter, and 0.68 Gy/min dose rate.

Absolute dosimetry of the X-ray system was conducted using an FC65-G Farmer type ionization chamber (IBA Dosimetry, Germany) together with a MAX-4000 electrometer (Standard Imaging, USA) according to IAEA report TRS-277 [21]. Dosimetry for the collimated case was performed using Gafchromic™ EBT3 dosimeter films at a source-surface distance representing the skin entrance of the mouse. Calibration was done using an unshielded beam. EBT3 films (lot No. 02122001) were irradiated and processed according to the recommended protocols specified for radiochromic film dosimetry in the report of AAPM Task Group 235 [22]. The reported dose for the X-ray group is the mean dose at the midpoint in the X-ray path through the mouse. Alanine dosimetry was used to measure delivered X-ray and proton

depth dose profiles, and the Monte Carlo method was used to simulate the dose in 3D (Figure 1C) (see [Supplementary Materials](#)).

Proton irradiation was performed using the Varian ProBeam clinical gantry with a pencil beam scanning dedicated nozzle (Varian, Medical Systems, Palo Alto, CA, USA) at the Danish Center for Particle Therapy at Aarhus University Hospital in Aarhus, Denmark. Two different proton treatment groups were included. The first proton treatment group (BP group) was irradiated with a total physical dose of 40.8 Gy given in six fractions over six days using a single-energy pristine Bragg peak (70 MeV degraded by 3 cm solid water). For this group, the distal edge of Bragg peak is located in the middle of the mouse. The second proton treatment group (TM group) was irradiated with a total physical dose of 44.8 Gy given in seven fractions over seven days with a single energy pristine Bragg peak (70 MeV degraded by 1 cm solid water). In this 'transmission mode', the Bragg peak ended up outside the mouse (Figure 1B). The proton entrance energy/range was estimated to be 25 MeV/6.8 mm and 60 MeV/31 mm for the BP and TM groups, respectively.

Day 0 was the time point where the first irradiation was performed. For X-ray and proton irradiation, mice were anesthetized using gas anesthesia with 4% Sevoflurane in O₂. Mice were positioned laterally, on the right side for the X-ray and BP groups and on the left side for the TM group, in a custom-made foam holder with the beam entering on the opposite side (Supplementary Figure 1). The mice in the TM group were positioned on the left side to approximately match the proton and X-ray dose distributions. A lead (for X-rays) or brass (for protons) collimator was custom-built to define a radiation field of 25 × 20 mm covering the oral cavity, pharynx, and major salivary glands and placed on top of the foam holder. The radiation field was carefully planned to only irradiate the tissues of interest and avoid exposure to the eyes and brain.

Experimental protocol and study groups

The experimental timeline for proton and X-ray experiments is presented in Figure 1A. On day –3, saliva collections were performed in all animals as baseline measurements. On days 0–4 and 7–11, X-ray-fractionated treatment was given once a day around 4 pm, as explained above. During the acute phase (days 8–35), mice were monitored daily, and examinations of the oral cavity were performed every second day in order to obtain documentation of the acute tissue responses. Oral mucositis and lip dermatitis were scored using modified scoring tables (Supplementary Tables 1 and 2) based on CTC v. 2.0 [23–25].

On days 0–4 and 7, proton-fractionated treatment was given once a day around 4 pm to both proton groups, as explained above. On day 8, irradiation treatment was terminated for the BP group due to substantial weight loss and observed oral mucositis. The TM group received one more fraction on day 8 and irradiation treatment was then terminated on day 9 due to substantial weight loss. To alleviate the pain from oral mucositis, analgesic treatment using

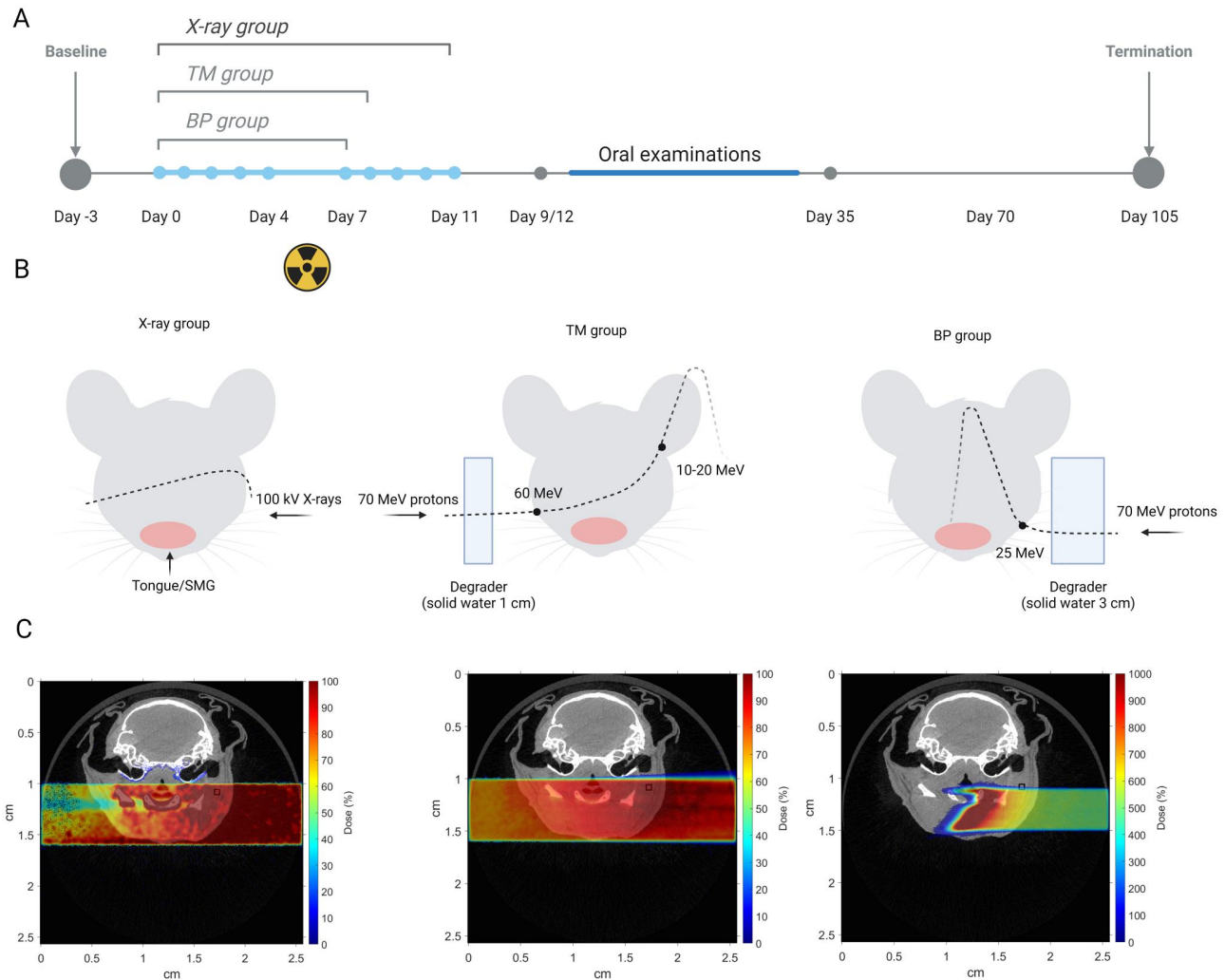


Figure 1. Timeline (A), Graphical treatment plan (B) and corresponding FLUKA MC simulations (C) of the X-ray and proton irradiation experiments.

Temgesic injections was started right after saliva collection (day 12 for the X-ray group and day 9 for the TM and BP groups) and administered to all mice through intraperitoneal injections every 8 h for 5 days. In addition, easily digestible and nutrition-rich gel fodder (DietGel Recovery, Clear H₂O) and saline injection (0.1–0.3 ml subcutaneously administered) were provided to all mice to avoid unnecessary mortality. However, several mice in the proton groups reached humane endpoints and were euthanized between days 12–18 according to the protocol approved by the national animal authorities. Additional samples of saliva were collected immediately after termination of irradiation treatment (day 12 for the X-ray group and day 9 for the BP and TM groups), and at the end of the acute phase on day 35. The maximum follow-up period was day 105 after the onset of fractionated irradiation. However, the acute phase was considered to be over on day 35, so only this period is included in the current study.

Saliva collection

Saliva volume measurements were used to assess salivary gland function and saliva production. Saliva collection was

performed as previously described [26,27]. Briefly, 0.375 mg/kg of pilocarpine (pilocarpine hydrochloride, Sigma) was intraperitoneally administered to the mice under anesthesia to stimulate saliva production. Saliva was collected into a cotton swab for 15 min and was then centrifuged at 7500 *g* and 4 °C for 2 min. The obtained volume was measured and stored at –80 °C. Data from two nonirradiated control groups from the involved research facilities were pooled.

Statistical analysis

Statistical analysis was performed using Prism 8 for Windows (Version 8.3.0, GraphPad Software, LLC). Saliva volume measurements were compared using a Mann–Whitney test with a significance level of 0.05.

Results

The dose distributions for X-ray and proton irradiations were measured using alanine dosimetry (Figure 2). The results for X-ray and TM groups showed that the depth dose profiles within the region of the irradiation field are virtually the same for two different radiation types with approximately

the same dose per fraction. Therefore, mice from X-ray and TM groups received the same dose distribution, gradually decreasing from the left to the right side. Because of the alanine pellet thickness and the narrow width of Bragg peak, the depth dose profile for BP proton irradiation cannot display the Bragg peak but a steep dose gradient is indeed seen. Thus, as also indicated by the Monte Carlo simulations, the distal edge of Bragg peak was likely located around the midplane of the mouse in the BP group, as planned.

The onset of lip dermatitis was seen on day 8 for all groups. The mean lip dermatitis severity score was quite similar in the X-ray and proton groups (Figure 3A); however, this score only represented the highest value observed locally in each mouse. In the BP group, we observed less severe dermatitis on the left side than on the right side of the lip, confirming that the Bragg peak was deposited in the middle of the mouse. The severity score on the right side of the lip in the BP group was equal to the severity score observed in the entire lip of the TM and X-ray groups. Moreover, we observed large areas of dry and moist desquamation followed by fur loss on the chest of TM and X-ray groups. In contrast, only dry desquamation followed by fur

loss was observed in similar areas of the chest in the BP group.

Mucositis of the tongue was observed in 100% of the mice exposed to both proton irradiation schemes, but only in 80% of the mice exposed to X-ray irradiation. The onset of mucositis was observed earlier for proton compared to X-ray-irradiated mice and the median severity score was higher (Figure 3B). In both proton groups, mucositis was observed on the ventral and dorsal surface of the tongue, while it was only observed on the ventral surface in the X-ray group (Figure 4). Even though the severity of the mucositis was similar in BP and TM mice, the locations were different. In the BP group, mucositis was only observed on the right side of the dorsal surface of the tongue, while it was more consistent on the entire dorsal surface in the TM group (Figure 4) further confirming the dose distributions seen by alanine dosimetry.

The saliva volume was significantly lower after X-ray and proton irradiation compared to controls right after termination of the radiotherapy (day 9 for BP and TM, day 12 for X-rays). However, at day 35 only the TM and X-ray group demonstrated significantly lower saliva volume compared to controls, while the BP group showed recovery of saliva production (Figure 5).

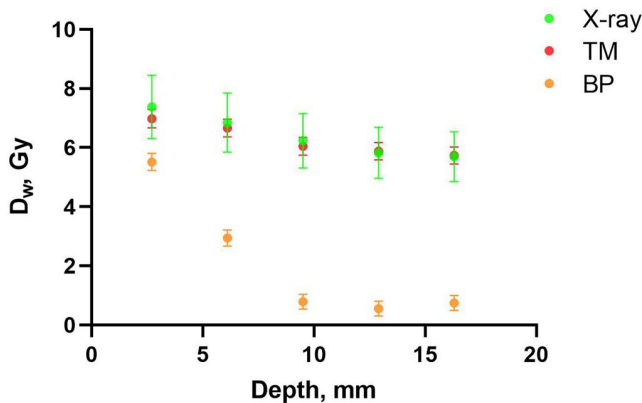


Figure 2. Depth dose profiles based on alanine dosimetry. All points represent the mean dose per pellet with 1 standard error indicated as error bars.

Discussion

Normal tissue complications after radiotherapy are dose-limiting and may prevent a successful treatment. Tissue damage can contribute both to interruption of planned treatment and to reduced quality of life for the patient. Proton therapy is considered a tissue-sparing modality because less normal tissue is irradiated compared to conventional X-rays. However, protons deposit their energy with an increasing LET at the end of the Bragg peak. To adjust for this, a constant RBE of 1.1 is used in most proton centers in USA and Europe [28]. However, data from *in vitro* and *in vivo* experiments demonstrate that the RBE increases along the proton beam track and that the average value may be higher than 1.1 [14–16].

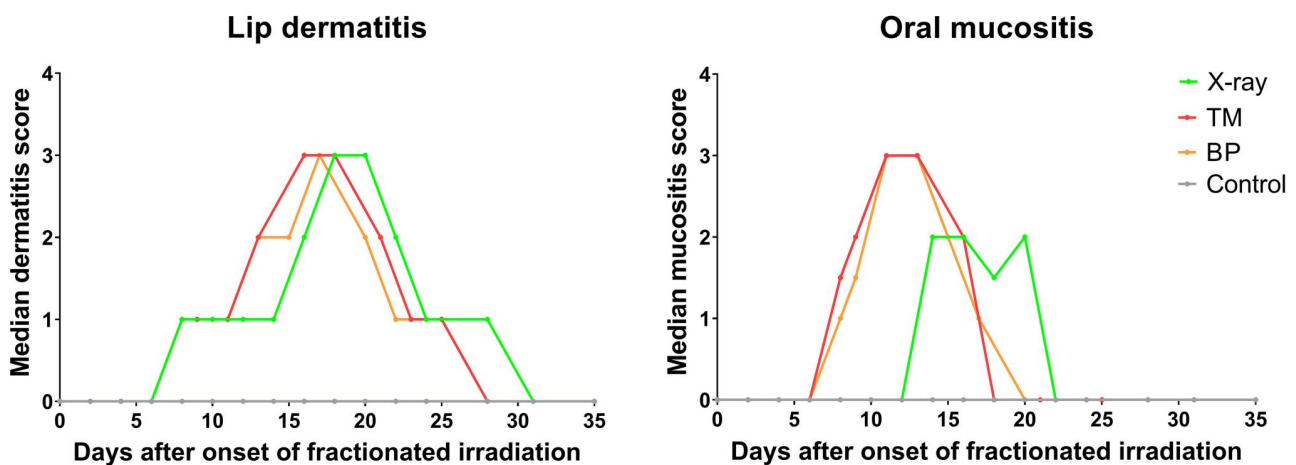


Figure 3. Timeline of median lip dermatitis score (A) and median oral mucositis score (B) in each treatment group after fractionated irradiation (X-rays $n = 9$, TM $n = 6$, BP $n = 5$, controls $n = 14$). The X-ray group received daily fractions on days 0–4 and 7–11, to a total dose of 65 Gy. The TM group received daily fractions on days 0–4 and 7–8, to a total dose of 45 Gy. The BP group received daily fractions on days 0–4 and 7, to a total dose of 41 Gy.

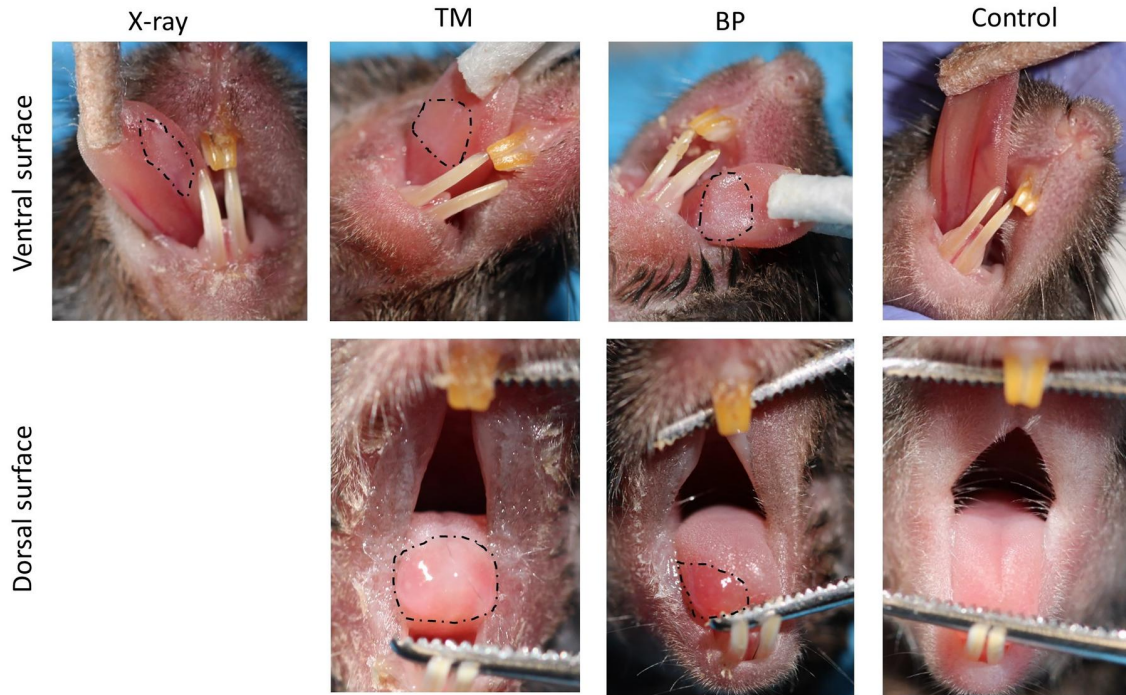


Figure 4. Representative images of observed oral mucositis on the ventral and dorsal surface of the tongue after proton- and X-irradiation (dotted lines). a control (nonirradiated) mouse is included for comparison.

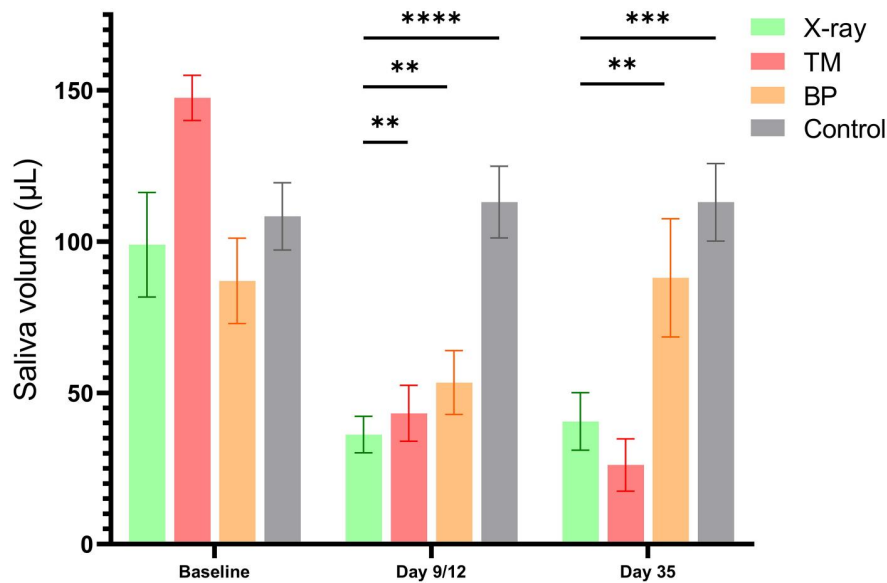


Figure 5. Saliva volume after X-ray and proton irradiation during the acute response phase. Data is represented as mean \pm SEM (** $p < 0.01$, *** $p < 0.001$, **** $p < 0.0001$; X-rays $n = 9$, TM $n = 6$, BP $n = 5$, controls $n = 14$).

Protons with dissimilar energies and LET have been shown to induce different biological effects [29], and more experiments to gain fundamental knowledge on biological effects in different tissues are needed to understand how RBE variations should be addressed in treatment planning.

In this study, we used two different proton beam delivery setups to study acute normal tissue responses. The BP group was irradiated with a pristine Bragg peak covering half of the mouse H&N region with the distal side of the Bragg peak located in the area of interest (oral cavity, salivary

glands). This may clinically reflect irradiation of normal tissues being located behind the tumor. On the other hand, the TM group was irradiated with a more homogeneous dose distribution where the Bragg peak ended up outside the mouse. We designed this approach to create a proton plan with a similar dose distribution as X-rays to be able to directly compare their biological effectiveness. The depth dose distribution measured by alanine dosimetry showed very similar dose distributions for the TM and X-ray group. Surprisingly, the biological effects were very high for the TM group compared to the X-ray group.

The fractionated treatment had to be terminated earlier than planned due to substantial weight loss in the BP and TM groups so that the total dose received was lower than that received by the X-ray group. The animals tolerated 1.5–1.6 times higher doses with X-rays compared to both proton groups. Therefore, for local H&N irradiation, protons were biologically more effective in causing acute tissue damage compared to X-rays. Moreover, the proton RBE for both treatment groups is likely higher than the clinical standard of 1.1.

In the present study, the saliva volume was significantly lower in all irradiated groups right after treatment termination (day 9/12) and on day 35, compared to controls. However, the BP group showed recovery of saliva production compared to the TM and X-ray groups on day 35. This may indicate a compensatory mechanism in the paired salivary glands that were outside the radiation field (as only half of the pair of glands were hit by the BP approach). Moreover, we observed a greater degree of oral mucositis after proton compared to X-ray irradiation. The oral mucositis mean score was about the same for TM and BP, but the extension on the tongue was different. The observed location and high score of oral mucositis on the dorsal surface of the tongue in BP mice indicates that there is an effect of high LET on normal tissue damage considering the much lower dose received by this area compared to the other irradiation groups. However, the low LET TM proton setup with a lower total dose compared to the X-ray setup also induced pronounced oral mucositis, which indicates that LET might not be the only decisive factor contributing to RBE in this case. Thus, for protons, it would seem that low irradiated volume and high LET (BP) give approximately the same mucositis as high volume and low LET (TM).

It is challenging to compare our results to clinical studies since the latter usually demonstrate a lower mean dose to the oral cavity after protons compared to X-rays as well as less irradiated volume [18–20,30–32]. Thus, in these clinical studies, the lower dose explained the reduced side effects, but the local RBE could still be higher due to differences in LET. No other preclinical data on oral mucositis after protons compared to X-rays have been published. However, Choi et al. studied acute normal tissue responses in the intestinal epithelium [33], which resembles oral epithelium in many ways [34]. They found that in mouse jejunum, protons induced a greater decrease in the number of crypts than X-rays, even when the same physical dose was used [33]. Our study also demonstrates larger acute tissue responses in the oral mucosa after protons compared to X-rays. Surprisingly, we observed this difference in oral mucosal response even using lower total physical doses of protons than X-rays.

In contrast to the increased score of oral mucositis after proton irradiation, we found similar dermatitis scores after proton- and X-irradiation. Similar acute responses in the skin have previously been shown in mice after a single dose of proton or X-irradiation of the leg [13,35]. The observed difference in the acute response of oral mucosa and skin in the present study is, however, intriguing. Oral mucosa and skin are intrinsically different in regard to wound healing, where oral mucosa generally heals faster than skin [36,37]. Relative

to X-irradiation, we observed an increase in oral mucositis compared to dermatitis following proton irradiation. This could indicate that the oral mucosa is affected not only by the type of radiation but also by the reduction in saliva production or changes in the saliva content. Differences in the degree of keratinization and proliferation rate between the two tissues can also contribute to the observed differences and need to be further elucidated.

Disclosure statement

No potential conflict of interest was reported by the authors.

Funding

This work was supported by UiO Life Science at the University of Oslo under grant reference 2018/10221 and South-Eastern Norway Regional Health Authority under grant number 2019050.

ORCID

Olga Zlygosteva  <http://orcid.org/0000-0002-2744-9663>

Data availability statement

The data that support the findings of this study are available from the corresponding author, EM, upon reasonable request.

References

- [1] Barazuol L, Coppes RP, van Luijk P. Prevention and treatment of radiotherapy-induced side effects. *Mol Oncol.* 2020;14(7):1538–1554. doi: 10.1002/1878-0261.12750.
- [2] Chibly AM, Aure MH, Patel VN, et al. Salivary gland function, development, and regeneration. *Physiol Rev.* 2022;102(3):1495–1552. doi: 10.1152/physrev.00015.2021.
- [3] Siddiqui F, Movsas B. Management of radiation toxicity in head and neck cancers. *Semin Radiat Oncol.* 2017;27(4):340–349. doi: 10.1016/j.semradonc.2017.04.008.
- [4] Tian X, Liu K, Hou Y, et al. The evolution of proton beam therapy: current and future status. *Mol Clin Oncol.* 2018;8(1):15–21. doi: 10.3892/mco.2017.1499.
- [5] Fontana AO, Augsburg MA, Grosse N, et al. Differential DNA repair pathway choice in cancer cells after proton- and photon-irradiation. *Radiother Oncol.* 2015;116(3):374–380. doi: 10.1016/j.radonc.2015.08.014.
- [6] Lupu-Plesu M, Claren A, Martial S, et al. Effects of proton versus photon irradiation on (lymph)angiogenic, inflammatory, proliferative and anti-tumor immune responses in head and neck squamous cell carcinoma. *Oncogenesis.* 2017;6(7):e354–e354. doi: 10.1038/oncsis.2017.56.
- [7] Nielsen S, Bassler N, Grzanka L, et al. Differential gene expression in primary fibroblasts induced by proton and cobalt-60 beam irradiation. *Acta Oncol.* 2017;56(11):1406–1412. doi: 10.1080/0284186X.2017.1351623.
- [8] Nielsen S, Bassler N, Grzanka L, et al. Comparison of coding transcriptomes in fibroblasts irradiated with low and high let proton beams and cobalt-60 photons. *Int J Radiat Oncol Biol Phys.* 2019; 103(5):1203–1211. doi: 10.1016/j.ijrobp.2018.11.065.
- [9] Vitti ET, Parsons JL. The radiobiological effects of proton beam therapy: impact on DNA damage and repair. *Cancers (Basel).* 2019;11(7):946. doi: 10.3390/cancers11070946.
- [10] Paganetti H. Mechanisms and review of clinical evidence of variations in relative biological effectiveness in proton therapy. *Int J*

- Radiat Oncol Biol Phys. 2022;112(1):222–236. doi: [10.1016/j.ijrobp.2021.08.015](https://doi.org/10.1016/j.ijrobp.2021.08.015).
- [11] McNamara AL, Schuemann J, Paganetti H. A phenomenological relative biological effectiveness (RBE) model for proton therapy based on all published in vitro cell survival data. *Phys Med Biol*. 2015;60(21):8399–8416. doi: [10.1088/0031-9155/60/21/8399](https://doi.org/10.1088/0031-9155/60/21/8399).
- [12] Paganetti H. Relative biological effectiveness (RBE) values for proton beam therapy. Variations as a function of biological endpoint, dose, and linear energy transfer. *Phys Med Biol*. 2014;59(22):R419–72. doi: [10.1088/0031-9155/59/22/R419](https://doi.org/10.1088/0031-9155/59/22/R419).
- [13] Sorensen BS, Horsman MR, Alsner J, et al. Relative biological effectiveness of carbon ions for tumor control, acute skin damage and late radiation-induced fibrosis in a mouse model. *Acta Oncol*. 2015;54(9):1623–1630. doi: [10.3109/0284186X.2015.1069890](https://doi.org/10.3109/0284186X.2015.1069890).
- [14] Sorensen BS, Bassler N, Nielsen S, et al. Relative biological effectiveness (RBE) and distal edge effects of proton radiation on early damage in vivo. *Acta Oncol*. 2017;56(11):1387–1391. doi: [10.1080/0284186X.2017.1351621](https://doi.org/10.1080/0284186X.2017.1351621).
- [15] Sorensen BS, Pawelke J, Bauer J, et al. Does the uncertainty in relative biological effectiveness affect patient treatment in proton therapy? *Radiother Oncol*. 2021;163:177–184. doi: [10.1016/j.radonc.2021.08.016](https://doi.org/10.1016/j.radonc.2021.08.016).
- [16] Saager M, Peschke P, Brons S, et al. Determination of the proton RBE in the rat spinal cord: is there an increase towards the end of the spread-out Bragg peak? *Radiother Oncol*. 2018;128(1):115–120. doi: [10.1016/j.radonc.2018.03.002](https://doi.org/10.1016/j.radonc.2018.03.002).
- [17] Jones B. Why RBE must be a variable and not a constant in proton therapy. *Br J Radiol*. 2016;89(1063):20160116. doi: [10.1259/bjr.20160116](https://doi.org/10.1259/bjr.20160116).
- [18] Meijer TWH, Scandurra D, Langendijk JA. Reduced radiation-induced toxicity by using proton therapy for the treatment of oropharyngeal cancer. *Br J Radiol*. 2020;93(1107):20190955. doi: [10.1259/bjr.20190955](https://doi.org/10.1259/bjr.20190955).
- [19] Cao J, Zhang X, Jiang B, et al. Intensity-modulated proton therapy for oropharyngeal cancer reduces rates of late xerostomia. *Radiother Oncol*. 2021;160:32–39. doi: [10.1016/j.radonc.2021.03.036](https://doi.org/10.1016/j.radonc.2021.03.036).
- [20] Blanchard P, Garden AS, Gunn GB, et al. Intensity-modulated proton beam therapy (IMPT) versus intensity-modulated photon therapy (IMRT) for patients with oropharynx cancer - A case matched analysis. *Radiother Oncol*. 2016;120(1):48–55. doi: [10.1016/j.radonc.2016.05.022](https://doi.org/10.1016/j.radonc.2016.05.022).
- [21] Andreo P, Cunningham JR, Hohlfield K, et al. Absorbed dose determination in photon and electron beams. An international Code of Practice. 1987.
- [22] Niroomand-Rad A, Chiu-Tsao ST, Grams MP, et al. Report of AAPM task group 235 radiochromic film dosimetry: an update to TG-55. *Med Phys*. 2020;47(12):5986–6025. doi: [10.1002/mp.14497](https://doi.org/10.1002/mp.14497).
- [23] Mallick S, Benson R, Rath GK. Radiation induced oral mucositis: a review of current literature on prevention and management. *Eur Arch Otorhinolaryngol*. 2016;273(9):2285–2293. doi: [10.1007/s00405-015-3694-6](https://doi.org/10.1007/s00405-015-3694-6).
- [24] Sonis ST, Elting LS, Keefe D, et al. Perspectives on cancer therapy-induced mucosal injury: pathogenesis, measurement, epidemiology, and consequences for patients. *Cancer*. 2004;100(9 Suppl):1995–2025. doi: [10.1002/cncr.20162](https://doi.org/10.1002/cncr.20162).
- [25] Trotti A, Byhardt R, Stetz J, et al. Common toxicity criteria: version 2.0. an improved reference for grading the acute effects of cancer treatment: impact on radiotherapy. *Int J Radiat Oncol Biol Phys*. 2000;47(1):13–47. doi: [10.1016/S0360-3016\(99\)00559-3](https://doi.org/10.1016/S0360-3016(99)00559-3).
- [26] Bagavant H, Trzeciak M, Papinska J, et al. A method for the measurement of salivary gland function in mice. *J Vis Exp*. 2018;(131):57203. doi: [10.3791/57203](https://doi.org/10.3791/57203).
- [27] Juvkam IS, Zlygosteva O, Arous D, et al. A preclinical model to investigate normal tissue damage following fractionated radiotherapy to the head and neck. *J Radiat Res*. 2023;64(1):44–52. doi: [10.1093/jrr/rrac066](https://doi.org/10.1093/jrr/rrac066).
- [28] Heuchel L, Hahn C, Pawelke J, et al. Clinical use and future requirements of relative biological effectiveness: survey among all european proton therapy centres. *Radiother Oncol*. 2022; 172: 134–139. doi: [10.1016/j.radonc.2022.05.015](https://doi.org/10.1016/j.radonc.2022.05.015).
- [29] Tommasino F, Durante M. Proton radiobiology. *Cancers (Basel)*. 2015;7(1):353–381. doi: [10.3390/cancers7010353](https://doi.org/10.3390/cancers7010353).
- [30] Holliday EB, Kocak-Uzel E, Feng L, et al. Dosimetric advantages of intensity-modulated proton therapy for oropharyngeal cancer compared with intensity-modulated radiation: a case-matched control analysis. *Med Dosim*. 2016;41(3):189–194. doi: [10.1016/j.meddos.2016.01.002](https://doi.org/10.1016/j.meddos.2016.01.002).
- [31] McDonald MW, Liu Y, Moore MG, et al. Acute toxicity in comprehensive head and neck radiation for nasopharynx and paranasal sinus cancers: cohort comparison of 3D conformal proton therapy and intensity modulated radiation therapy. *Radiat Oncol*. 2016; 11(1):32. doi: [10.1186/s13014-016-0600-3](https://doi.org/10.1186/s13014-016-0600-3).
- [32] Romesser PB, Cahlon O, Scher E, et al. Proton beam radiation therapy results in significantly reduced toxicity compared with intensity-modulated radiation therapy for head and neck tumors that require ipsilateral radiation. *Radiother Oncol*. 2016;118(2): 286–292. doi: [10.1016/j.radonc.2015.12.008](https://doi.org/10.1016/j.radonc.2015.12.008).
- [33] Choi C, Lee C, Shin SW, et al. Comparison of proton and photon beam irradiation in Radiation-Induced intestinal injury using a mouse model. *Int J Mol Sci*. 2019;20(8):1894. doi: [10.3390/ijms20081894](https://doi.org/10.3390/ijms20081894).
- [34] Suarez LJ, Arboleda S, Angelov N, et al. Oral versus gastrointestinal mucosal immune niches in homeostasis and allostasis. *Front Immunol*. 2021;12:705206. doi: [10.3389/fimmu.2021.705206](https://doi.org/10.3389/fimmu.2021.705206).
- [35] Nielsen S, Bassler N, Grzanka L, et al. Proton scanning and X-ray beam irradiation induce distinct regulation of inflammatory cytokines in a preclinical mouse model. *Int J Radiat Biol*. 2020;96(10): 1238–1244. doi: [10.1080/09553002.2020.1807644](https://doi.org/10.1080/09553002.2020.1807644).
- [36] Turabelidze A, Guo S, Chung AY, et al. Intrinsic differences between oral and skin keratinocytes. *PLoS One*. 2014;9(9): e101480. doi: [10.1371/journal.pone.0101480](https://doi.org/10.1371/journal.pone.0101480).
- [37] Waasdorp M, Krom BP, Bikker FJ, et al. The bigger picture: why oral mucosa heals better than skin. *Biomolecules*. 2021;11(8): 1165. doi: [10.3390/biom11081165](https://doi.org/10.3390/biom11081165).

Supplementary materials and methods

Alanine dosimetry

We applied cylindrical alanine pellets (diameter 4.8 mm and height 2.7 mm) from Harwell Dosimeters Ltd, UK. Seven pellets were stacked on top of each other and placed in an Eppendorf tube. The tubes with pellets were positioned inside the foam holder in the area of mouse oral cavity and irradiated with the same settings and dose per fractions as mice in all treatment groups (X-rays, BP, TM). The pellets were read out using a Bruker EMX micro spectrometer, where the specific read out procedure is described in [1]. The system was calibrated in a cobalt-60 field with traceability to PTB in Germany. Beam quality correction factor (k_Q) relative to cobalt for the 100 kV x-ray beam was estimated to be $k_Q = 1.43$ with an uncertainty $u(k_Q)=0.14$ ($k=1$) based on [2,3]. Beam quality correction factors for the proton irradiations were estimated to be $k_Q = 1.022$ for the plateau and $k_Q = 1.033$ for the measurements in or near the Bragg peak based on [4,5]. The uncertainty of the proton beam-quality corrections was estimated to $u(k_Q)=0.02$ ($k=1$). Depth dose distributions for all experiments were plotted using D_w and position of the pellet in the stack, where the pellet thickness was translated into water equivalent thickness (WET) [6].

Monte Carlo simulations

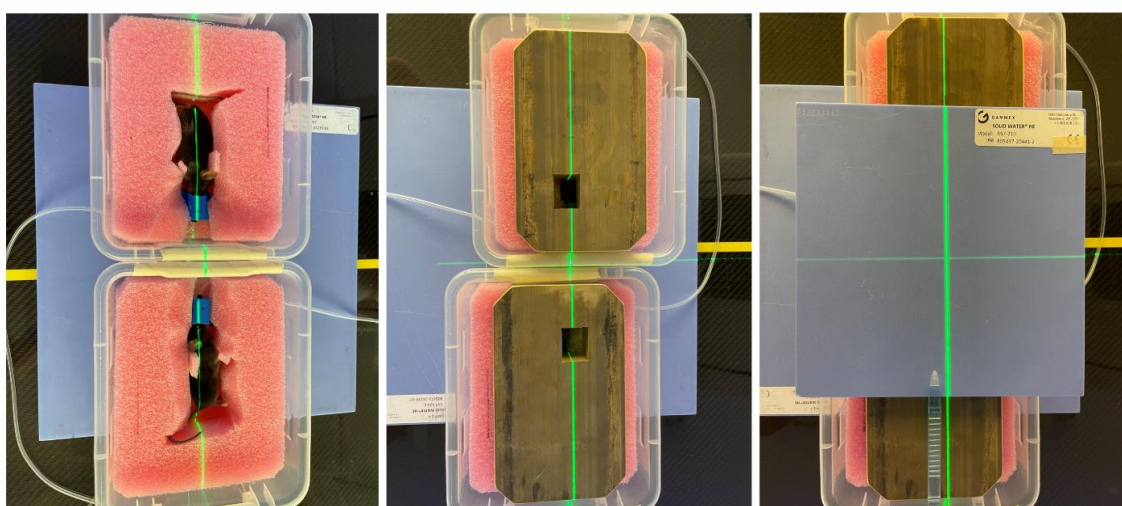
Monte Carlo (MC) simulations of the three-dimensional (3D) dose distribution in mice were conducted in FLUKA 4–3.2 [7,8] and Flair 3.2-4.3 [9]. Briefly, the simulations were performed in computed tomography (CT) images of one euthanized male mouse (11 weeks old). For the X-ray irradiation setup, a 100 kV spectrum attenuated through a 2 mm aluminum filter was simulated. For the proton irradiation setup, nominal energy of 24 MeV and 60 MeV with a Gaussian energy distribution of 3 MeV and 2 MeV full width at half maximum (FWHM) spread were simulated, respectively. The MC simulations were run using standard FLUKA physics settings (cf. PRECISION defaults in the FLUKA manual). The absorbed dose was scored on a voxel-by-voxel basis (using the USRBIN option in FLUKA). The mean LET in the irradiated part of the mouse was crudely estimated to be 3.3 and 4.2 keV/ μm for TM and BP, respectively, while it was around 1.0 keV/ μm for X-rays. It is stressed the local LET approximately mid-plane in the animal will be much higher for the BP approach.

References

1. Ankjærgaard C, Johansen, A.Z., von Staffeldt, M.M.K., Andersen, C.E., Madsen, D.H., Behrens, C.F. Irradiation of subcutaneous mouse tumors with a clinical linear accelerator validated by alanine dosimetry. *Radiation Measurements* 2021;147 (106636).
2. Hjørringgaard JG. Dosimetry for Low Energy X-rays: Efficiency of the Alanine Pellet Dosimeter. DTU Orbit: Technical University of Denmark; 2021.
3. Hjørringgaard JG, Ankjærgaard, C., Andersen, C.E. The microdosimetric one-hit detector model for calculating the relative efficiency of the alanine pellet dosimeter in low energy X-ray beams. *Radiation Measurements* 2022;150(106659).
4. Carlino A, Gouldstone C, Kragl G, et al. End-to-end tests using alanine dosimetry in scanned proton beams. *Phys Med Biol.* 2018 Feb 26;63(5):055001.
5. Palmans H, Carlino, A., Gouldstone, C., Sharpe, P. Cross calibration of alanine for scanned proton beams. National Physics Laboratory: National Physics Laboratory 2018.

6. Zhang R, Newhauser WD. Calculation of water equivalent thickness of materials of arbitrary density, elemental composition and thickness in proton beam irradiation. *Phys Med Biol.* 2009 Mar 21;54(6):1383-95.
7. Ahdida C, Bozzato D, Calzolari D, et al. New capabilities of the FLUKA multi-purpose code. *Frontiers in Physics.* 2022:705.
8. Battistoni G, Boehlen T, Cerutti F, et al. Overview of the FLUKA code. *Annals of Nuclear Energy.* 2015;82:10-18.
9. Vlachoudis V, editor *FLAIR: a powerful but user friendly graphical interface for FLUKA.* Proc. Int. Conf. on Mathematics, Computational Methods & Reactor Physics (M&C 2009), Saratoga Springs, New York; 2009.

Supplementary figures and tables



Supplementary Figure 1. Pictures of the irradiation set-up for proton irradiation.

Supplementary Table 1: Dermatitis scoring table based on CTC v. 2.0

Dermatitis score	Observed effects
0 None	No change over baseline
1 Mild	Faint erythema, mild edema and dry desquamation
2 Moderate	Bright erythema, moderate edema and patchy moist desquamation
3 Severe	Severe erythema and edema, confluent moist desquamation
4 Life threatening	Ulceration, necrosis, hemorrhage

Supplementary Table 2: Mucositis scoring table based on CTC v. 2.0

Mucositis score	Observed effects
0 None	No change over baseline
1 Mild	Erythema
2 Moderate	Patchy mucositis
3 Severe	Confluent, fibrinous mucositis
4 Life threatening	Ulceration, necrosis, hemorrhage

Supplementary Table 3: Individual raw data

Mouse ID		Saliva volume (microliter)			Mucositis on the tongue												
		Baseline	Day 9/12	Day 35	Day 8	Day 10	Day 12	Day 14	Day 16	Day 18	Day 20	Day 22	Day 24	Day 28	Day 31	Day 35	
11-1	X-rays 1	35	25	20	0	0	0	1	0	0	0	0	0	0	0	0	
11-3	X-rays 2	60	30	10	0	0	0	2	2	0	0	0	0	0	0	0	
11-6	X-rays 3	80	40	15	0	0	0	2	2	2	2	2	1	0	0	0	
11-7	X-rays 4	105	2	-	0	0	2	2	2	2	-	-	-	-	-	-	
11-9	X-rays 5	70	20	20	0	0	0	2	1	1	2	0	0	0	1	0	
12-1	X-rays 6	35	40	45	0	0	0	2	2	0	0	0	0	0	0	0	
12-4	X-rays 7	200	60	45	0	0	0	0	2	2	2	2	2	2	2	2	
12-5	X-rays 8	155	65	60	0	0	0	0	2	2	2	2	1	2	2	0	
12-8	X-rays 9	150	50	100	0	0	0	0	0	0	0	0	0	0	0	0	
12-10	X-rays 10	100	30	50	0	0	2	2	2	2	2	2	2	0	0	0	
15-11	TM1		62	30	2	2	3	3	3	1	0	0	0	0	0	0	
15-12	TM2		60	40	2	2	3	3	2	0	0	0	0	0	0	0	
16-6	TM3	140	13	10	2	2	3	3	2	1	0	0	0	0	0	0	
16-7	TM4	155	62	10	1	2	3	3	2	0	0	0	0	0	0	0	
18-1	TM5		70	-	0	2	3	3	1	0	-	-	-	-	-	-	
18-2	TM6		7	-	0	2	-	-	-	-	-	-	-	-	-	-	
18-3	TM7		56	7	2	2	3	3	1	1	0	0	0	0	0	0	
18-4	TM8		16	60	1	2	3	3	1	0	0	0	0	0	0	0	
15-2	BP1	100	28	-	1	2	3	3	2	2	-	-	-	-	-	-	
15-3	BP2	130	75	-	1	1	3	3	2	1	-	-	-	-	-	-	
15-4	BP3	70	25	150	1	2	3	3	2	1	0	0	0	0	0	0	
15-5	BP4	35	92	-	1	2	3	-	-	-	-	-	-	-	-	-	
15-6	BP5	60	80	110	1	2	3	3	1	1	0	0	0	0	0	0	
15-7	BP6	20	25	-	1	1	3	-	-	-	-	-	-	-	-	-	
15-8	BP7	90	22	50	1	1	3	3	2	1	0	0	0	0	0	0	
15-9	BP8	72	105	85	1	2	3	3	2	1	0	0	0	0	0	0	
16-1	BP9	160	17	-	1	1	3	-	-	-	-	-	-	-	-	-	
16-2	BP10	133	65	45	1	1	3	3	1	1	0	0	0	0	0	0	

15-1	Control protons 1	70	82	-	0	0	0	0	0	0	0	0	0	0	0	0	0
16-3	Control protons 2	175	97	35	0	0	0	0	0	0	0	0	0	0	0	0	0
16-4	Control protons 3	100	112	160	0	0	0	0	0	0	0	0	0	0	0	0	0
16-5	Control protons 4	30	172	155	0	0	0	0	0	0	0	0	0	0	0	0	0
16-8	Control protons 5	172	77	190	0	0	0	0	0	0	0	0	0	0	0	0	0
17-1	Control protons 6	110	152	190	0	0	0	0	0	0	0	0	0	0	0	0	0
17-10	Control protons 7	135	240	150	0	0	0	0	0	0	0	0	0	0	0	0	0
11-2	Control X-rays 1	120	160	60	0	0	0	0	0	0	0	0	0	0	0	0	0
11-4	Control X-rays 2	65	90	70	0	0	0	0	0	0	0	0	0	0	0	0	0
11-5	Control X-rays 3	20	60	55	0	0	0	0	0	0	0	0	0	0	0	0	0
11-8	Control X-rays 4	105	45	60	0	0	0	0	0	0	0	0	0	0	0	0	0
11-10	Control X-rays 5	90	90	105	0	0	0	0	0	0	0	0	0	0	0	0	0
12-2	Control X-rays 6	110	140	-	0	0	0	0	0	0	0	0	0	0	0	0	0
12-3	Control X-rays 7	115	100	110	0	0	0	0	0	0	0	0	0	0	0	0	0
12-6	Control X-rays 8	160	125	130	0	0	0	0	0	0	0	0	0	0	0	0	0
12-7	Control X-rays 9	170	60	120	0	0	0	0	0	0	0	0	0	0	0	0	0
12-9	Control X-rays 10	95	120	105	0	0	0	0	0	0	0	0	0	0	0	0	0

Abbreviations: TM = Transmission Mode proton treatment plan. BP = Bragg Peak proton treatment plan

Dermatitis on the lip												
Day 8	Day 10	Day 12	Day 14	Day 16	Day 18	Day 20	Day 22	Day 24	Day 28	Day 31	Day 35	
1	1	1	2	2	3	3	2	1	1	0	0	0
1	1	1	1	1	2	2	2	2	1	0	0	0
1	1	1	1	2	3	3	2	2	1	0	0	0
0	1	1	2	2	3	-	-	-	-	-	-	0
1	1	1	2	2	3	3	2	1	1	0	0	0
1	1	1	1	2	3	3	2	2	1	0	0	0
1	1	1	1	2	3	3	2	1	1	0	0	0
0	1	1	1	2	2	2	2	1	1	0	0	0
1	1	1	1	1	1	1	1	1	1	0	0	0
1	1	1	2	2	2	2	2	2	1	0	0	0
1	1	2	3	3	3	2	1	1	0	0	0	0
1	1	2	3	3	3	2	1	1	0	0	0	0
1	1	1	2	3	3	2	1	1	0	0	0	0
1	1	1	2	2	2	1	1	1	0	0	0	0
1	1	1	2	3	3	-	-	-	-	-	-	0
1	1	-	-	-	-	-	-	-	-	-	-	0
1	1	1	2	2	2	2	1	1	0	0	0	0
1	1	2	2	3	2	1	1	1	0	0	0	0
1	1	2	2	3	3	-	-	-	-	-	-	0
1	1	2	2	3	3	-	-	-	-	-	-	0
1	1	2	2	3	3	2	1	1	0	0	0	0
1	1	2	-	-	-	-	-	-	-	-	-	0
1	1	1	2	2	2	1	1	1	0	0	0	0
1	1	1	-	-	-	-	-	-	-	-	-	0
1	1	1	2	2	3	2	1	1	0	0	0	0
1	1	1	2	2	2	1	1	1	0	0	0	0
1	1	1	-	-	-	-	-	-	-	-	-	0
1	1	1	1	2	2	2	1	1	0	0	0	0

0	0	0	0	0	0	-	-	-	-	-	-	0
0	0	0	0	0	0	0	0	0	0	0	0	0
0	0	0	0	0	0	0	0	0	0	0	0	0
0	0	0	0	0	0	0	0	0	0	0	0	0
0	0	0	0	0	0	0	0	0	0	0	0	0
0	0	0	0	0	0	0	0	0	0	0	0	0
0	0	0	0	0	0	0	0	0	0	0	0	0
0	0	0	0	0	0	0	0	0	0	0	0	0
0	0	0	0	0	0	0	0	0	0	0	0	0
0	0	0	0	0	0	0	0	0	0	0	0	0
0	0	0	0	0	0	0	0	0	0	0	0	0
0	0	0	0	0	0	0	0	0	0	0	0	0
0	0	0	0	0	0	0	0	0	0	0	0	0
0	0	0	0	0	0	0	0	0	0	0	0	0
0	0	0	0	0	0	0	0	0	0	0	0	0
0	0	0	0	0	0	0	0	0	0	0	0	0
0	0	0	0	0	0	0	0	0	0	0	0	0
0	0	0	0	0	0	0	0	0	0	0	0	0
0	0	0	0	0	0	0	0	0	0	0	0	0
0	0	0	0	0	0	0	0	0	0	0	0	0
0	0	0	0	0	0	0	0	0	0	0	0	0
0	0	0	0	0	0	0	0	0	0	0	0	0
0	0	0	0	0	0	0	0	0	0	0	0	0
0	0	0	0	0	0	0	0	0	0	0	0	0

Paper IV

**Proton compared to X-irradiation
leads to more acinar atrophy and
greater hyposalivation accompanied
by a differential cytokine response**

